Laurien Stubbé

Influence of a reconfigurable wheelbase on lateral vehicle dynamics

MSc Thesis

TU Delft

Thesis

Influence of a reconfigurable wheelbase on lateral vehicle dynamics

Laurien Stubbé

In partial fulfillment of the requirements for the degree of

Master of Science in Mechanical Engineering
Track: Vehicle Engineering
Specialisation: Dynamics and Control

at the Delft University of Technology

Student number: 4367049
Graduation committee: Dr. ir. Riender Happee, Chair, Associate Professor, CoR-IV
Dr. Barys Shyrokau, Supervisor, Assistant Professor, CoR-IV
Mr. Alberto Bertipaglia, PhD Student, CoR-IV

September 23, 2022

TU Delft Delft University of Technology

Cognitive Robotics

Acknowledgements

I would like to acknowledge and sincerely thank my supervisor Dr. Barys Shyrokau for helping me carry out this research. Without his teachings, advice, and feedback it would not be what it is now. I would also like to thank him for giving the Vehicle Dynamics and Vehicle Control courses during my masters, which I enjoyed very much. My enthusiasm for those courses caused me to make the switch from the Materials specialization to the Dynamics and Control specialization, from where this topic originated. Additionally, I would like to thank Dr. ir. Riender Happee and Mr. Alberto Bertipaglia for being part of the committee to evaluate my work.

Lastly, I would like to thank my family and friends for supporting me throughout my studies and pushing me to do my very best.

Laurien Stubbé
Vreeland, September 6, 2022

Abstract

This thesis describes the concept of a reconfigurable wheelbase for a car as a way to improve agility at higher velocities. Altering the longitudinal position of each wheel with respect to the centre of gravity, leads to a change in lateral wheel forces. This affects the car's yaw rate, therefore making it possible to influence its agility. Available literature has shown that this subject is still quite weakly investigated, which makes it an interesting topic of research. To investigate this influence of actively reconfiguring the wheelbase, simulations were done using IPG Carmaker together with MATLAB/Simulink, during which a simplified vehicle model of a Toyota Camry was used. A proportional derivative controller combined with control allocation was designed to regulate the reconfigurable wheelbase system. It features a reference generator that returns a desired yaw rate and activation logic which ensures that the controller is only activated in a velocity range of $60\,km/h$ to $110\,km/h$ and when a steering input is given. Furthermore, a benchmark study is designed, using a fuzzy logic controller that is based on a simplified version of one presented by Soltani et al. [1]. This controller uses the same reference generator and activation logic for consistency. The rules and membership functions of the fuzzy logic block are adopted from the mentioned paper. The performance of both these controllers and a baseline vehicle without any control, are evaluated for a step steer manoeuvre, an increasing circle manoeuvre and a double lane change, at different velocities and/or steering amplitudes. Based on the results of these tests, it is shown that both controllers are able to influence the lateral dynamics positively during most of these manoeuvres and are therefore able to improve the vehicle's agility in the velocity range in which the controller is active.

Contents

List of Figures

List of Tables

1. Introduction

1.1 Background

Over the last few decades, there have been great improvements in vehicle automation. All kinds of subsystems have been designed to aid the driver, with safety and comfort in mind. One category of these subsystems is vehicle dynamics control. Where some other systems are just there to alert the driver of certain hazardous situations, vehicle dynamics control systems influence the dynamics in such a way to avoid these hazards. An example of such, is a yaw moment control system, which, as implied by the name, affects the vehicle's yaw moment. There are different systems available to achieve this control, both directly and indirectly, but all of them mainly have the goal to achieve lateral vehicle stability. In order to do so, during heavy oversteer or understeer conditions, the system will produce a stabilizing yaw moment to counteract this behaviour. Direct systems accomplish this by controlling the braking or traction of the vehicle, whereas indirect systems control the steering and suspension [3, 4]. However, both suffer from limitations. The direct systems are lacking on roads with variable friction coefficients, and their operation can disturb the driver and even lead to an increase in stopping distances during braking-in-turn manoeuvres [5]. The indirect systems show flaws when performing in the non-linear operational zone of the vehicle [6]. The performance can be increased by using such a system in combination with an active suspension, but this is very expensive in terms of power consumption [7, 8].

Another reason to influence the lateral dynamics of a vehicle, is agility and manoeuvrability, which can be influenced by the same vehicle systems as mentioned or combinations thereof. However, affecting these dynamics can also be done differently, through actively changing the geometry of the chassis, which is something that is not implemented on the road yet.

The subject of cars with a reconfigurable geometry does peak the interest of certain car manufacturers. A few concepts of cars with an extendable wheelbase can be found, such as the Renault MORPHOZ. This concept car is designed to have a larger travel configuration, as well as a smaller city configuration [9]. The travel configuration is shown in Figure 1.1a. Audi has presented a similar idea, named Audi Skysphere, which features a sports car configuration with an enlarged wheelbase, in addition to a smaller city configuration as well [10]. The enlarged version is shown in Figure 1.1b. Furthermore, a Polish company called Triggo has presented a concept of a car that can vary its wheel track to improve agility. This small electric car features

(a) Renault MORPHOZ [9]. (b) Audi Skysphere [10]. (c) Triggo [11].

Figure 1.1: Concepts by different car manufacturers of cars with a reconfigurable wheelbase or track.

a wider configuration to enjoy the stability of a regular car for longer trips, but it can retract its wheels to a shorter configuration to have the agility of a motorcycle to move through traffic or find a parking spot [11]. This car with both its configurations can be seen in Figure 1.1c. Since the different configurations of these cars are designed for specific applications, there is no mention of any active control. All of these ideas are also still very much at a conceptual level, but this does demonstrate the interest the vehicle branch has in the subject of changeable chassis, which confirms the relevance of this research.

This research will concentrate on actively varying the wheelbase of a vehicle during driving, to study the effect this has on its yaw rate, from which the manoeuvrability and agility can be evaluated. Manoeuvrability is desirable in low speed applications, such as urban settings, whereas agility is wanted for higher velocity manoeuvres. The focus in this research will be on operation at high speed, so the agility of the vehicle will be analysed.

1.2 Previous Research

The concept of a reconfigurable wheelbase is explored based on collected research. The term reconfigurable wheelbase, as used in this report, refers to a wheelbase that can actively vary the longitudinal distance of each of the four wheels to the vehicle's centre of gravity (CG), see Figure 1.2. In doing so, the normal load on each tyre changes, which in turn changes the lateral and longitudinal forces of each tyre [1]. Additionally, the effective arm of a tyre is modified when this tyre is relocated. The difference in both the tyre forces and the effective arms affects the yaw moment, which influences the understeer-oversteer characteristics, as well as the stability and handling of the vehicle.

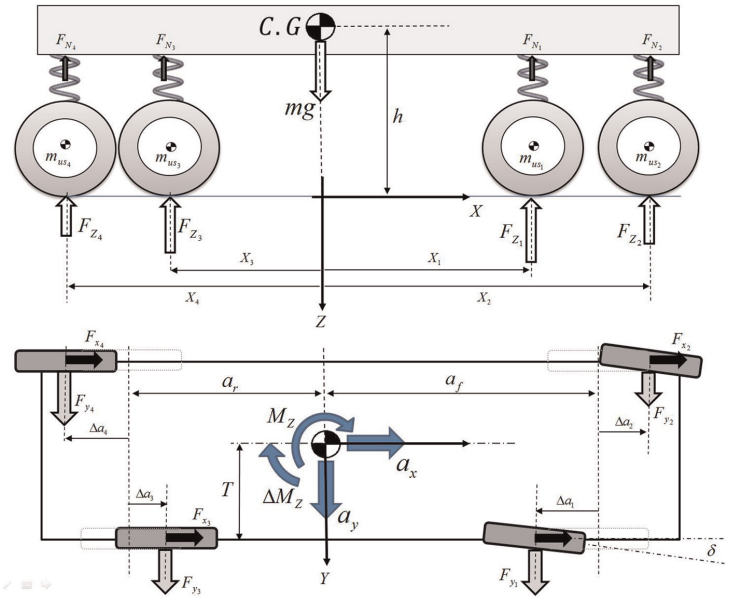

Figure 1.2: Side and top view respectively of the concept of a reconfigurable wheelbase [1].

The effect of using such a reconfigurable wheelbase on the vehicle dynamics is examined in a 2017 paper of Soltani et al. [1]. This begins with the performance of a linear analysis to determine the normal loads on each wheel and using this to investigate the stability and steerability of the vehicle. First, the normal loads F_{z_i} that each wheel exerts on a flat road are determined using

Figure 1.2. These loads are made up of the spring forces F_{N_i} and the unsprung masses m_{us_i}. In order to make the system statically determinate, the deflections of the suspension need to be considered [12]. Assuming that the chassis of the vehicle is rigid on a flat road and combining this mathematically with all other features mentioned, a linearized version of the normal force of the tyres is expressed as follows

$$F_{z_i} \approx F_{n_i} + \sum_{j=1}^{4} K_{ij} \Delta a_j, \qquad i = 1, 2, 3, 4 \tag{1.1}$$

where F_{n_i} represents the nominal normal forces on the wheels for $\Delta a_i = 0$ for $i = 1, 2, 3, 4$. K_{ij} is defined as

$$K_{ij} = \frac{\partial F_{z_i}}{\partial X_j}, \qquad i, j = 1, 2, 3, 4 \tag{1.2}$$

From Equation 1.1 it is clear that the normal loads of all tyres are dependent on the longitudinal position of each wheel. Since the changes of these normal forces affect other lateral and longitudinal forces, a yaw moment can be created by varying the tyre positions. Accordingly, a system that actively varies these positions can be classified as an indirect yaw moment control system [1].

Hereafter, the stability of the vehicle is analysed, using the typical approach for linear systems, where the fact is used that for a small slip angle α, its relation to the lateral force is practically linear [13] and given by the following formula

$$F_{y_i} = C_{\alpha_i} \alpha_i \tag{1.3}$$

Here C_α represents the cornering stiffness of the tyre, which is calculated by taking a second-order function of the normal load. The slip angles of each tyre are defined as

$$\alpha_i = \delta_i - \frac{v + X_i r}{u}, \qquad i = 1, 2, 3, 4 \tag{1.4}$$

where δ_i is the steering angle of each wheel, which is zero for the rear wheels, v and u are the lateral and longitudinal velocity respectively and r is the yaw rate of the vehicle. With these calculations, the stability analysis can be done, which is performed using a 2DOF planar vehicle model. The model's equations of motion are given by

$$m(\dot{v} + ur) = \sum_{i=1}^{4} F_{y_i} \tag{1.5}$$

$$I_z \dot{r} = \sum_{i=1}^{4} F_{y_i} X_i \tag{1.6}$$

By substituting the above Equations into each other, the state-space Equations of the described linear model are obtained. Using these Equations, the transfer function can be derived. This transfer function can then be used to determine the characteristic Equation. In this case, the characteristic Equation will be of the second order, which means that the system can only be stable if the eigenvalues are all positive [13]. The stability condition is thus obtained by performing some mathematical operations and reads as follows

$$\frac{\sum_{i=1}^{2} \sum_{j=3}^{4} C_{\alpha_i} C_{\alpha_j} (X_i - X_j)}{m I_z u^2} \left(\frac{u^2}{g} K_{us} + L_{ef} \right) > 0 \tag{1.7}$$

where K_{us} is the understeer gradient and L_{ef} is the effective wheelbase, which are given by Equation 1.8 and 1.9 respectively. It can be concluded from Equation 1.7 that a vehicle with understeer characteristics is always stable, since a positive understeer gradient will always satisfy the stability condition [13, 14].

$$K_{us} = \frac{-\sum_{i=1}^{4} mgC_{\alpha_i}X_i}{\sum_{i=1}^{2}\sum_{j=3}^{4} C_{\alpha_i}C_{\alpha_j}(X_i - X_j)} \tag{1.8}$$

$$L_{ef} = \frac{\sum_{i=1}^{3}\sum_{j=i+1}^{4} C_{\alpha_i}C_{\alpha_j}(X_i - X_j)^2}{\sum_{i=1}^{2}\sum_{j=3}^{4} C_{\alpha_i}C_{\alpha_j}(X_i - X_j)} \tag{1.9}$$

Both of these Equations can be rewritten to functions of the positions of the wheels, by substituting the function of the cornering stiffness. After some more calculations, K_{us} and L_{ef} can be given in the following linearized forms

$$\Delta K_{us} \approx \sum_{i=1}^{4}(V_{i1} + a_y V_{i2} + a_x V_{i3})\Delta a_i, \qquad i = 1, 2, 3, 4 \tag{1.10}$$

$$\Delta L_{ef} \approx \sum_{i=1}^{4}(W_{i1} + a_y W_{i2} + a_x W_{i3})\Delta a_i, \qquad i = 1, 2, 3, 4 \tag{1.11}$$

Here the terms V_{ij} and W_{ij} can be expressed in Equations containing some technical parameters of the vehicle, such as the height of the CG, the track and the weight. Assuming that $a_x = 0$ and that the lateral acceleration is positive, conclusions can be drawn from how these terms relate to each other. For instance, it shows that at low lateral acceleration, repositioning the front right wheel and rear left wheel to the front of the vehicle will increase the vehicle's oversteer behaviour. At high lateral acceleration, this same action will increase the vehicle's understeer behaviour. Furthermore, repositioning the front left wheel closer to the vehicle's CG or moving the rear right wheel away from the CG will noticeably increase the understeer behaviour, which has a positive effect on the stability of the vehicle. This means, for example, that for high lateral acceleration and $a_x = 0$, a shape in which the front right and rear left wheel move forwards and the front left and rear right wheel move backwards will improve vehicle stability [1].

Now, the steerability of the vehicle will be linearly analysed, for which the yaw rate gain is the most commonly used parameter [14]. This parameter can be expressed by the following equation

$$Y_g = \frac{r}{\delta}\Big|_{ss} = \frac{u}{L_{ef} + K_{us}u^2/g} \tag{1.12}$$

Going through a similar process as with the stability analysis, the following Equation is obtained

$$\Delta Y_g = -\frac{Y_{g0}^2}{u}\sum_{i=1}^{4}(P_{i1} + a_y P_{i2} + a_x P_{i3})\Delta a_i \tag{1.13}$$

with

$$P_{ij} = W_{ij} + \frac{u^2}{g}V_{ij} \tag{1.14}$$

Unless at very high speed, the W_{ij} term can be ignored as it is much smaller than the second term in such situations. Substituting this information in Equation 1.13 and then combining it with Equation 1.10 gives the following

$$\Delta Y_g = -\frac{uY_{g0}^2}{g}\Delta K_{us} \Rightarrow \frac{\Delta Y_g}{\Delta K_{us}} = -\frac{uY_{g0}^2}{g}\Delta K_{us} < 0 \tag{1.15}$$

This Equation should be interpreted as that for each configuration of the wheels that is favourable to the stability, the opposite shape is favourable to the steerability. From this linear stability and steerability analysis, it can thus be concluded that by using a reconfigurable wheelbase, the vehicle can be made more sensitive to the steering input in situations where the vehicle is totally stable but experiences understeer characteristics. Oppositely, the understeer behaviour of the vehicle can be increased when it is showing oversteer behaviour in situations where the yaw velocity is too high [1].

Of course, the actual behaviour of the tyres is non-linear, as opposed to what was assumed before. Therefore, another analysis is performed, which focuses on the non-linear operation zone of the tyres and the effect the reconfigurable wheelbase has here when producing a stabilizing yaw moment [1]. This effect is studied as the alteration in the lateral and longitudinal forces of the tyre, as well as in the yaw moment. Using the combined slip magic formula tyre model [15] with the assumption of no camber angle, gives the longitudinal and lateral forces of the tyres as non-linear functions of the slip angles α_i, the longitudinal slips κ_i and the normal forces on these tyres F_{z_i}. Combining this information with Equation 1.1, gives the total longitudinal and lateral force of the vehicle as functions of the slip angles, the longitudinal slips and all wheel positions. The yaw moment of the vehicle is a function of the longitudinal and lateral tyre forces and the longitudinal and lateral position of the wheels with respect to the CG. Using the conclusions drawn about the longitudinal and lateral forces, it now becomes clear that the yaw moment can thus also be described as a function of the slip angles, longitudinal slips and longitudinal positions of the wheels. This means that the longitudinal and lateral forces, F_x and F_y respectively, as well as the yaw moment M_z can be controlled by changing the longitudinal positions of the wheels. With the help of Taylor expansions and using the assumption of small Δa_i, the following Equations can be written

$$\frac{dF_x}{dX_i} = \sum_{j=1}^{4} \frac{\partial F_{x_j}}{\partial X_i} \Rightarrow \Delta F_x = \sum_{j=1}^{4} \frac{\partial F_{x_j}}{\partial X_i}\Delta a_i, \qquad i = 1,2,3,4 \tag{1.16}$$

$$\frac{dF_y}{dX_i} = \sum_{j=1}^{4} \frac{\partial F_{y_j}}{\partial X_i} \Rightarrow \Delta F_y = \sum_{j=1}^{4} \frac{\partial F_{y_j}}{\partial X_i}\Delta a_i, \qquad i = 1,2,3,4 \tag{1.17}$$

$$\Delta M_z = \frac{\partial M_z}{\partial(\Delta a_i)}\Delta a_i, \qquad i = 1,2,3,4 \tag{1.18}$$

Figure 1.3 shows plots made by Soltani et al., which illustrate the derivation of the changes in the longitudinal forces, the lateral forces and the yaw moment associated with the changes in wheel positions of the reference vehicle model [1]. This model utilizes 195/65R15 tyres and the forces and yaw moments are plotted against the longitudinal acceleration for three different values of lateral acceleration, namely $a_x = 0$, $a_x = 0.3g$ and $a_x = -0.6g$. The slip angles of both front tyres and separately of both rear tyres are assumed to be equal, and the longitudinal slips are assumed to be equal for all wheels. From these plots it can be concluded that for zero longitudinal acceleration, moving the front-left and rear-right wheel to the front of the car will lead to a positive yaw moment, whereas moving the front-right and rear-left wheels will give a yaw moment of which the value is fluctuating between positive and negative, as well as being quite small. Therefore, these wheels are disregarded when finding the optimal configuration for stability or steerability. For each situation, a similar analysis can be conducted, which

leads again to the conclusion that changing the longitudinal position of the wheels can improve stability and steerability of a vehicle [1].

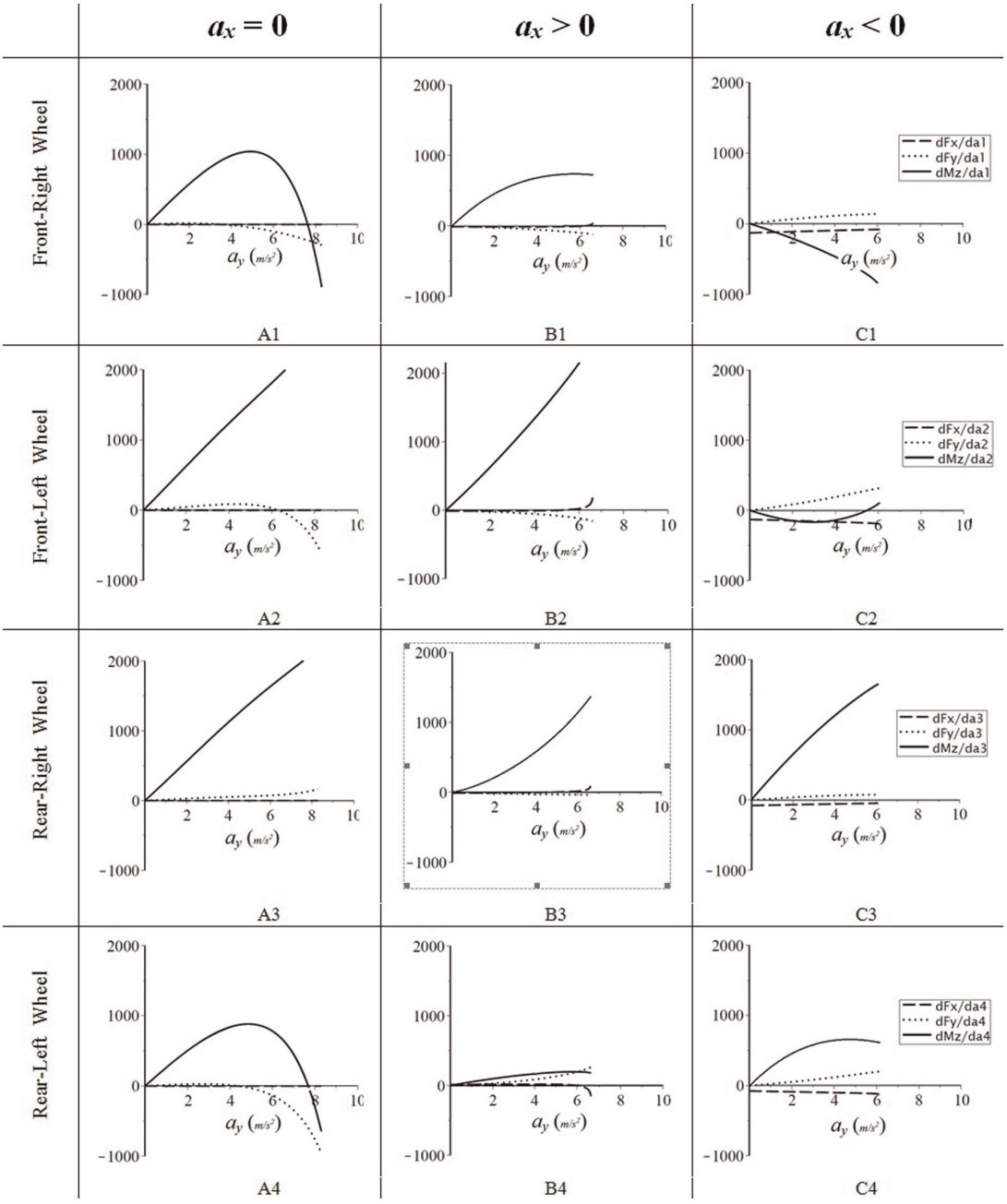

Figure 1.3: Derivation of the changes in the longitudinal forces, the lateral forces and the yaw moment associated with the changes in wheel positions of the reference vehicle model [1].

1.3 Problem Definition

This work studies how an actively reconfigurable wheelbase can improve the lateral vehicle dynamics during high speed manoeuvres. Cars implementing this concept do as of yet not exist, and it is quite weakly investigated in literature. However, it can be theoretically derived that there could be certain benefits in changing these geometrical values, as it comes to agility.

Implementing such a system, with a controller that optimizes its use during driving, could lead to a vehicle that is better drivable at higher velocities.

1.4 Contributions

The main contribution of this research, is a closer reference yaw rate following of a car by active control of the longitudinal wheel positions at higher speeds. This is achieved by implementing a system using PD control to generate the control demand. Then control allocation is applied, to optimally distribute it over the four longitudinal wheel positions, in order to change the yaw rate. The system's performance is evaluated by doing simulations for three manoeuvres that are commonly used to evaluate the vehicle behaviour and comparing its results to a benchmark fuzzy controller that performs the same manoeuvres.

1.5 Thesis Layout

This report is divided into five chapters. Chapter 1 is an introduction to the subject of cars with a reconfigurable wheelbase. It provides the motivation behind this research, as well as a summary of the literature that was found on the subject during the previously conducted literature study. Furthermore, the problem definition is stated and the contributions of this work are listed. In Chapter 2 a theoretical analysis is presented. The first Section explains the theoretical contribution that changing the wheelbase has on vehicle dynamics. These findings are then compared to simulations for both steady state and transient behaviour, using different fixed values for the wheelbase. Chapter 3 is about the design of the reconfigurable wheelbase controller, which starts by determining the feedforward contribution by normalizing and analysing the simulations from the previous Chapter. This is followed by a section about the controller design, featuring an overview of the system, an explanation of the reference model and a description of the PD controller and control allocation part. The next section is about the benchmark study and the fuzzy control system that was designed for comparison, which was based on the paper of Soltani et al. [1]. In Chapter 4 the simulations done using the designed controller and the benchmark controller are presented. First the test manoeuvres are discussed and then the results of both controllers are compared for these situations. Finally, Chapter 5 contains the conclusions of this work, as well as some recommendations for future research.

2. Theoretical Analysis

2.1 Theoretical Effect of Wheelbase on Vehicle Dynamics

The first step in understanding the benefits that an actively reconfigurable wheelbase might bring to vehicle dynamics, is to gain insight in what the effect of the wheelbase is on these dynamics. Intuitively, it is quite obvious that changing the wheelbase affects the turn radius of a vehicle. This is demonstrated by large trucks or buses that need a lot more room to make a turn than regular passenger cars would need. In other words, a longer wheelbase results in a wider turn radius for the same steering angle. This relation between the wheelbase and the steering angle for low speed turns is expressed in the following Equation

$$\delta_o \cong \frac{L}{R + 0.5B} < \delta_i \cong \frac{L}{R - 0.5B} \tag{2.1}$$

Here δ_o is the steering angle of the outer wheel and δ_i is the steering angle of the inner wheel. The wheel track is represented by B, the wheelbase is given by L and R is the radius of curvature for the CG of the vehicle. From this relation it is apparent that by enlarging the wheelbase, the steering angles of both wheels would have to be increased to be able to make a turn of the same radius.

In return, a longer wheelbase will result in more stability in corners, which will lead to a safer feeling for the driver. This can be deduced from the formula for the yaw velocity response gain, as is given in Equation 1.12. The yaw rate gain represents the steady state ratio of the yaw velocity to the steering angle. A higher yaw rate gain means that the vehicle is more sensitive to the steering input, but this also makes the vehicle less stable. It can be derived from the formula that a larger wheelbase L, would lead to a smaller yaw rate gain and vice versa. This is illustrated by Figure 2.1, where the steady state yaw rate response gain is plotted against the longitudinal velocity for a simple vehicle using the bicycle model. This is done for a baseline vehicle, as well as that same vehicle with its wheelbase increased by 10% and decreased by 10%. This 10% is chosen because that would lead to a change of about 20 cm per wheel, which is roughly a maximum of what a mechanism build inside a car can be expected to facilitate. From Figure 2.1 it is visible that at the same speed for a shorter wheelbase, the vehicle has a higher yaw rate gain and therefore more sensitive handling. For a longer wheelbase, the vehicle has a lower yaw rate gain and therefore is less responsive.

The shape of the curve in the Figure is defined by understeer characteristics. This remains the same due to the understeer gradient staying the same. This is the case because this understeer gradient is calculated as follows

$$K_{us} = \frac{mg}{L}\left(\frac{l_r}{C_{\alpha f}} - \frac{l_f}{C_{\alpha r}}\right) \tag{2.2}$$

Here, l_r and l_f represent the length of the rear and front wheelbase measured from the CG respectively, and $C_{\alpha f}$ and $C_{\alpha r}$ are the front and rear cornering stiffness, respectively. By changing both the front and rear lengths of the wheelbase by 10%, this cancels each other out, resulting in K_{us} staying the same. Changing the rear and front wheelbase with a different factor, would show more of a difference in shape.

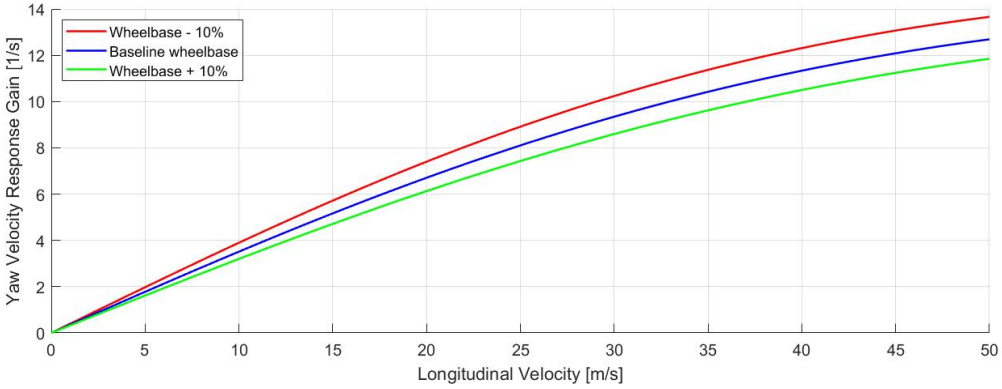

Figure 2.1: Yaw rate response gain plotted against the longitudinal speed for the baseline vehicle, the baseline with wheelbase increased by 10% and the baseline with wheelbase decreased by 10%.

Furthermore, the wheelbase also plays a role in the Ackermann geometry of a vehicle. This is a geometric arrangement that makes both front wheels turn in a slightly different angle, such that their radii originate from a common centre. This is necessary to prevent the wheels from scrubbing. This principle can be described using the following formula, not taking any kingpin offsets into account

$$cot\delta_o - cot\delta_i = \frac{B}{L} \tag{2.3}$$

From this Equation it is obvious that by enlarging the wheelbase, the track would have to be reduced by the same factor to keep the steering angles the same, which would render a very unstable geometry for the vehicle.

These contributions of changing the wheelbase, are roughly summarized by a formula for the steering angle, that is derived from the force balance during steady state motion, which is as follows

$$\delta = \frac{L}{R} + K_{us}\frac{a_y}{g} \tag{2.4}$$

Where K_{us} is obtained as per Equation 2.2. The first component is related to the kinematic contribution, so the Ackermann geometry, and the second component is related to the dynamic characteristic of the vehicle itself, so using the understeer gradient. This Equation too, shows that by enlarging the wheelbase, the steering angle will have to be enlarged as well. However, it can also be derived from this formula, that at low lateral acceleration the effect of changing the wheelbase will be more significant, whereas that significance will fade out with an increasing lateral acceleration.

2.2 Analysis of the Wheelbase Effect Using Advanced Simulation Setup

2.2.1 Steady State Behaviour

To confirm the theoretical effect of changing the wheelbase, simulations were done to compare the outcome. These simulations were run using the software of IPG CarMaker, combined with MATLAB and Simulink. For these simulations, the vehicle model of a Toyota Camry was used

Description	Symbol	Value	Unit
Gravitational acceleration	g	9.81	m/s^2
Vehicle mass	m	1619.96	kg
Wheelbase	L	2.8	m
Front wheelbase	l_f	1.075	m
Rear wheelbase	l_r	1.725	m
Front cornering stiffness	$C_{\alpha F}$	146000	N/rad
Rear cornering stiffness	$C_{\alpha R}$	105000	N/rad
Inertia tensor around z-axis	I_{zz}	2840.385	kgm^2

Table 2.1: Vehicle Parameters of the Toyota Camry model.

and altered via Simulink to feature changes in the wheelbase of ±10%. The vehicle parameters are given in Table 2.1. First, this model was used to assess its steady state behaviour, by having it drive in a circle with a radius of 100 m while slowly increasing speed. Doing this for each different configuration of the wheelbase, yields data of which some interesting plots can be constructed.

In Figure 2.2, the steering angle is plotted against the lateral acceleration for this manoeuvre. The figure compares the situation for different lengths of the wheelbase. It is visible from the image that in the beginning a larger steering angle is required for a vehicle with a larger wheelbase, which is indeed what was expected from Equation 2.4.

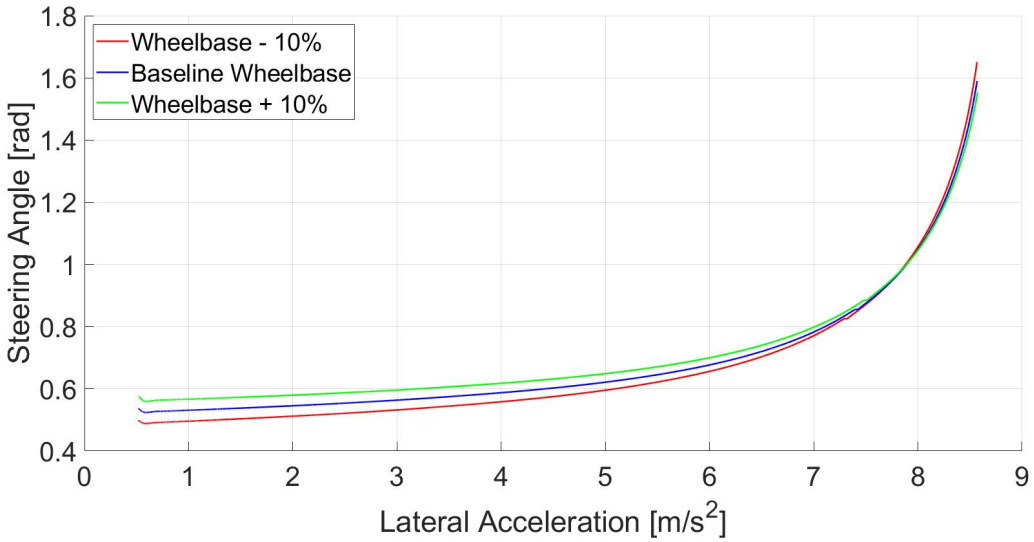

Figure 2.2: Steering angle plotted against lateral acceleration during a steady state circular manoeuvre for different lengths of the wheelbase.

In Figure 2.3, the yaw rate is plotted against the velocity. As seen from the graph, enlarging the wheelbase leads to a less responsive vehicle.

In Figure 2.4, the sideslip angle is plotted against the lateral acceleration. From the image, it is observed that the sideslip angle is slightly higher for a larger wheelbase at lower lateral

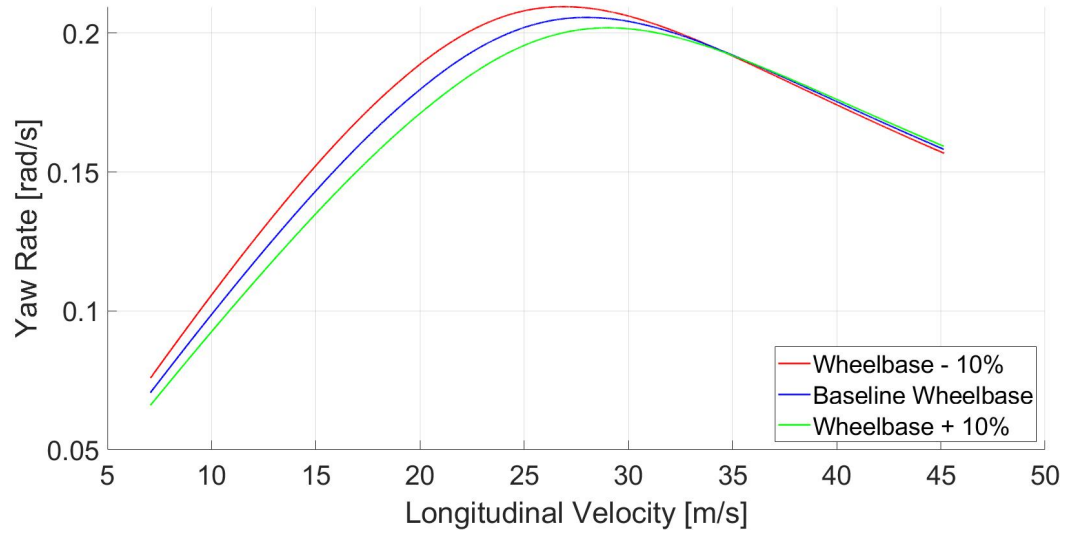

Figure 2.3: Yaw rate plotted against longitudinal velocity during a steady state circular manoeuvre for different lengths of the wheelbase.

accelerations. However, this difference is very small and becomes even smaller for larger lateral accelerations, so the difference can be regarded as insignificant. The values of each configuration stay within stable driving conditions, which is approximated by a sideslip angle that is smaller than 5°. This is an interesting plot to study for the effects that changing these parameters has on the stability, but these results will not be used to determine the feedforward contribution of the controller, whereas both other plots above will be.

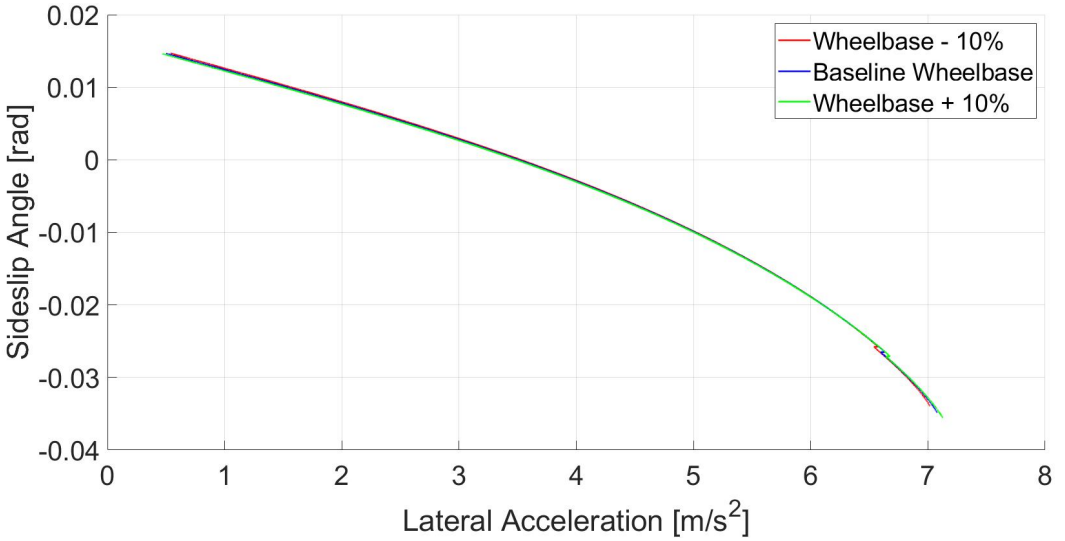

Figure 2.4: Sideslip angle plotted against lateral acceleration during a steady state circular manoeuvre for different lengths of the wheelbase.

In Figure 2.5, the roll angle is plotted against the lateral acceleration. The graph yields no significant results. The steepness of the lines of these plots estimates the roll angle gradient of the vehicle, and the larger a roll gradient is, the less comfortable a vehicle drives. This too is

interesting to study, however it will not be used to determine the feedforward contribution either.

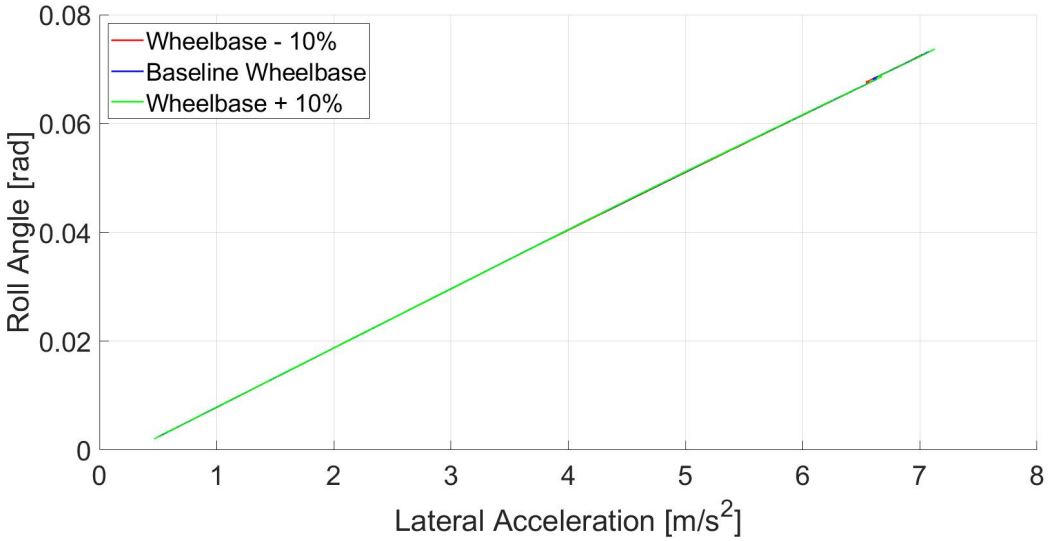

Figure 2.5: Roll angle plotted against lateral acceleration during a steady state circular manoeuvre for different lengths of the wheelbase.

2.2.2 Transient Behaviour

After the steady state analysis, the transient behaviour of the car was analysed. This was done by using the same vehicle model in IPG CarMaker, but now having the vehicle drive a step steer manoeuvre. The vehicle was given an initial velocity of 80 km/h and it starts the manoeuvre by three seconds of steady state driving, after which the step steer is implemented for one second, and it ends with four seconds of holding this steering angle.

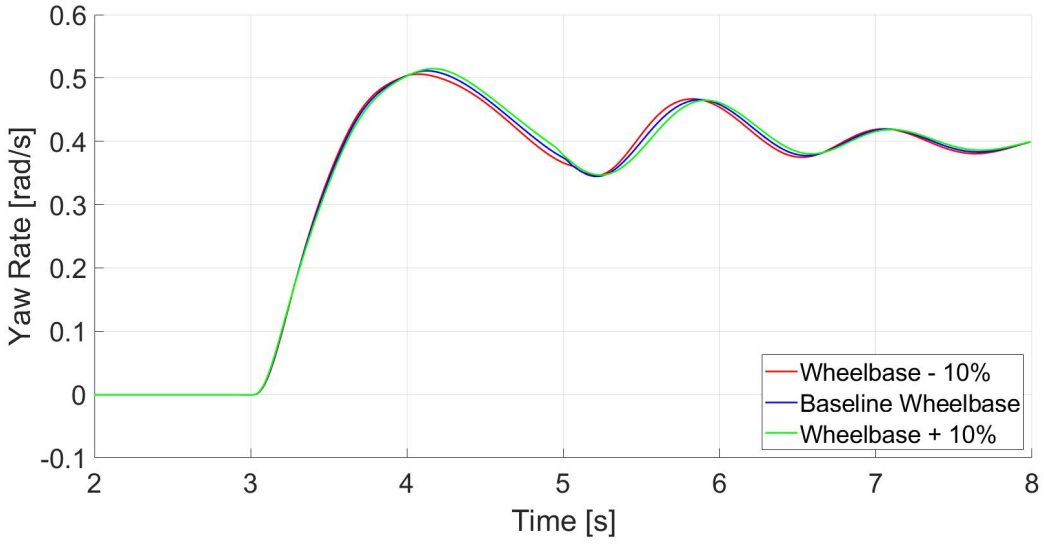

Figure 2.6: Yaw rate plotted against time during a step steer manoeuvre with a steering amplitude of 150° for different lengths of the wheelbase.

First, the steering angle was given an amplitude of 150°, which was used to investigate the extreme cases. The yaw rate plotted against time for this situation is shown in Figure 2.6. From here, it can be observed that changing the wheelbase barely influences the results, apart from the fact that the smaller wheelbase reacts a bit faster.

In Figure 2.7, the lateral acceleration is plotted against time, which too shows very little difference.

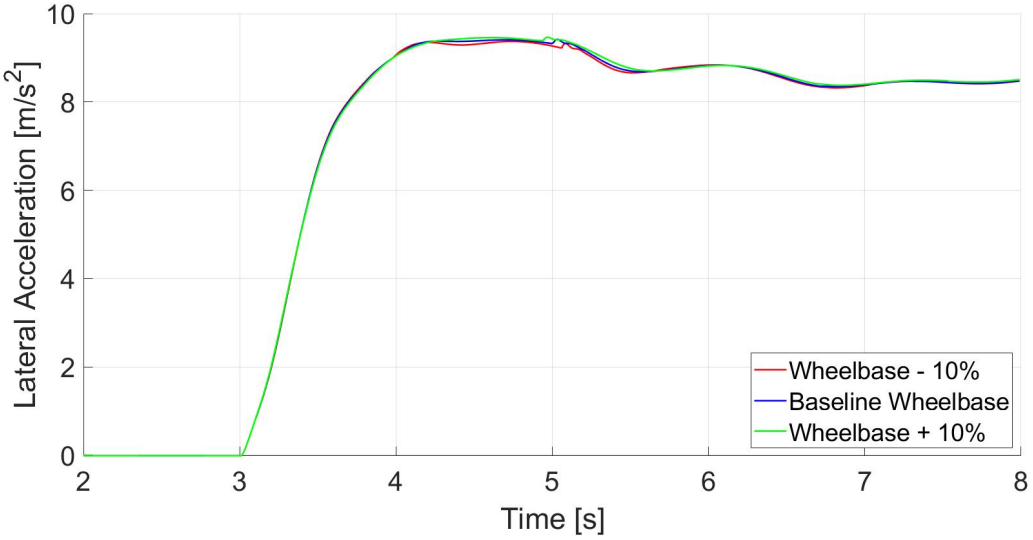

Figure 2.7: Lateral acceleration plotted against time during a step steer manoeuvre with a steering amplitude of 150° for different lengths of the wheelbase.

Hereafter, the same manoeuvre is again simulated, but now for a smaller steering angle amplitude. This amplitude was chosen to be 50°, which was used to illustrate a non-extreme case, unlike before.

In Figure 2.8, the yaw rate is plotted against time. A small difference is visible, where the larger wheelbase shows a smaller yaw rate.

In Figure 2.9, the lateral acceleration is plotted against time. Here again, it is seen that changing the wheelbase has some influence. The configuration with a smaller wheelbase reaches a higher lateral acceleration and therefore more overshoot in that department.

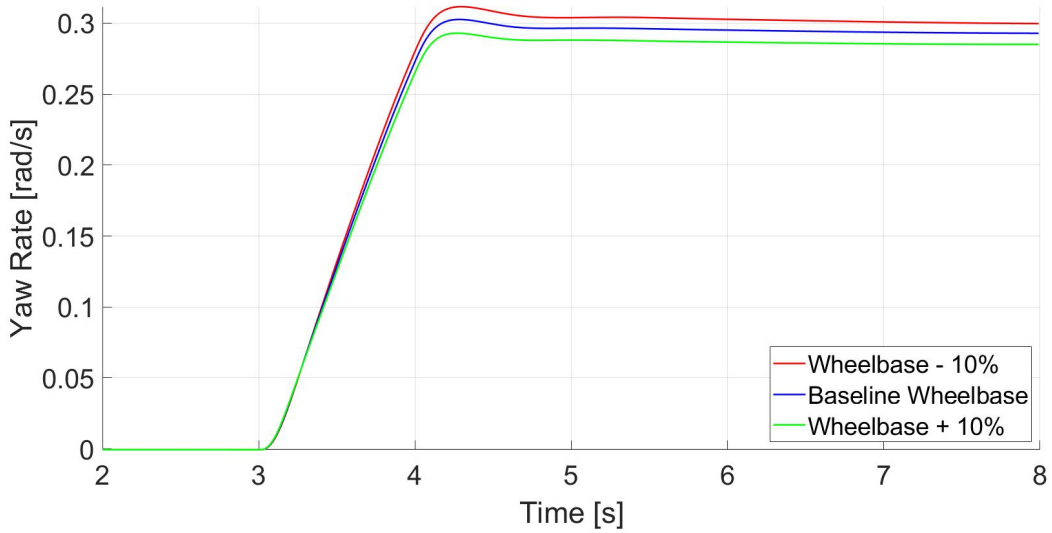

Figure 2.8: Yaw rate plotted against time during a step steer manoeuvre with a steering amplitude of 50° for different lengths of the wheelbase

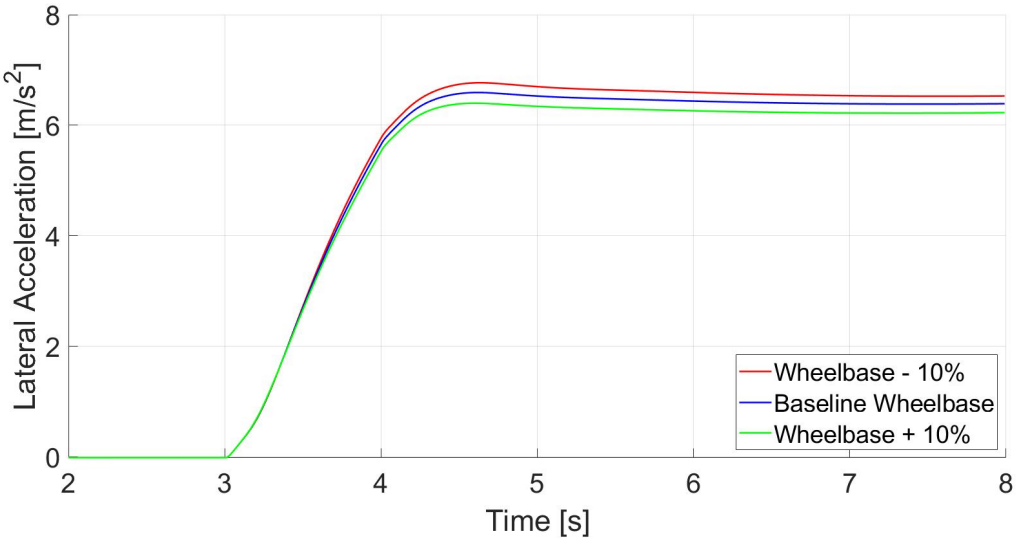

Figure 2.9: Lateral acceleration plotted against time during a step steer manoeuvre with a steering amplitude of 50° for different lengths of the wheelbase

2.3 Summary

In this Chapter, a theoretical analysis was performed to determine the effect that the size of the wheelbase has on vehicle dynamics. First, this is done by explaining the theoretical effect that the size of the wheelbase has on vehicle dynamics. Several formulas containing this value are given, such as for the understeer gradient and the Ackermann geometry. Consecutively, the influence of the wheelbase on these formulas is explained. Hereafter, the theoretical effect is compared to simulations done with IPG Carmaker and Simulink. The vehicle model of a Toyota Camry was used for this. First, the steady state behaviour is assessed, by running a simulation of the car driving in a circle of 100 m. Plots of the understeer gradient, vehicle stability, yaw rate

and roll angle gradient are analysed. Next, the transient response was evaluated by performing a step steer simulation. This was done at a velocity of 80 km/h and a steering amplitude of 150° for an extreme case and 50° for a more normal one. For both situations, plots of the yaw rate and the lateral acceleration against time were analysed.

3. Reconfigurable Wheelbase Controller

3.1 Feedforward Contribution

In order to find the feedforward contribution, the non-extreme step steer simulations are assessed. The graphs that were shown in the previous Chapter are normalized, such that the overshoot and response time can be calculated.

Figure 3.1 shows the normalized yaw rate response plotted against time, from which even the differences for the wheelbase are no longer visible. However, using this graph, the yaw velocity response time and overshoot can be calculated, which will quantify the feedforward contribution of the different configurations.

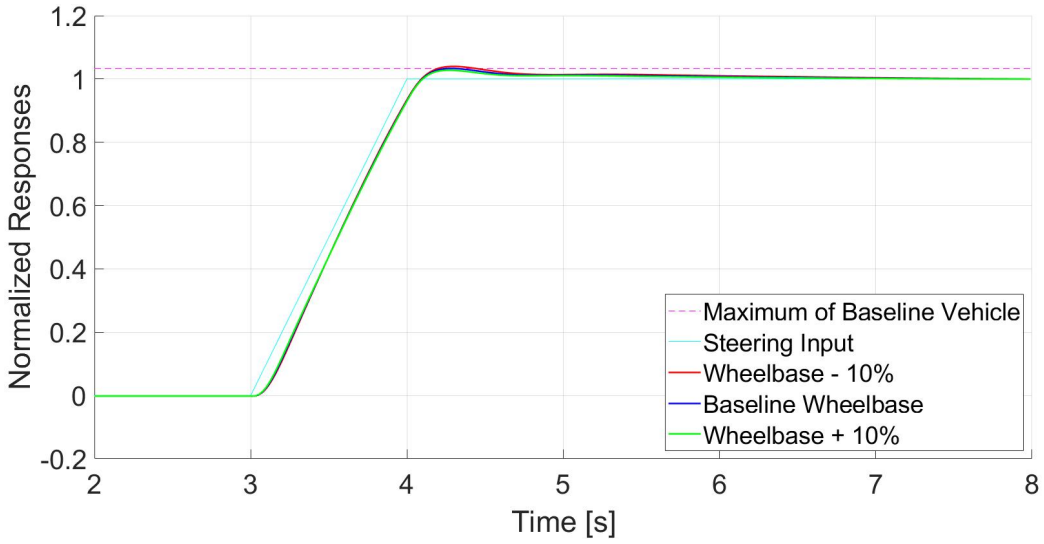

Figure 3.1: Normalized yaw rate plotted against time during a step steer manoeuvre with a steering amplitude of 50° for different lengths of the wheelbase.

In Figure 3.2, the normalized lateral acceleration is plotted against time. Here too, the slight differences in the wheelbase plot are no longer visible, but the plot will be used to calculate the lateral acceleration overshoot and response time.

Calculating the overshoot and response time of both the normalized yaw rate r and the normalized lateral acceleration a_y, yield the results as given in Table 3.1. Here it can be noted that a smaller wheelbase leads to more yaw rate overshoot. A 10% reduction in wheelbase leads to a 21.5% increase in overshoot compared to the baseline, whereas increasing the wheelbase by 10% leads to a 15.3% decrease in yaw rate overshoot. The response time is almost the same for every configuration, except that it is only slightly shorter for the smaller wheelbase. The lateral acceleration overshoot is also larger for a smaller wheelbase. A 10% reduction in wheelbase leads to a 15.7% increase in overshoot compared to the baseline, whereas increasing the wheelbase by 10% leads to a 13.2% decrease in lateral acceleration overshoot. The response time is nearly the same for every configuration, it is only slightly shorter for a larger wheelbase. The accuracy of

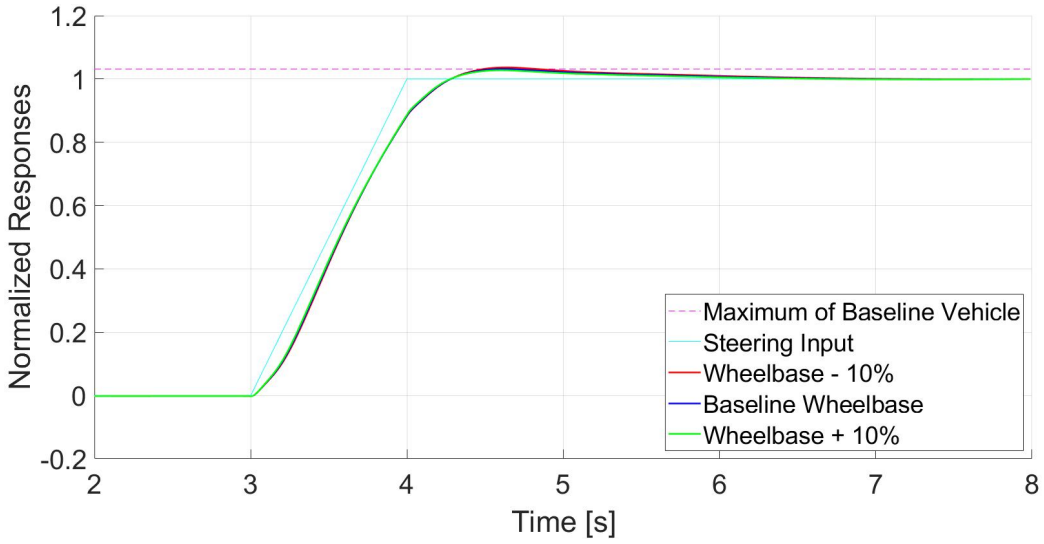

Figure 3.2: Normalized lateral acceleration plotted against time during a step steer manoeuvre with a steering amplitude of 50° for different lengths of the wheelbase.

	Wheelbase -10%	Baseline Wheelbase	Wheelbase +10%
Overshoot r [%]	3.9675	3.3266	2.7662
Response Time r [s]	0.46	0.47	0.47
Overshoot a_y [%]	3.6608	3.1642	2.7468
Response Time a_y [s]	0.53	0.53	0.52

Table 3.1: Numerical values of the normalized responses for different lengths of the wheelbase.

these time values is however due to the time step the IPG simulation takes, which is not precise enough to draw any clear conclusions from.

3.2 Controller Design

3.2.1 Overview

For the design of the controller, the same software and vehicle model of a Toyota Camry was used as in Section 2.2. A block diagram, which gives a simplified overview of the designed low level automation system, is shown in Figure 3.3. The vehicle model provides the system with its inputs, which are the yaw rate, steering wheel angle, longitudinal vehicle velocity and lateral wheel forces. The reference model uses the longitudinal vehicle velocity and steering wheel angle to generate a reference yaw rate. From this reference, the actual yaw rate is subtracted, which gives the error. This error is the input of the proportional derivative (PD) controller, the output of which is multiplied by the longitudinal vehicle velocity and the steering wheel angle and given to the control allocation block as control input. Furthermore, this block uses the lateral wheel forces as input data to then solve the control allocation problem, yielding the allocated demand and the command of longitudinal wheel positions, which is sent to the vehicle model and back into the control allocation block as input for the next iteration.

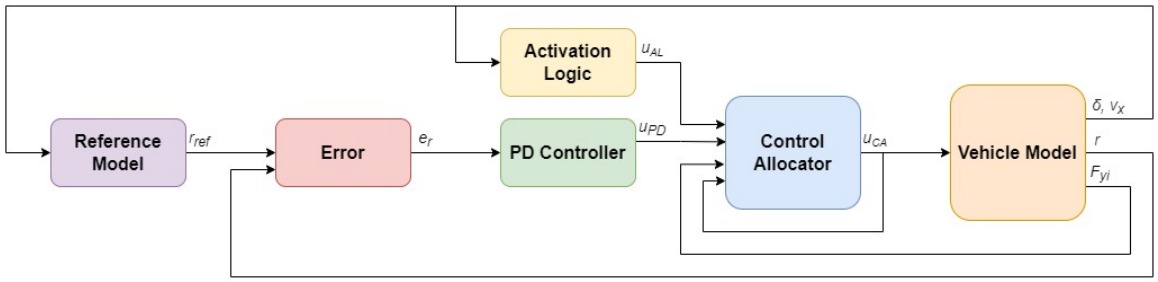

Figure 3.3: Simplified block diagram of the designed control system.

3.2.2 Reference Model

As seen from Figure 3.3, the reference generator receives the longitudinal velocity as well as the steering angle as inputs. Before its input, the longitudinal velocity is multiplied by a saturation block, that limits the range of the reference generator from $20km/h$ to $200km/h$. This lower limit was chosen because the generator reacts more intensely at lower speeds, yielding an unsteady reference in that area. The upper limit was chosen, because the behaviour at higher speeds is outside the scope of this research. The steering wheel angle is divided by 18.4382 to account for the steering ratio. These sets of data are then used to calculate the steady state yaw rate and the maximum reference yaw rate, using the following equations

$$r_{ss} = \frac{u}{L + \frac{K_{us}u^2}{g}} \delta \tag{3.1}$$

$$r_{max} = 0.85 \frac{\mu g}{u} \tag{3.2}$$

Here, K_{us} is calculated according to Equation 2.2 and μ is the friction coefficient, which was assigned a value of 1.0. All other variables were assigned values in accordance with the Toyota Camry model from Table 2.1. The reference generator then sets a value for saturated reference yaw rate according to the following Equation

$$r_{sat} = \begin{cases} r_{ss}, & |r_{ss}| \leq |r_{max}| \\ \pm r_{max}, & |r_{ss}| > |r_{max}| \end{cases} \tag{3.3}$$

Lastly, $r_{d_{sat}}$ is multiplied by a second order transfer function to account for the dynamic vehicle response, which results in the reference yaw rate, as can be seen in the following Equation

$$r_{ref} = \frac{\omega_0^2 \tau s + \omega_0^2}{s^2 + 2\zeta\omega_0 s + \omega_0^2} r_{sat} \tag{3.4}$$

Here, ω_0 is the yaw frequency, τ is the yaw delay and ζ is the yaw damping. These values were set to a fixed value of 14.5, 0.002 and 0.7 respectively. To get a more realistic simulation of the dynamic vehicle response, these values should change in correspondence with speed, but for this research it was chosen to keep them fixed to values that are reasonable within the velocity range of the test manoeuvres, as to focus on other parts of the controller. Finally, the reference yaw rate is obtained, from which the actual yaw rate is then subtracted to find the yaw rate error of the system.

3.2.3 PD Controller

The yaw rate error is given as input to the PD block, the output of which is calculated according to the following Equation

$$u_{PD} = K_p e_r + K_d \frac{de_r}{dt} \tag{3.5}$$

Here, u_{PD} represents the output and e_r is the yaw rate error signal. The values K_p and K_d are the proportional and derivative gain, which were set to 20 and 3 respectively. These values were found by tuning the controller to the non-extreme step steer manoeuvre of Subsection 2.2.2, so at a velocity of $80\,km/h$ and an amplitude of 50°.

3.2.4 Activation Logic

The output of the PD controller is then multiplied by the longitudinal vehicle velocity and the steering wheel angle. However, both these values were first multiplied by a lookup table to implement the range in which the controller should be active, which is the activation logic.
For the longitudinal speed, it was decided to have the controller start working at $60\,km/h$, reaching its full effect at $100\,km/h$, after which its effect reduces to zero for $110\,km/h$. These values were chosen like this by using a simulation in which the vehicle drives with a constant steering amplitude of 30° at increasing speeds. The results below $20\,km/h$ were disregarded here, because of the saturation implemented for the reference generator. From the resulting yaw rate, it was noticeable that it followed the reference quite closely for lower speeds, but starts diverging at a velocity around $75\,km/h$. Furthermore, after reaching a velocity of about $100\,km/h$ the yaw rate starts decreasing, whereas the reference yaw rate is still increasing. This is due to the constraint, which is imposed in the control allocation block, of a maximum wheel movement of $\pm 20\,cm$, as was used by Soltani et al. [1].

The steering wheel angle was multiplied by a lookup table that alters the value of the absolute steering wheel angle in the range of 0° to 5° to the values of $tanh(0)$ to $tanh(5)$. This is done to make sure that the controller does not change anything when the driver gives no steering input, hereafter it slowly builds up its effect for those first few degrees.

3.2.5 Control Allocation

The output of the controller is now multiplied by this activation logic from the vehicle model and put into the control allocation block, together with the lateral wheel forces, which were obtained directly from the vehicle model, and the previous output of this block. The control allocation block then solves a weighted least squares problem to obtain the best combination of actuator commands that leads to the desired yaw rate. This weighted least squares problem is given by the following equation

$$u_{wls} = arg \min_{u_{lim}^{low} \leq u_{prev} \leq u_{lim}^{up}} \left(\|W_u u_{prev}\|_2^2 + \xi \|W_v (B u_{prev} - v^*)\|_2^2 \right) \tag{3.6}$$

Here, u_{wls} is the output of the cost function and u_{prev} is the output value of the previous integration step of the control allocation block. The limit constraints u_{lim}^{low} and u_{lim}^{up} are given as follows

$$u_{lim}^{low} = max(-disp_{max}, u_{prev} - rate_{fs} * ts) \tag{3.7}$$

$$u_{lim}^{up} = min(disp_{max}, u_{prev} + rate_{fs} * ts) \tag{3.8}$$

The value $disp_{max}$ is the maximum displacement of the wheels, which is set to 0.2 to prevent the wheels from moving more than $\pm 20\,cm$, as mentioned before. The rate of change is expressed as $rate_{fs}$ and is set to 0.1. The time step ts is set to 0.001. In Equation 3.6, the weights W_u for the variable configuration, W_v for the allocation error and ξ for the second term of the cost function are set to 1, 1 and 0.001 respectively. Furthermore, v is the control input, coming from the PD controller output multiplied by the modified longitudinal velocity and steering wheel angle, and the control effectiveness matrix B is given as

$$B = \begin{bmatrix} \frac{-F_{y_{FL}}}{I_{zz}} & \frac{-F_{y_{FR}}}{I_{zz}} \\ \frac{F_{y_{RL}}}{I_{zz}} & \frac{F_{y_{RR}}}{I_{zz}} \end{bmatrix} \tag{3.9}$$

In this matrix, $F_{y_{FL}}$, $F_{y_{FR}}$, $F_{y_{RL}}$ and $F_{y_{RR}}$ represent the lateral forces on the front left, front right, rear left and rear right wheel respectively, as received from the vehicle model. They are divided by I_{zz}, which is the inertia tensor around the yaw axis, given by $2840.385 kgm^2$ in accordance with the vehicle model.

Since this weighted least squares could return an unconstrained value when using the step size, the output is optimized to yield the following output u_{CA} of the control allocation block

$$u_{CA} = max\left(u_{lim}^{low}, min(u_{lim}^{up}, u_{wls})\right) \tag{3.10}$$

This output contains four signals, one for each wheel, which are multiplied by a first order transfer function as follows

$$u_c = \frac{1}{\tau s + 1}\, u_{CA} \tag{3.11}$$

This was done to reduce the chutter in the commanded position, and the time constant τ was tuned to do so. Now each signal is used as an input that assigns a new wheel position to the corresponding wheel in the vehicle model. Lastly, the output u_{CA} is multiplied by the control effectiveness matrix B to obtain the allocated demand v_{out}.

3.3 Benchmark Study

3.3.1 Overview

To test the performance of the PD controller from Section 3.2, a benchmark controller was made. This controller is based on a simplified version of the controller described by Soltani et al. [1], with a few alterations to make it comparable to the other controller. A block diagram is shown in Figure 3.4 to give a simplified overview of the benchmark controller. The vehicle model provides the system with its inputs, which are the yaw rate, steering wheel angle and longitudinal vehicle velocity. The reference model is exactly the same as the one described in Subsection 3.2.2, so it also uses the longitudinal vehicle velocity and steering wheel angle to generate a reference yaw rate. From this reference, again the actual yaw rate is subtracted, which gives the error. This error is the input of the fuzzy controller, the output of which is the velocity of the longitudinal displacement, or the derivative of the longitudinal wheel positions. This is integrated to obtain these positions, which are then sent to the vehicle model as a command.

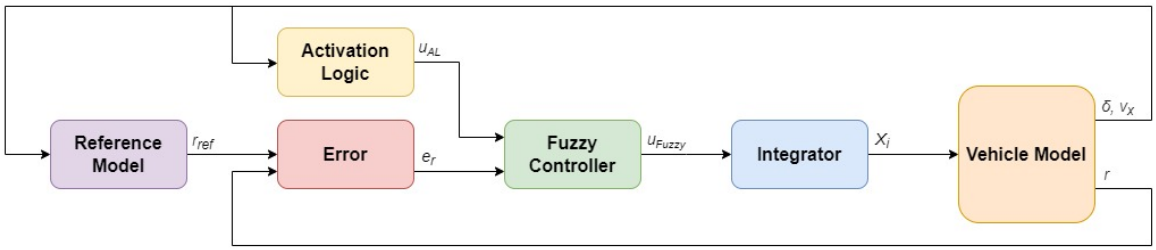

Figure 3.4: Simplified block diagram of the benchmark control system.

3.3.2 Fuzzy Controller

After the yaw rate error is calculated as in Subsection 3.2.2, it is multiplied by a gain of $180/\pi$ to change it from radians to degrees. Hereafter, the signal is guided through a rate transition block that changes the sample time from continuous to $0.01\,s$, to be a suitable input signal for the fuzzy controller. This signal is now multiplied by the longitudinal vehicle velocity and the steering wheel angle, both of which were first multiplied by exactly the same activation logic as the PD controller and then also guided through a rate transition block to set the sampling time to $0.01\,s$. After the multiplication of the yaw rate error with this activation logic, the resulting signal is given as the input to the fuzzy controller.

The original controller of Soltani et al. features five inputs, longitudinal acceleration, lateral acceleration, sideslip angle, steering wheel angle and the yaw rate error, each with their own membership functions [1]. For this benchmark study, the fuzzy controller was simplified to only have the one input signal that is described above, for which the membership function was based on that of the yaw rate error input from Soltani et al. The membership function plots have the same shape, but instead of a range of $-10°$ to $10°$, it has a range of $-3°$ to $3°$, as shown in Figure 3.5. This range was selected, because the used input signal is noticeably reduced by the multiplication with the longitudinal speed and steering angle, so the larger range would lead to the controller barely having any effect on the wheel positions. In this plot, the abbreviations BN, SN, Z, SP and BP stand for big negative, small negative, zero, small positive and big positive respectively.

The system has four output signals that represent the derivative of the longitudinal wheel positions, the membership functions of which are loosely based on those of Soltani et al. The plots are made symmetrical around the axis and are given a range of -0.1 to $0.1\,m/s$ instead of -10 to $6\,m/s$. This range is chosen to correspond with the rate of change of the PD controller, to make a fair comparison. Furthermore, the outer two plots are made into a Gaussian shape instead of a triangular one, to make the outputs of the fuzzy controller a little more smooth around its limits.

Soltani's controller featured 54 rules, whereas this simplified version only has 5, due to the lack of other inputs. The 5 rules that were implemented were chosen by assuming the situation in which the longitudinal acceleration is zero, the lateral acceleration is small positive and the sideslip angle is small. Then the rules are given as:

1. $(e_r == BN) => (dDa_1 = SN)(dDa_2 = BN)(dDa_3 = BN)(dDa_4 = SN)$
2. $(e_r == SN) => (dDa_1 = Z)(dDa_2 = SN)(dDa_3 = SN)(dDa_4 = Z)$
3. $(e_r == Z) => (dDa_1 = Z)(dDa_2 = Z)(dDa_3 = Z)(dDa_4 = Z)$

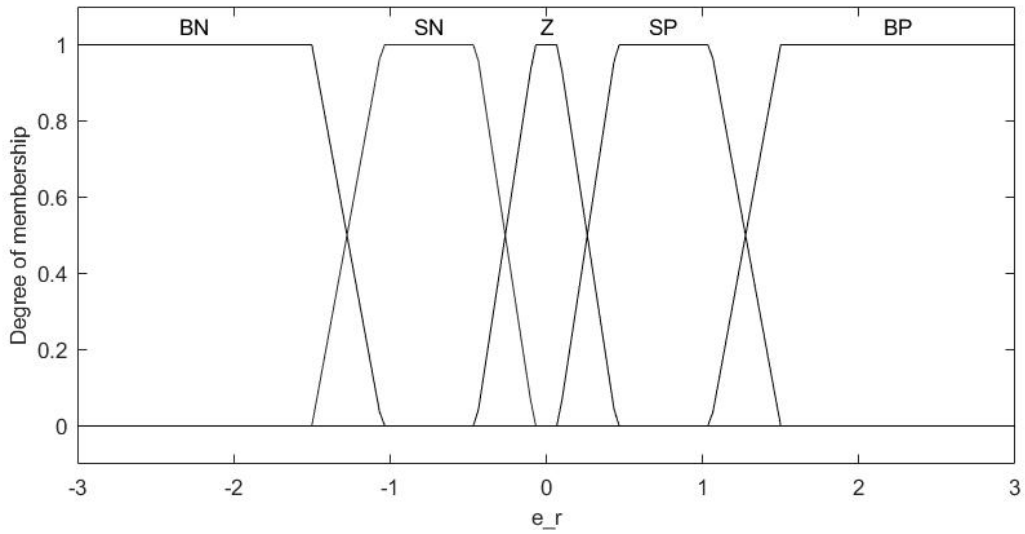

Figure 3.5: Membership function of the input signal, where the signal is given in degrees.

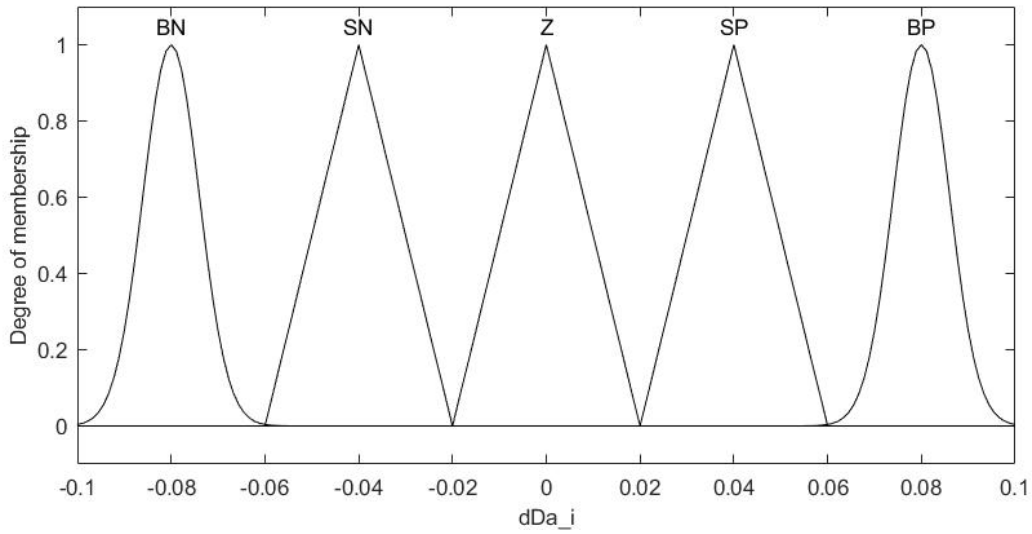

Figure 3.6: Membership function of the output signals, where the signal is given in m/s.

4. $(e_r == SP) => (dDa_1 = Z)(dDa_2 = SP)(dDa_3 = SP)(dDa_4 = Z)$
5. $(e_r == BP) => (dDa_1 = SP)(dDa_2 = BP)(dDa_3 = BP)(dDa_4 = SP)$

Here the output numbers 1, 2, 3 and 4 are assigned to the front right, front left, rear right and rear left wheels respectively.

3.3.3 Integrator

The output of the fuzzy controller is then multiplied by a gain of $[1 \ -1 \ \ 1 \ -1]$, to make the wheels of the fuzzy controller move in the same direction as the corresponding wheels do from the PD controller, again to make the controllers more comparable. Hereafter, the signal enters the integrator, which is given an upper and lower saturation limit of $0.2\,m$ and $-0.2\,m$

respectively, as corresponds to the displacement limits implemented in the PD controller. The signal is put through another rate transition block to obtain a sample time of $0.001s$, before the signal is split four ways. It is then multiplied by the same transfer function of Equation 3.11, again for consistence while comparing. Lastly, each signal is used to assign the commanded longitudinal wheel position to the corresponding wheel.

3.4 Summary

In this Chapter, the design of the reconfigurable wheelbase controllers is explained. First, the feedforward contribution for the controller was determined by taking the normalized values of the yaw rate and the lateral acceleration, to determine their overshoot and response time. Hereafter, the controller design of the PD controller combined with control allocation is made clear by giving an overview of the system and then explaining each component. This starts with the reference model, by providing the used formulas and design choices. Then the PD control block and how it was tuned are explained. The next part mentions the activation logic that was used to make the controller work only in the velocity range of $60\,km/h$ to $110\,km/h$ and when a steering input is given. As the last part of this controller, the control allocation block and the weighted least squares problem that it solves are explained. After this, the benchmark controller is dissected, starting with an overview as well. Since the reference model and the activation logic are kept the same as for the previous system, these are not explained a second time. The fuzzy control block, that was based on a simplified version presented by Soltani et al. [1], is of course explained. Images of the membership functions that were used are presented, as well as the set of rules that were implemented. After this, the integrator block is explained as the last step of this system.

4. Simulation and Results

4.1 Manoeuvres

4.1.1 Step Steer

The controllers were tested for three common test manoeuvres, the first of which is a step steer manoeuvre. This test was already mentioned in Subsection 2.2.2, as it is used to evaluate the transient behaviour of a vehicle when making a turn. For the simulation on which the controller was tuned, the vehicle was given an initial speed of $80\,km/h$, as mentioned before. After three seconds of steady state driving, the step steer is implemented for one second with a steering amplitude of 50°, which is then maintained for the next four seconds, after which the manoeuvre is finished. For completeness, the performance was tested for more values in the range of the controllers. The $80\,km/h$ scenario was also tested for an amplitude of 30° and the controllers were tested for both amplitudes at velocities of $100\,km/h$ and $105\,km/h$ as well. To analyse the borderline cases, this manoeuvre was performed with a 50° amplitude and a speed of $60\,km/h$ and $110\,km/h$ too.

4.1.2 Increasing Circle

The next test manoeuvre is the increasing circle. Here the vehicle is given no initial velocity, but directly starts slowly increasing its speed, while holding a constant steering amplitude. This results in the vehicle driving in an increasing circle. The manoeuvre is performed for a steering amplitude of 30° and 50°.

4.1.3 Double Lane Change

The last manoeuvre for which the controllers were tested is the double lane change. This is a slightly more complicated manoeuvre than the first two. The vehicle is given an initial speed of $80\,km/h$, after which a move to the left lane is commanded, directly followed by a move back to the right lane. The manoeuvre and its measurements are shown in Figure 4.1. This manoeuvre was tested at different velocities of $100\,km/h$ and $105\,km/h$ as well.

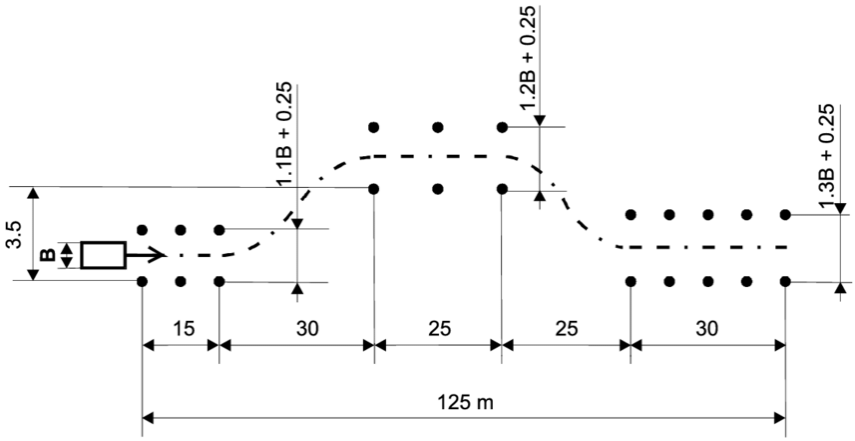

Figure 4.1: Double lane change manoeuvre, as determined by ISO [2].

4.2 Controller Comparison

4.2.1 Step Steer

Velocity of $80\,km/h$ and Steering Amplitude of $50°$

For every scenario mentioned in Subsection 4.1.1, the step steer manoeuvre was run with both controllers and the baseline vehicle without any control. To compare the performance, the yaw rate was plotted against time in the same Figure for each of these situations, as well as the reference yaw rate. At a velocity of $80\,km/h$ and a steering amplitude of $50°$, this graph is shown in Figure 4.2.

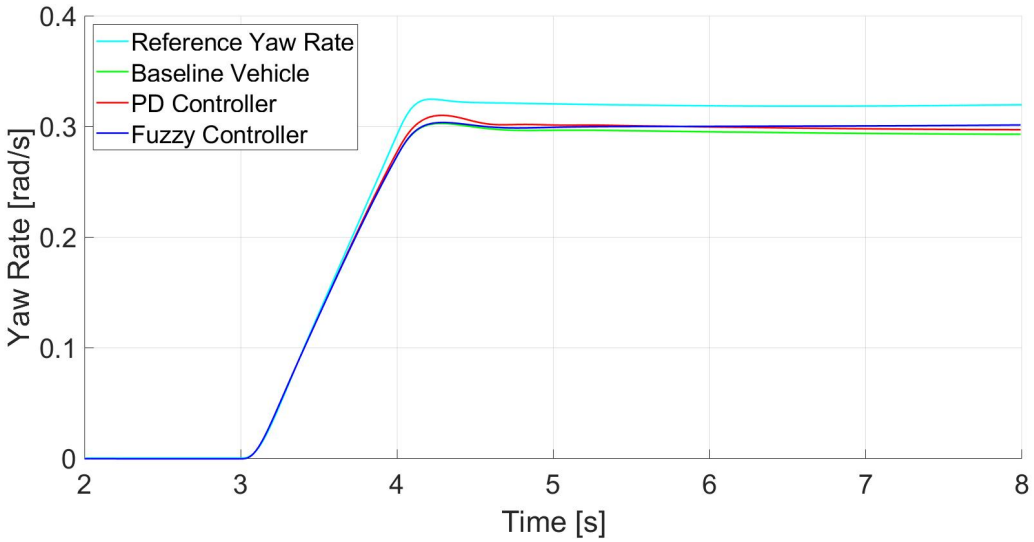

Figure 4.2: Yaw rate against time for different controllers during the step steer manoeuvre at a velocity of $80\,km/h$ and a steering amplitude of $50°$.

As can be seen from this Figure, the lines of the baseline, PD controller and fuzzy controller are quite close together. To get a better view of what is going on at the most important part, around four seconds, Figure 4.3 shows a close-up of that area.

From this Figure it becomes clear that the PD controller has the most overshoot and follows the reference yaw rate the closest. From Figure 4.2 it is observable that after about six seconds, the fuzzy controller intersects the line of the PD controller and follows the reference slightly closer for the remainder of the manoeuvre. This result however, can be regarded as inferior, since it is the behaviour during the turn that is to be evaluated with a step steer manoeuvre. The PD controller and the fuzzy controller equal the baseline in the beginning, but after their wheels start moving they do outperform the baseline for the rest of the manoeuvre. Plots of the yaw rate error and the control demand of the PD controller are given in the Appendix by Figure A.1 and A.2 respectively.

Another interesting plot to study, is the commanded wheel displacements for both controllers. This is shown in Figure 4.4. Here it is visible that the controllers start working at different times in the manoeuvre. The fuzzy controller starts later due to the range of the imposed membership functions. From the left figure it can be seen that the wheels regulated by the PD controller form into a trapezoid, with both right wheels moving closer to the CG, while the left wheels also

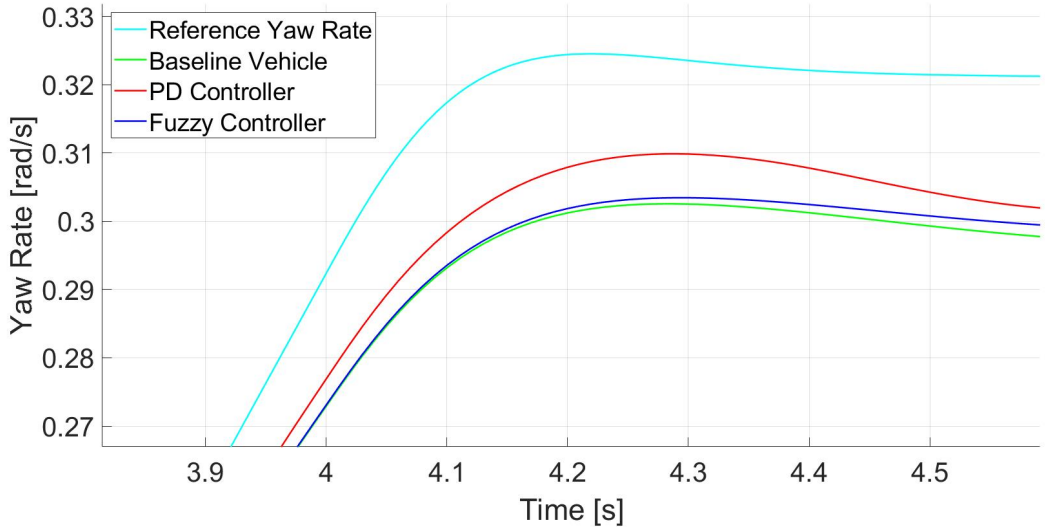

Figure 4.3: Zoomed in version of the yaw rate against time for different controllers during the step steer manoeuvre at a velocity of 80 km/h and a steering amplitude of 50°.

move closer, but not quite as much. The fuzzy controller, on the other hand, steers the wheels more into a parallelogram, since the front left and rear right move closer to the CG, while the other two stay in place. It should also be noted, that the displacement for the fuzzy controller moves towards the limits, whereas the PD commands stay in a smaller range and look like they are converging.

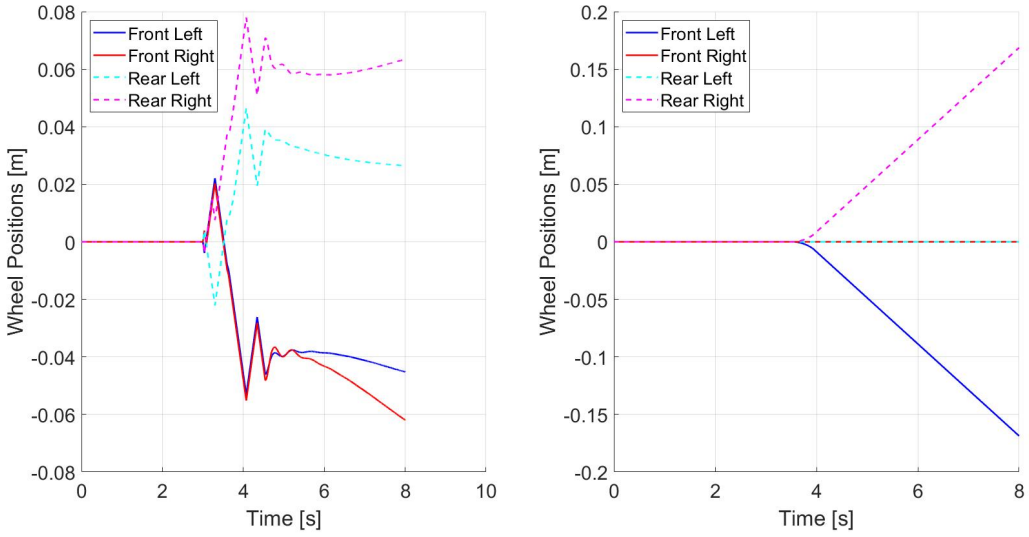

Figure 4.4: Commanded wheel displacement in longitudinal direction against time for the PD controller (left) and the fuzzy controller (right), during the step steer manoeuvre at a velocity of 80 km/h and a steering amplitude of 50°.

Velocity of $80\,km/h$ and Steering Amplitude of $30°$

The same manoeuvre was tested again for a velocity of $80\,km/h$, but this time with a steering amplitude of $30°$. The yaw rate against time for this situation was plotted in Figure 4.5.

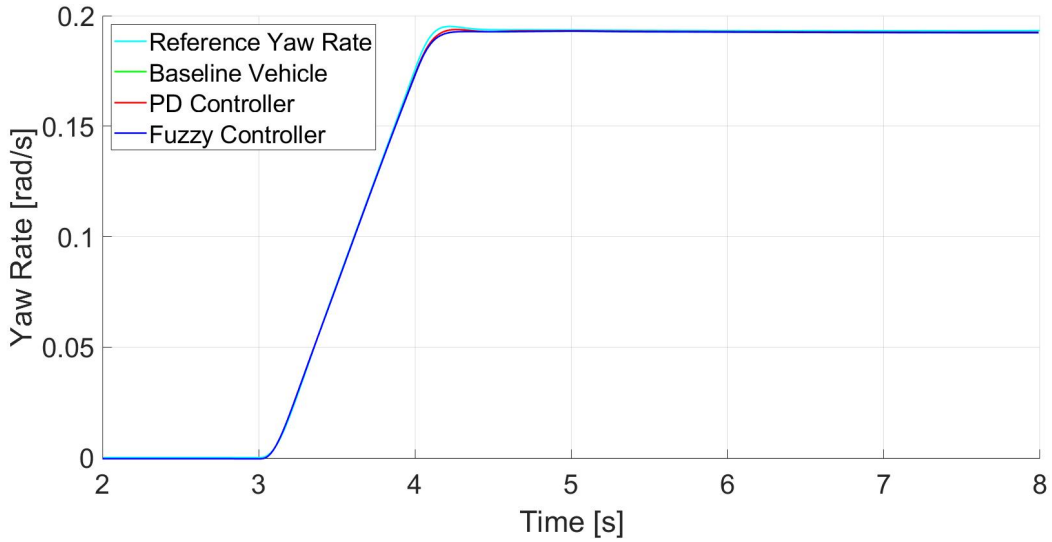

Figure 4.5: Yaw rate against time for different controllers during the step steer manoeuvre at a velocity of $80\,km/h$ and a steering amplitude of $30°$.

The lines are very close together, so a zoomed in version is given in Figure 4.6. From here, it is visible that the PD controller follows the reference closer than the fuzzy controller, but by a very small margin. The baseline vehicle appears to be invisible, but by zooming in even more, it shows to be hidden by the fuzzy line, which is nearly exactly the same, but just outperforms it by an even smaller margin. This small margin comes from the commanded wheel displacement of the fuzzy controller, which is very small too in this situation. Plots of the commanded wheel displacement, the yaw rate error and the control demand of the PD controller are given in Figures A.3, A.4, and A.5 respectively.

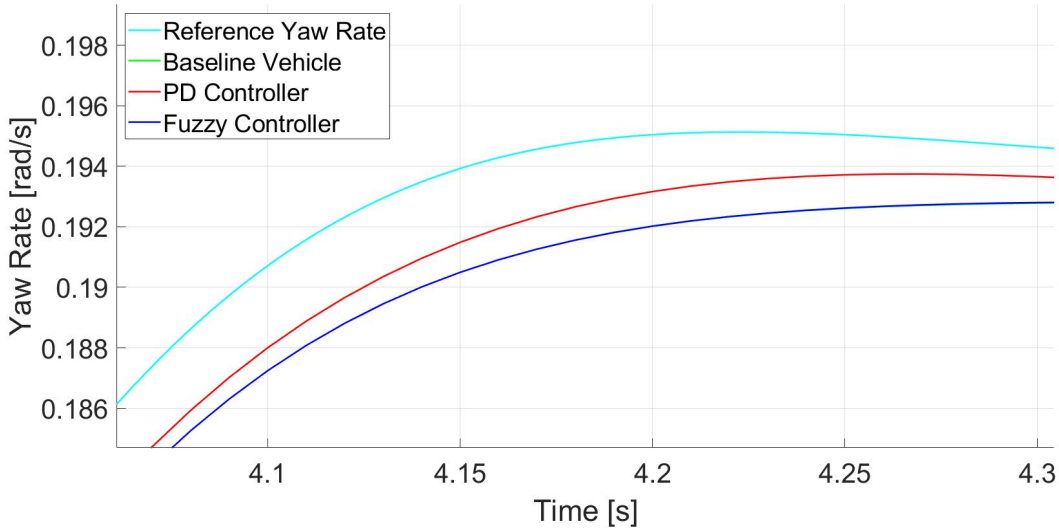

Figure 4.6: Zoomed in version of the yaw rate against time for different controllers during the step steer manoeuvre at a velocity of 80 km/h and a steering amplitude of 30°.

Velocity of 100 km/h **and Steering Amplitude of** 50°

The yaw rate against time for the step steer manoeuvre at a velocity of 100 km/h and a steering amplitude of 50° is presented in Figure 4.7.

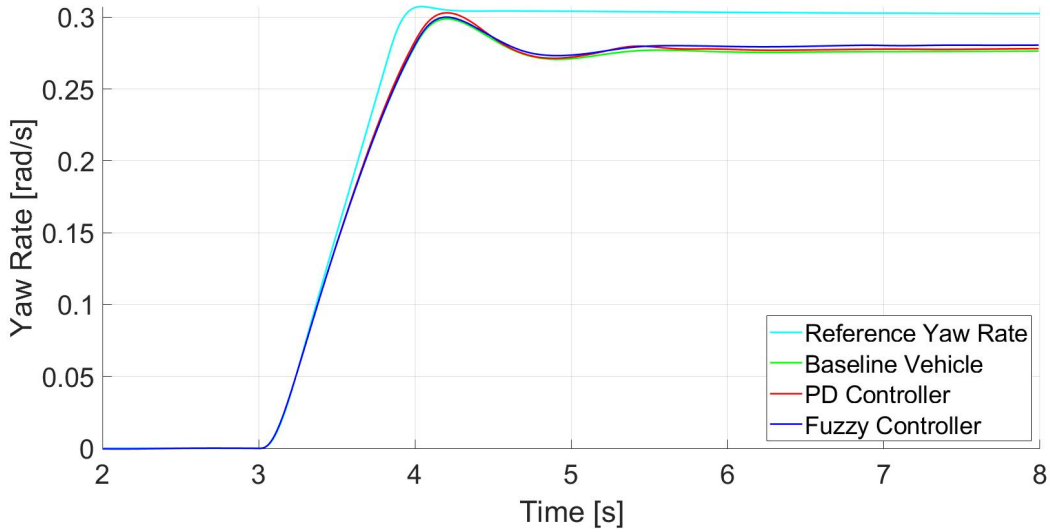

Figure 4.7: Yaw rate against time for different controllers during the step steer manoeuvre at a velocity of 100 km/h and a steering amplitude of 50°.

The zoomed in version of this plot is given in Figure 4.8, which shows the difference more clearly. Again, the PD controller has the closest yaw rate following, with the fuzzy controller coming in second and the baseline coming in last. Plots of the commanded wheel displacement, the yaw rate error and the control demand of the PD controller are given in Figures A.6, A.7, and A.8 respectively.

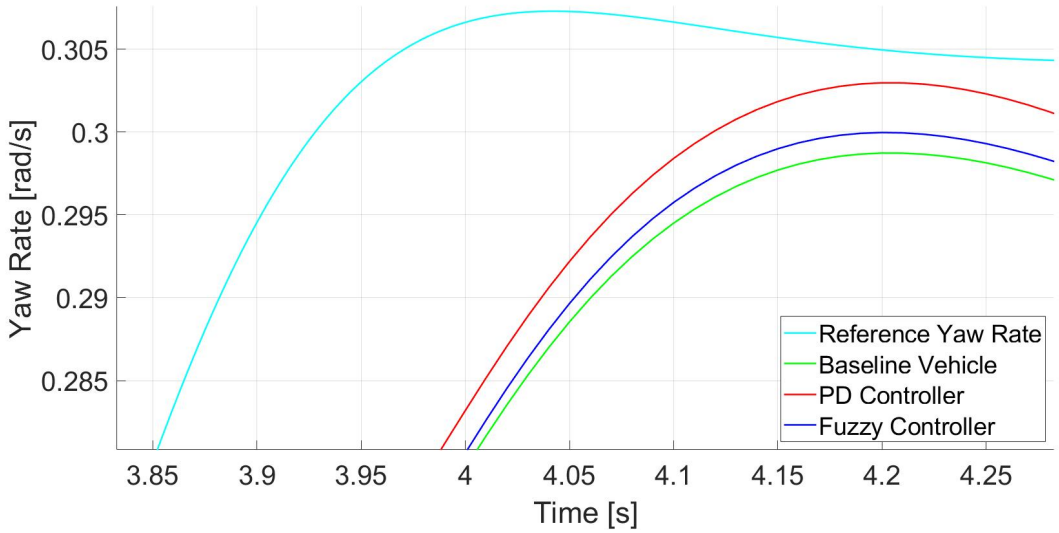

Figure 4.8: Zoomed in version of the yaw rate against time for different controllers during the step steer manoeuvre at a velocity of 100 km/h and a steering amplitude of 50°.

Velocity of 100 km/h **and Steering Amplitude of** 30°

The same velocity of 100 km/h was also tested with a steering amplitude of 30°, of which the yaw rate against time result is shown in Figure 4.9. From here, it is already visible that the PD controller is the closest to the reference yaw rate again.

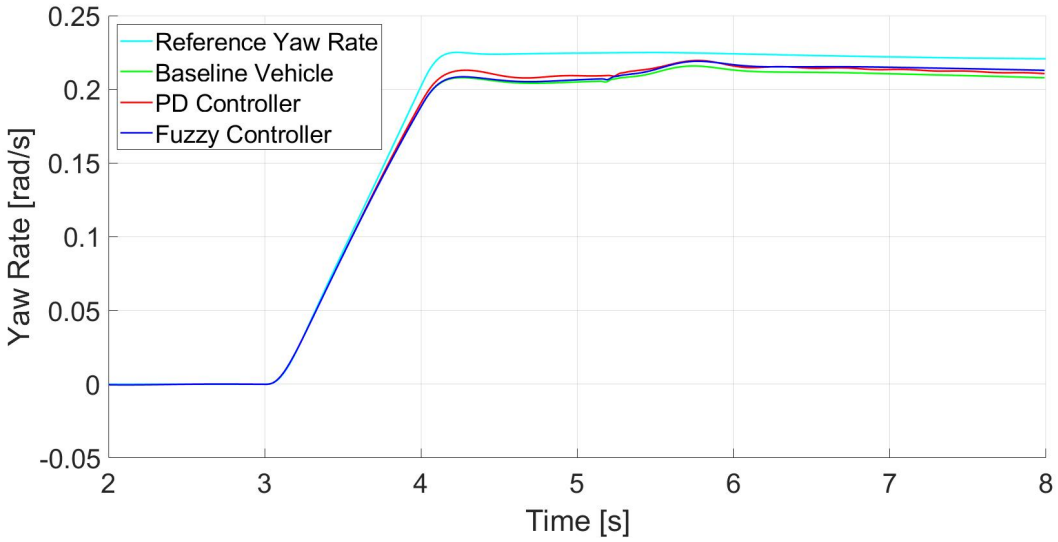

Figure 4.9: Yaw rate against time for different controllers during the step steer manoeuvre at a velocity of 100 km/h and a steering amplitude of 30°.

To make a better distinction between the line of the fuzzy controller and the baseline, a zoomed in version is given in Figure 4.10. The fuzzy controller just outperforms the baseline again with a very small margin. Plots of the commanded wheel displacement, the yaw rate error and the control demand of the PD controller are given in Figures A.9, A.10, and A.11 respectively.

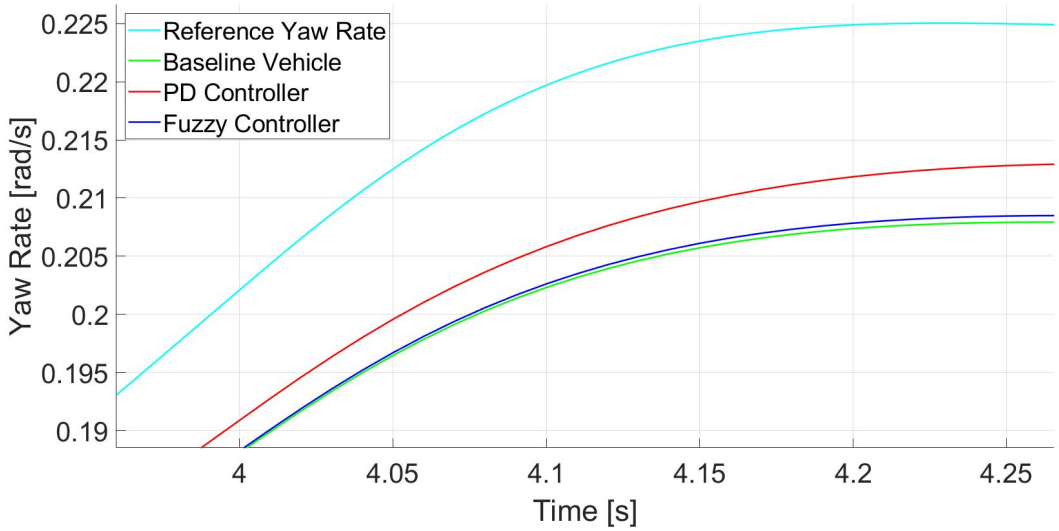

Figure 4.10: Zoomed in version of the yaw rate against time for different controllers during the step steer manoeuvre at a velocity of 100 km/h and a steering amplitude of 30°.

Velocity of 105 km/h **and Steering Amplitude of** 50°

The yaw rate against time for the scenario with a velocity of 105 km/h and a steering amplitude of 50° is given in Figure 4.11. From this plot, it is visible that the yaw rate following becomes less steady at a higher speed and higher amplitude.

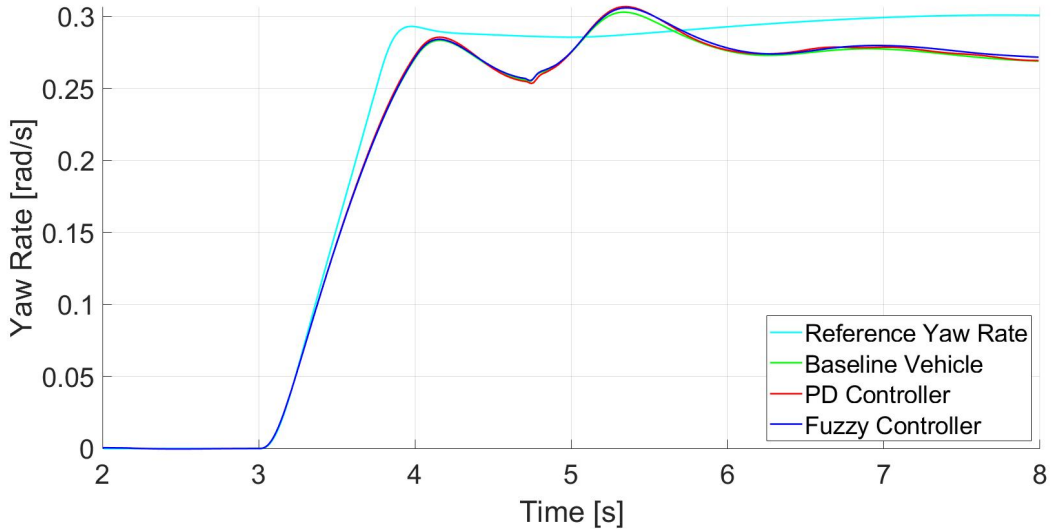

Figure 4.11: Yaw rate against time for different controllers during the step steer manoeuvre at a velocity of 105 km/h and a steering amplitude of 50°.

From the zoomed in version of the yaw rate plot, which is shown in Figure 4.12, it can be seen that again the PD controller is closest to the reference, followed by the fuzzy controller and then the baseline vehicle. Plots of the commanded wheel displacement, the yaw rate error and the control demand of the PD controller are given in Figures A.12, A.13, and A.14 respectively.

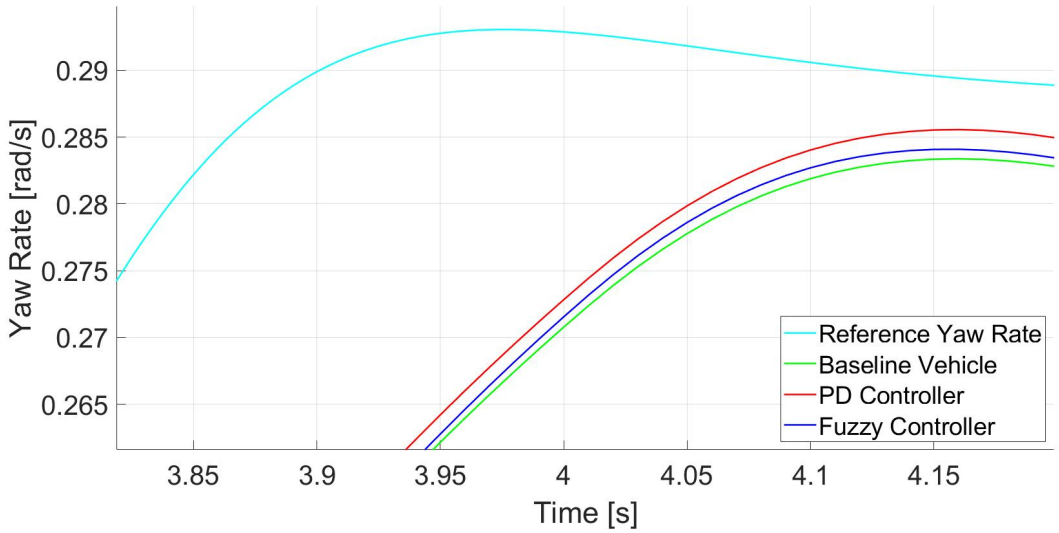

Figure 4.12: Zoomed in version of the yaw rate against time for different controllers during the step steer manoeuvre at a velocity of 105 km/h and a steering amplitude of 50°.

Velocity of 105 km/h **and Steering Amplitude of** 30°

The same velocity of 105 km/h was again tested with a smaller amplitude of 30°. The yaw rate against time for this scenario is given in Figure 4.13. From this Figure it can be noted that the smaller steering amplitude leads to a more stable yaw rate following of all controllers than an amplitude of 50° does. Furthermore, the PD line can already be identified as the closest to the reference yaw rate.

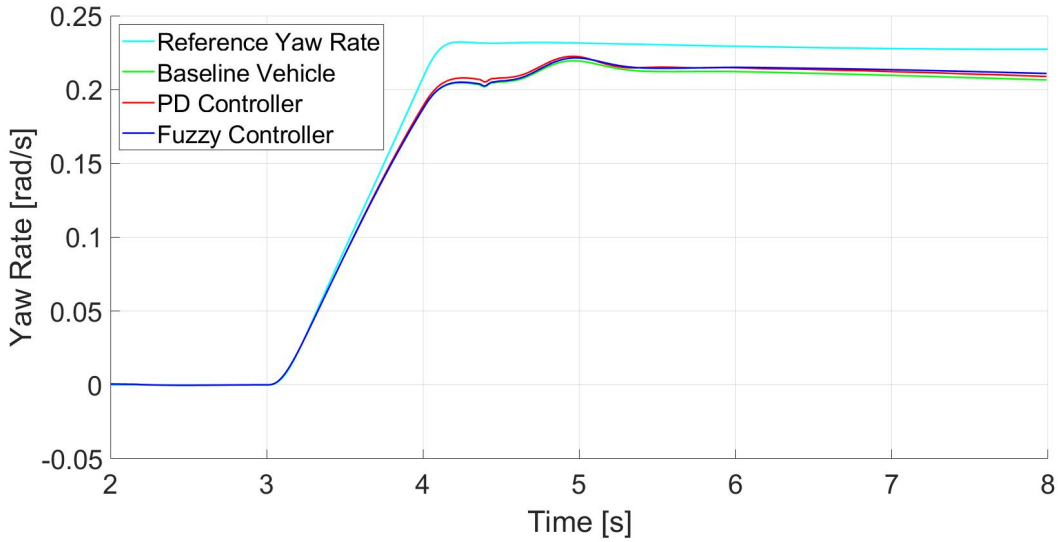

Figure 4.13: Yaw rate against time for different controllers during the step steer manoeuvre at a velocity of 105 km/h and a steering amplitude of 30°.

The zoomed in version of the yaw rate plot of this scenario is shown in Figure 4.14. Here, a clearer view of the order of the lines is obtained, from which it is visible that the fuzzy controller

line is slightly higher than the baseline again. Plots of the commanded wheel displacement, the yaw rate error and the control demand of the PD controller are given in Figures A.15, A.16, and A.17 respectively.

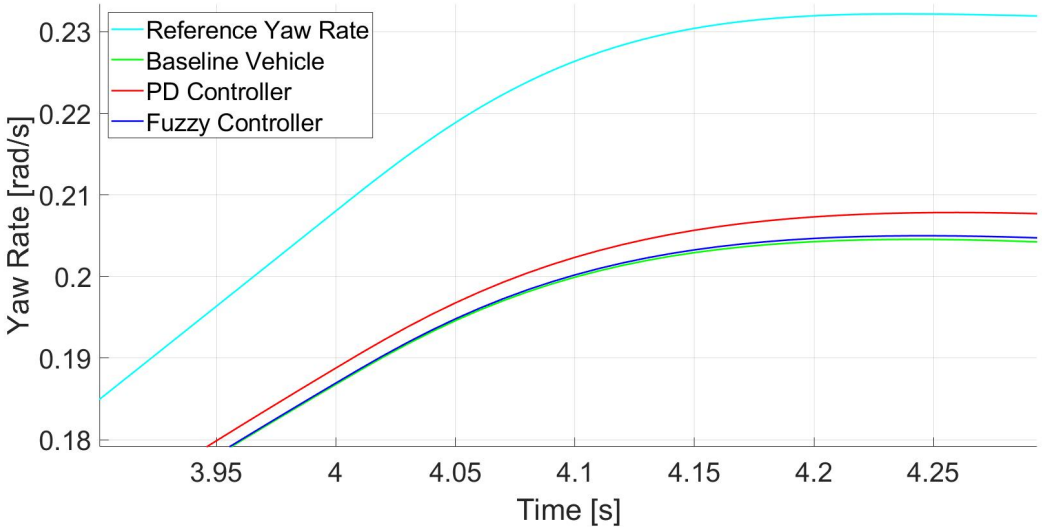

Figure 4.14: Zoomed in version of the yaw rate against time for different controllers during the step steer manoeuvre at a velocity of 105 km/h and a steering amplitude of 30°.

Velocity of 60 km/h and Steering Amplitude of 50°

To check the borderline cases of the range of the controller, this manoeuvre is also performed for a velocity of 60 km/h, at which the influence of the controller should be zero. The yaw rate against time for this manoeuvre is given in Figure 4.15. As can be seen, the lines seem to be almost identical, but they behave a bit unstable. This is due to the driver settings of the simulation having a relatively higher influence on the manoeuvre at lower speeds. They were kept the same for every manoeuvre performed for consistency.

The zoomed in version of the yaw rate plot is shown in Figure 4.16. This shows that the lines of the fuzzy controller and the baseline are in fact nearly identical, but the PD controller is still slightly higher. This is also due to the driver settings, because these make that the car does not drive at 60 km/h perfectly, which is why the controller is lightly activated. The fuzzy controller reacts less obvious to this because of the membership functions it was given, as was explained earlier in this Section. A plot of the commanded wheel displacement is given in Figure A.18, from where it is visible that the range of movement is indeed very small. It was chosen to only do this manoeuvre for a steering amplitude of 50°, since this already sufficiently demonstrates the boundary behaviour.

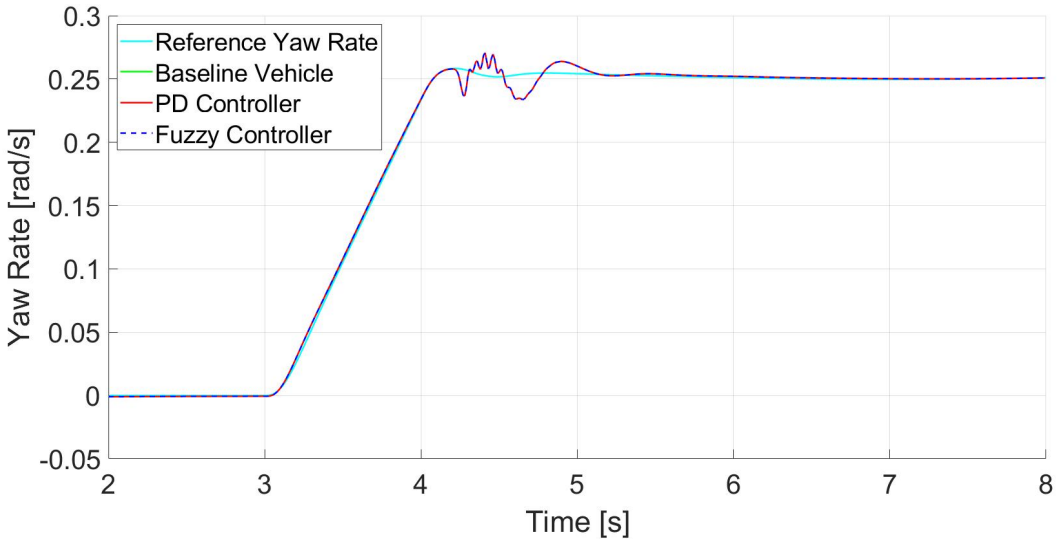

Figure 4.15: Yaw rate against time for different controllers during the step steer manoeuvre at a velocity of 60 km/h and a steering amplitude of 50°.

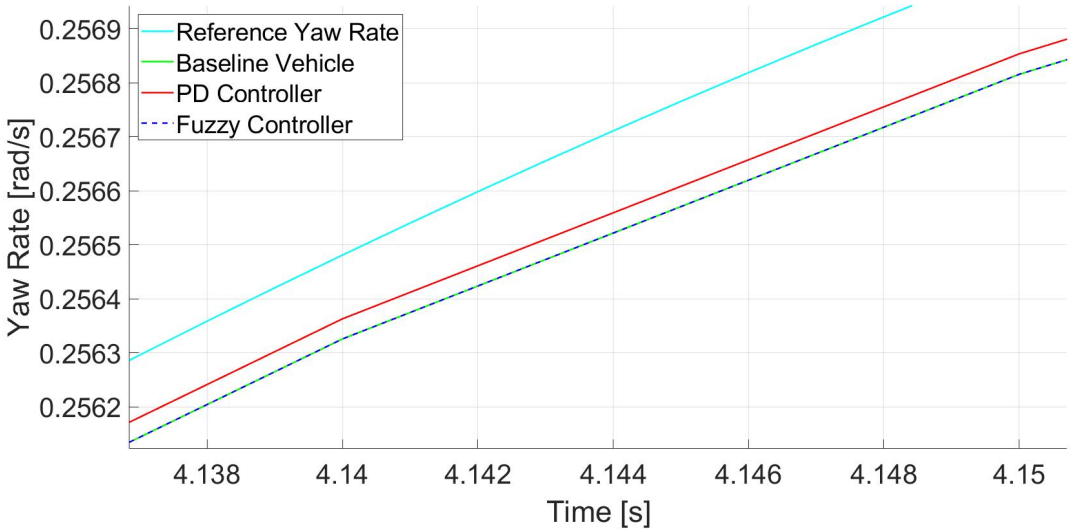

Figure 4.16: Zoomed in version of the yaw rate against time for different controllers during the step steer manoeuvre at a velocity of 60 km/h and a steering amplitude of 50°.

Velocity of 110 km/h and Steering Amplitude of 50°

To check the higher bounds of the controller range, the manoeuvre was also tested for a velocity of 110 km/h. The yaw rate against time for this scenario was plotted in Figure 4.17. It is again visible that the lines become unsteady for this higher speed manoeuvre, and they seem to follow the same line for all control situations.

From the zoomed in version given in Figure 4.18, a similar situation is shown as for a velocity of 60 km/h and this can be explained by the same reasoning. A plot of the commanded wheel displacement is given in Figure A.18, which again shows a very small range of movement.

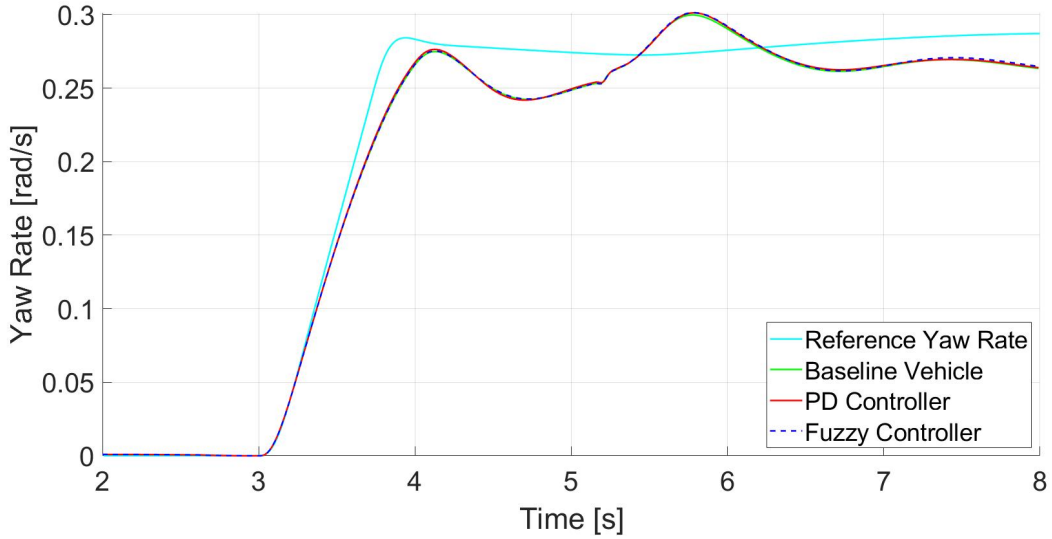

Figure 4.17: Yaw rate against time for different controllers during the step steer manoeuvre at a velocity of 110 km/h and a steering amplitude of 50°.

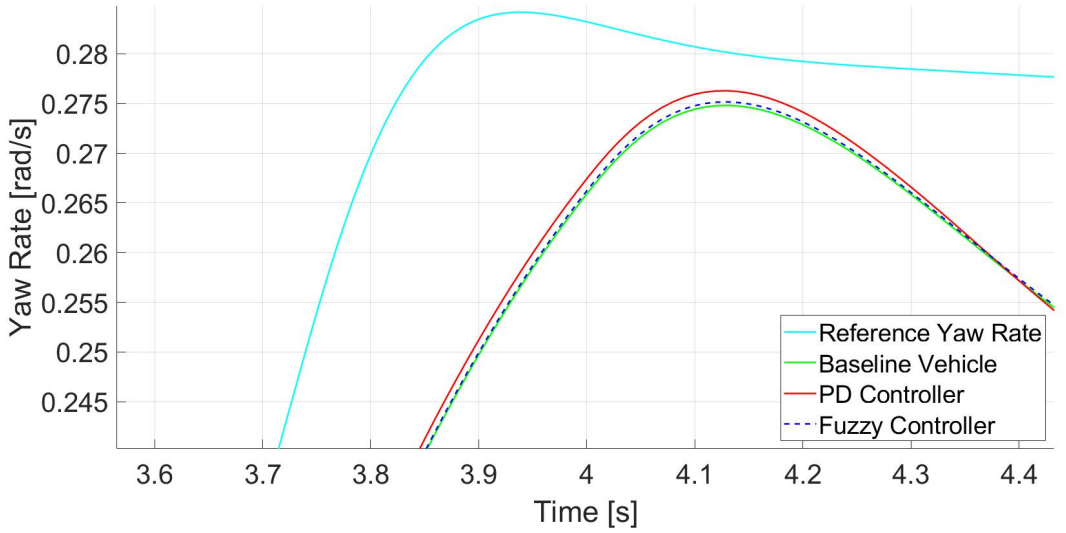

Figure 4.18: Zoomed in version of the yaw rate against time for different controllers during the step steer manoeuvre at a velocity of 110 km/h and a steering amplitude of 50°.

Numerical Results

The results of every different combination of velocity and steering angle, except for the borderline cases, are expressed numerically in Table 4.1. It gives the ratio of actual yaw rate to the reference yaw rate in percentages at three measuring points, for all three control situations, so the baseline vehicle, the PD controller and the fuzzy controller. The first measuring point is at 50% of the steering input, the second is at 90% of the steady state yaw rate of that particular control situation and lastly a measurement was done at 4.2 seconds. The last was chosen like this, because this is just after the steering input gets held at a constant value, and around this time almost all lines come closest to the reference. From these numbers, it becomes clear that the PD controller indeed outperforms both other control situation almost every time. Only during

both manoeuvres, at a velocity of 80 km/h, is the PD controller very slightly behind the other two. The fuzzy controller does indeed show very similar results during the first measurements, but performs less good during the second, even though the line in the graph is closer to the reference at this point during the different manoeuvres. This is due to the steady state values being different for every control situation, which means they are measured at different points. During the last measurements, the results are more clear with the PD controller performing the best, followed by the fuzzy controller for every situation. In the bottom row, the average of the measurements during all different velocity and steering amplitude combinations is given for that particular measuring point and control situation. This shows that at a steering input of 50%, the PD controller outperforms the baseline by 0.077%, whereas the fuzzy controller performs the same. At 90% of the respective steady state yaw rate, the PD controller outperforms the baseline by 0.886% and the fuzzy controller actually performs 0.008% worse on average. Lastly, at the measuring point of 4.2 seconds, the PD controller outperforms the baseline vehicle by 1.345% and the fuzzy controller outperforms it by 0.2%.

	50% of Steering Input			90% of Yaw Rate			At 4.2 seconds		
	Base	PD	Fuzzy	Base	PD	Fuzzy	Base	PD	Fuzzy
80 km/h, 50°	96.198	96.124	96.198	92.866	94.152	92.494	92.827	94.889	93.025
80 km/h, 30°	97.257	97.209	97.257	97.559	97.807	97.559	98.420	99.007	98.422
100 km/h, 50°	92.898	93.102	92.899	86.845	87.879	87.024	97.993	99.383	98.399
100 km/h, 30°	94.917	95.048	94.916	92.153	93.523	92.067	92.178	94.158	92.385
105 km/h, 50°	91.014	91.175	91.017	85.349	85.773	85.779	97.928	98.669	98.145
105 km/h, 30°	93.484	93.576	93.483	88.885	89.840	88.690	88.026	89.334	88.196
Average	94.295	94.372	94.295	90.610	91.496	90.602	94.562	95.907	94.762

Table 4.1: Ratio of actual yaw rate to reference yaw rate, given in percentage, during the step steer manoeuvre at different combinations of velocity and steering amplitude.

4.2.2 Increasing Circle

Steering Amplitude of 30°

Both controllers were also tested on the increasing circle manoeuvre, of which similar graphs were made. Figure 4.19 shows the yaw rate against time for this manoeuvre at a steering amplitude of 30°. Again, the lines are quite close to each other. At higher speeds, it can be seen that the fuzzy controller follows the reference better, but what happens before is not quite visible.

A zoomed in version of this plot is given in Figure 4.20. From here, it is observable that the PD controller actually follows the reference closer than the fuzzy controller until about 76 s into the manoeuvre. Hereafter, the line of the fuzzy controller intersects with the line of the PD controller and proceeds to follow the reference closer for the remainder of the manoeuvre. For the lower velocities, the fuzzy controller performs almost exactly the same as the baseline again, but after a significant wheel displacement is commanded, it outperforms this baseline.

The commanded wheel displacements for both controllers are shown in Figure 4.21. Here the wheel commands yield a similar configuration as for the step steer manoeuvre, so a trapezoid for the PD controller and a parallelogram for the fuzzy controller. Here it is clearly visible that the fuzzy controller has reached the limit constraint before the end of the manoeuvre, whereas

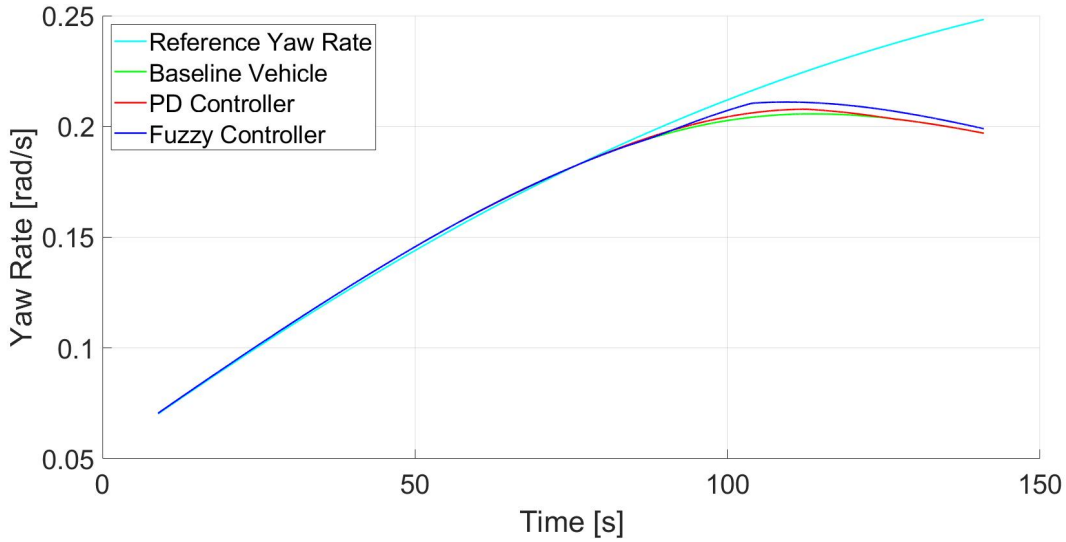

Figure 4.19: Yaw rate against time for different controllers during the increasing circle manoeuvre at a steering amplitude of 30°.

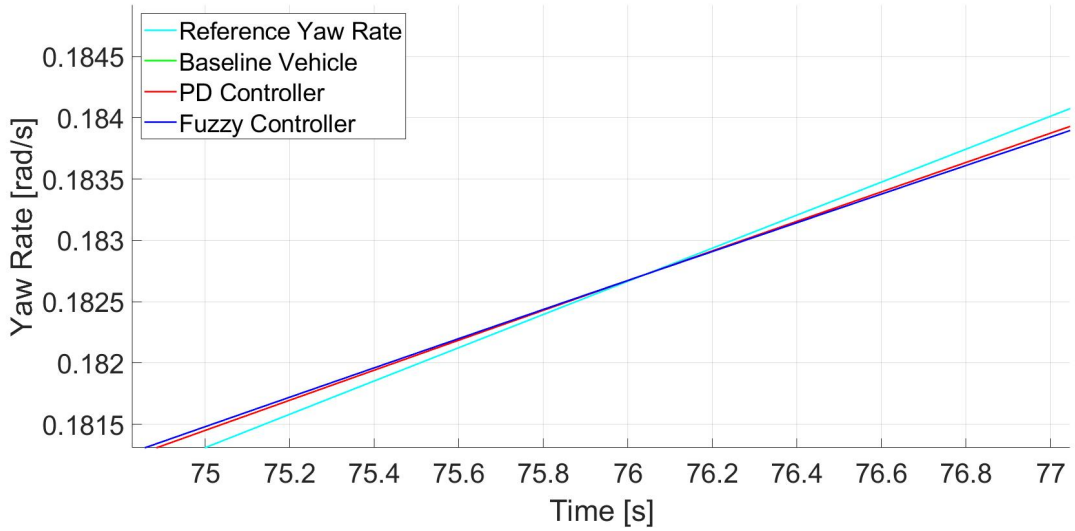

Figure 4.20: Zoomed in version of yaw rate against time for different controllers during the increasing circle manoeuvre at a steering amplitude of 30°.

the wheels commanded by the PD controller are returned to their original positions when the velocity limit of 110 km/h is reached. The fuzzy controller does not command the wheels to go back to their original state, which is why they remain at the limit. It should also be noted that right after the peaks of the PD controller, a little chuttering is visible. This is so small however, that it can be disregarded.

Another interesting result from this manoeuvre is plotted in Figure 4.22. This graph presents the control input and the allocated demand plotted against time, which are almost exactly the same. This shows that the controller is successfully allocating the demand for this manoeuvre. Here again that bit of chuttering is visible right after the peak, but this can be ignored as well.

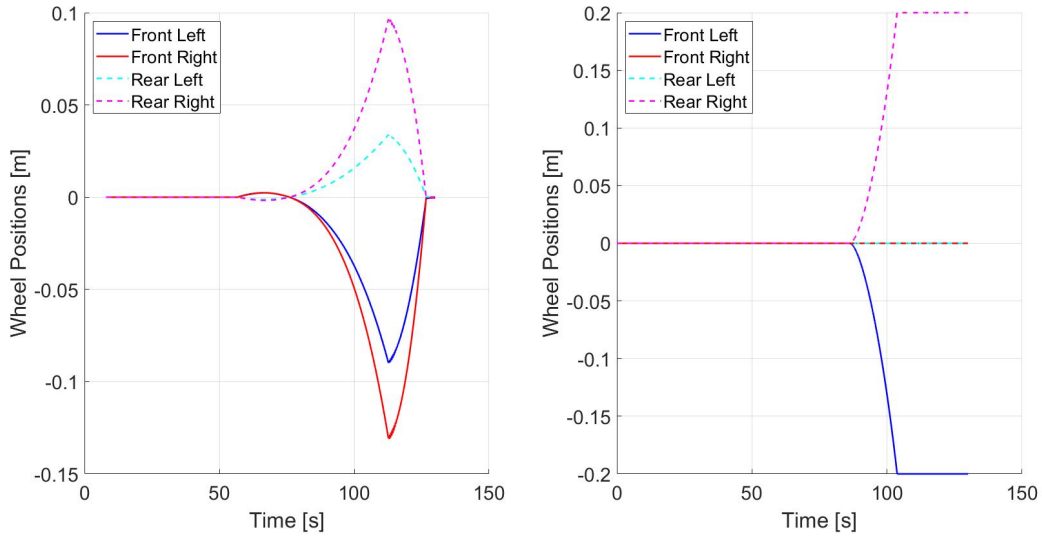

Figure 4.21: Commanded wheel displacement in longitudinal direction against time for the PD controller (left) and the fuzzy controller (right), during the increasing circle manoeuvre at a steering amplitude of 30°.

Plots of the yaw rate against velocity and the yaw rate error are given in Figures A.20 and A.21 respectively.

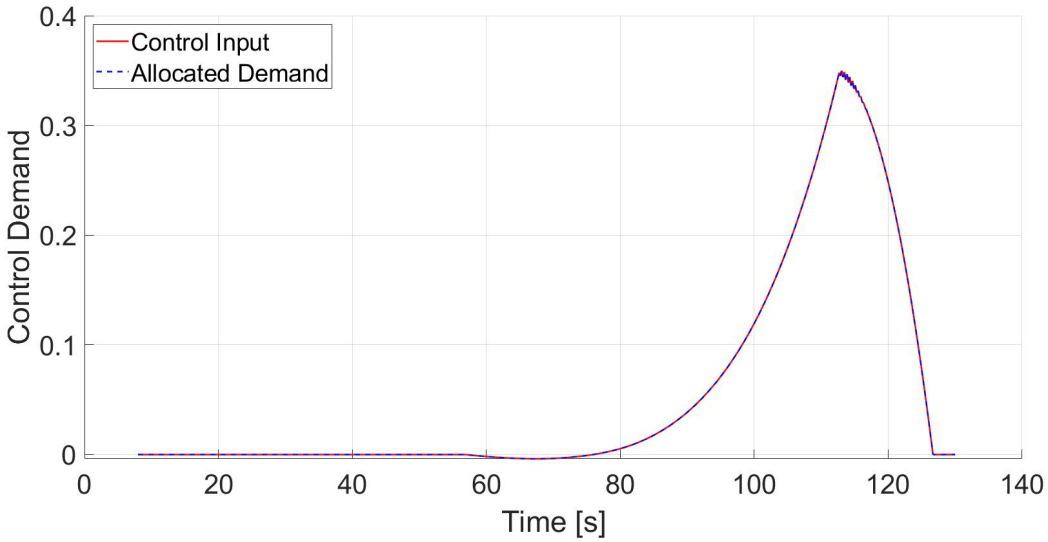

Figure 4.22: Control demand of the PD controller against time during the increasing circle manoeuvre at a steering amplitude of 30°.

Steering Amplitude of 50°

The increasing circle manoeuvre was also performed for a steering angle of 50°, of which the yaw rate is plotted against time in Figure 4.23. The fuzzy controller seems to follow the reference the closest again, followed by the PD controller and the baseline.

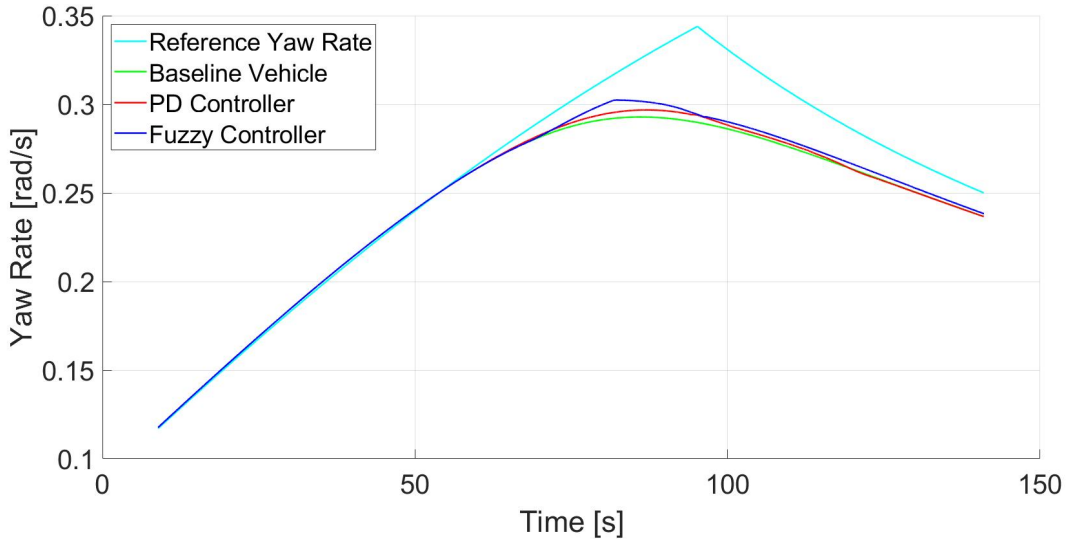

Figure 4.23: Yaw rate against time for different controllers during the increasing circle manoeuvre at a steering amplitude of 50°.

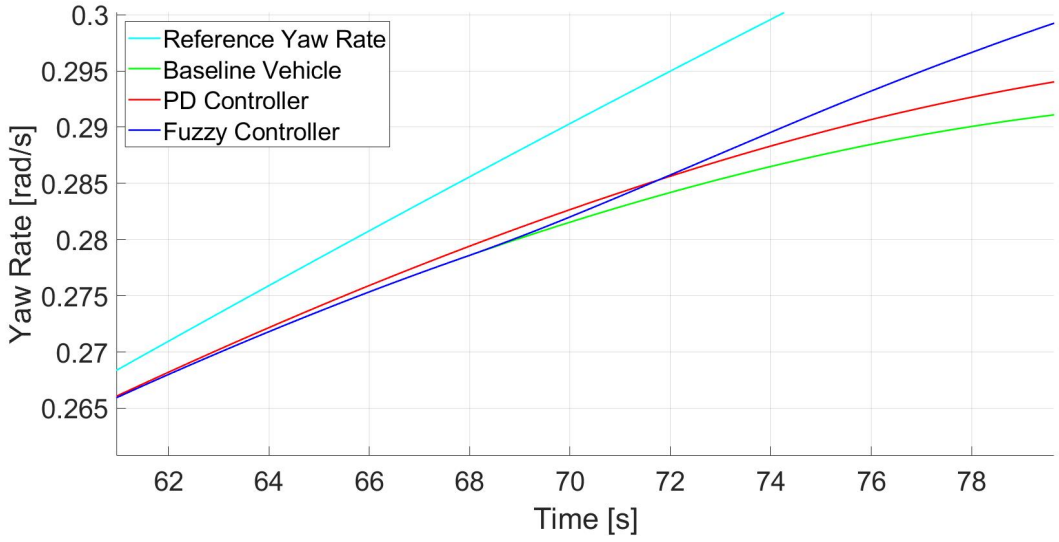

Figure 4.24: Zoomed in version of yaw rate against time for different controllers during the increasing circle manoeuvre at a steering amplitude of 50°.

To get a clearer view of what happens before the peaks, a zoomed in version is made and given in Figure 4.24. Again, this shows that the PD controller actually follow the reference closer in the beginning, but is then intersected by the fuzzy controller very soon after this one separates from the baseline. Plots of the yaw rate against velocity, the commanded wheel displacement, the yaw rate error and the control demand of the PD controller are given in Figures A.22, A.23, A.24, and A.25 respectively.

Numerical Results

The results of both different steering amplitudes, are expressed numerically in Table 4.2. This again gives the ratio of the actual yaw rate to the reference yaw rate in percentages at three

measuring points for all three control situations. The first measuring point is at a velocity of $80\,km/h$, the second is at a velocity of $100\,km/h$ and the third is at a velocity of $105\,km/h$. Here can be seen that the PD controller outperforms the baseline for all but one value, which is during the manoeuvre with an amplitude of 50°, at the $105\,km/h$ measuring point, which is just after the PD controller and baseline vehicle cross each other in Figure 4.23. The fuzzy controller outperforms both other control situations almost every time. The only exception is during the manoeuvre with an amplitude of 30°, at the $80\,km/h$ measuring point, where the fuzzy controller is equal to the baseline and the PD controller outperforms them both. Again, the averages per measuring point for each control situation are computed, rendering the bottom row. Since this manoeuvre is tested for just two different amplitudes, and they have quite different values at each measuring point, especially at the first, it should be noted that these averages are a little less reliable. Nevertheless, this shows that on average at a velocity of $80\,km/h$, the PD controller outperforms the baseline vehicle by 0.656% and the fuzzy controller outperforms it by 1.389%. At a velocity of $100\,km/h$, the PD controller outperforms it by 0.742% and the fuzzy controller by $1,716$%. Lastly, at a velocity of $100\,km/h$, the PD controller outperforms the baseline by 0.178%, whereas the fuzzy outperforms this baseline by 1.44%.

	$80\,km/h$			$100\,km/h$			$105\,km/h$		
	Base	PD	Fuzzy	Base	PD	Fuzzy	Base	PD	Fuzzy
30°	98.936	99.149	98.936	91.399	92.329	93.692	88.625	89.008	90.466
50°	90.552	91.711	93.390	90.633	91.187	91.771	92.124	92.097	93.164
Average	94.774	95.430	96.163	91.016	91.758	92.732	90.375	90.553	91.815

Table 4.2: Ratio of actual yaw rate to reference yaw rate, given in percentage, during the increasing circle manoeuvre at different steering amplitudes.

4.2.3 Double Lane Change

Velocity of $80\,km/h$

Lastly, the double lane change manoeuvre was executed at different velocities. For a velocity of $80\,km/h$, the yaw rate is plotted against time in Figure 4.25, but this time only for the PD controller and fuzzy controller to highlight the difference between these two in this more complicated manoeuvre. However, as is visible from the graph, the lines are nearly equal.

The commanded wheel displacements for this manoeuvre, looks much more eventful than for others, as can be expected from such a manoeuvre. It is shown in Figure 4.26. Especially the PD controller behaves in a somewhat erratic way. The fuzzy controller fluctuates a bit as well, but much less and in a smaller range. The control demand of the PD controller, as plotted in Figure 4.27 explain why this happens. From this graph, it is obvious that the control input moves too fast for the controller to catch up. These dips and peaks in the actuator commands are caused by the controller's constant need to correct itself before it reaches its goal.

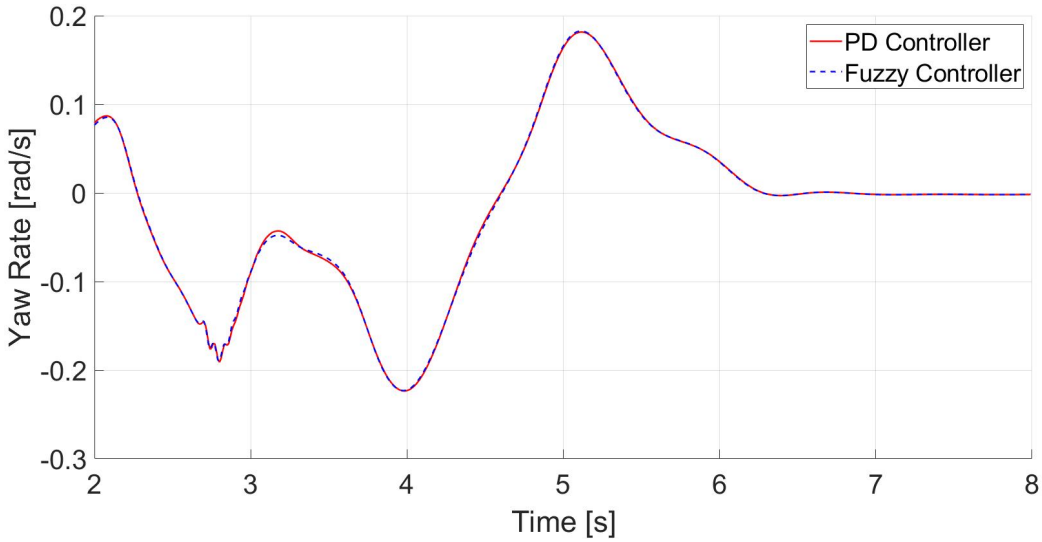

Figure 4.25: Yaw rate against time for the PD controller and the fuzzy controller during the double lane change manoeuvre at a velocity of 80 km/h.

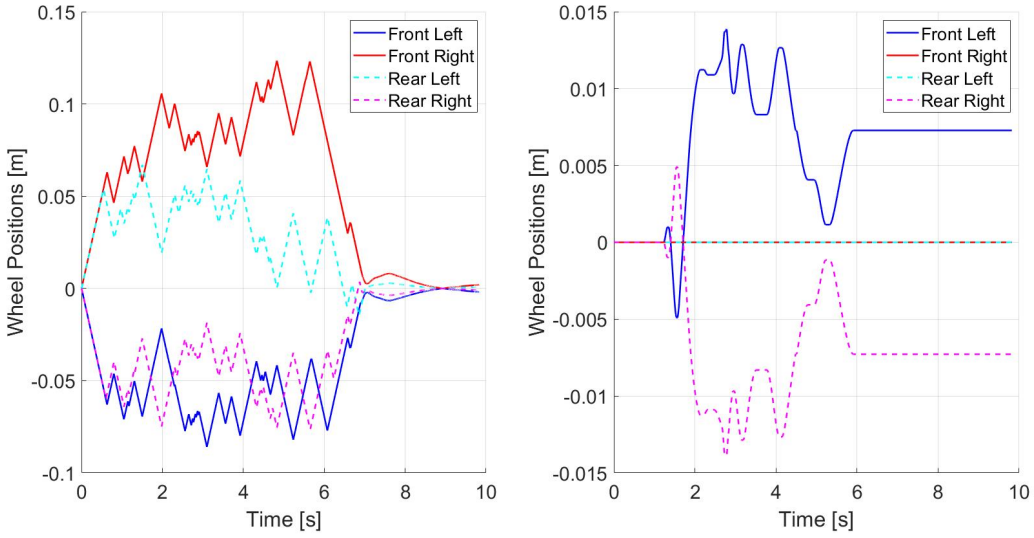

Figure 4.26: Commanded wheel displacement in longitudinal direction against time for the PD controller (left) and the fuzzy controller (right), during the double lane change manoeuvre at a velocity of 80 km/h.

In Figure 4.28 the steering angle is plotted against time for all three control situations. This shows that they are roughly the same, only the PD controller deviates a bit from the other two. Figure 4.29 shows a zoomed in version of the highest peak, from which it is visible that indeed the fuzzy controller and the baseline are nearly the same again. This is explained by the much smaller range of movement that is commanded by the fuzzy controller compared to the PD controller, as was explained in Figure 4.26. A plot of the yaw rate error is given in Figure A.26.

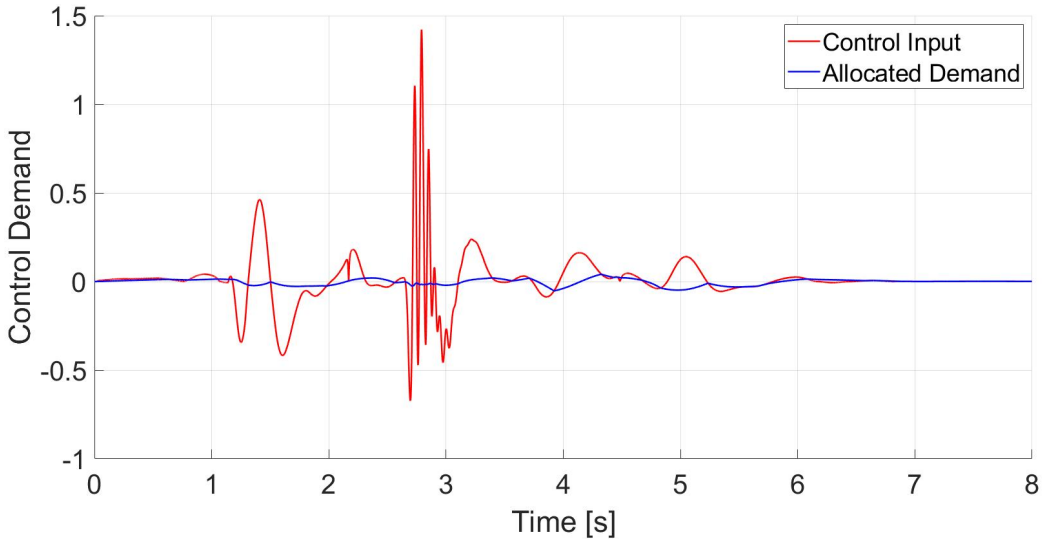

Figure 4.27: Control demand of the PD controller against time during the double lane change manoeuvre at a velocity of 80 km/h.

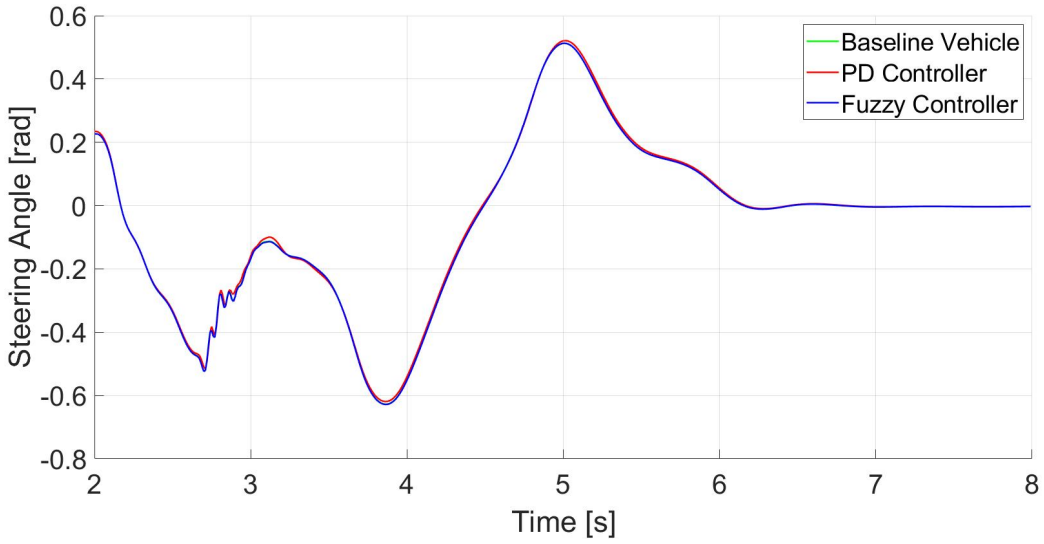

Figure 4.28: Steering angle against time for the PD controller and the fuzzy controller during the double lane change manoeuvre at a velocity of 80 km/h.

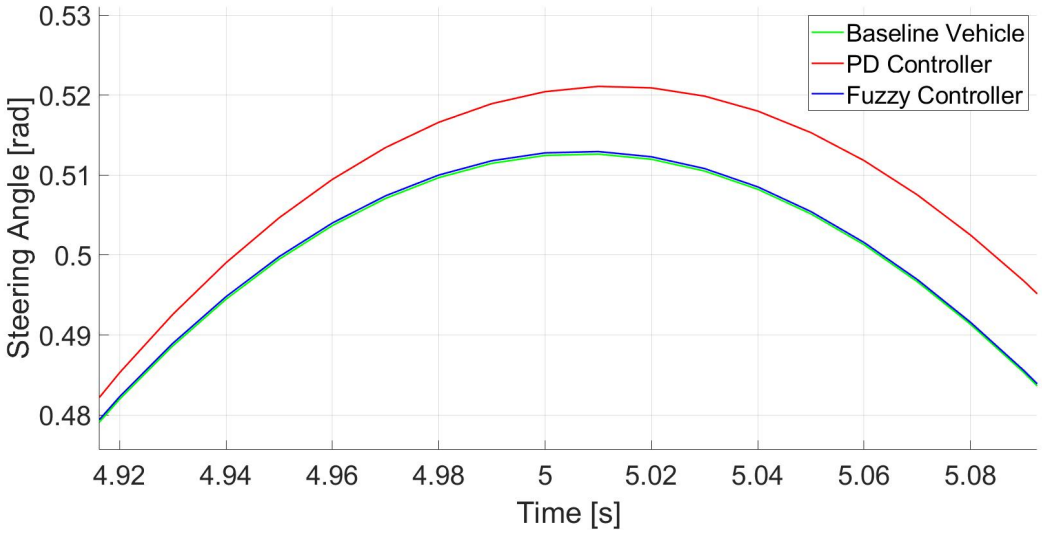

Figure 4.29: Zoomed in version of the steering angle against time for the PD controller and the fuzzy controller during the double lane change manoeuvre at a velocity of 80 km/h.

Velocity of 100 km/h

This manoeuvre is then performed at a velocity of 100 km/h, for which the yaw rate was plotted against time in Figure 4.30. Again, the lines are quite similar, apart from some small deviations.

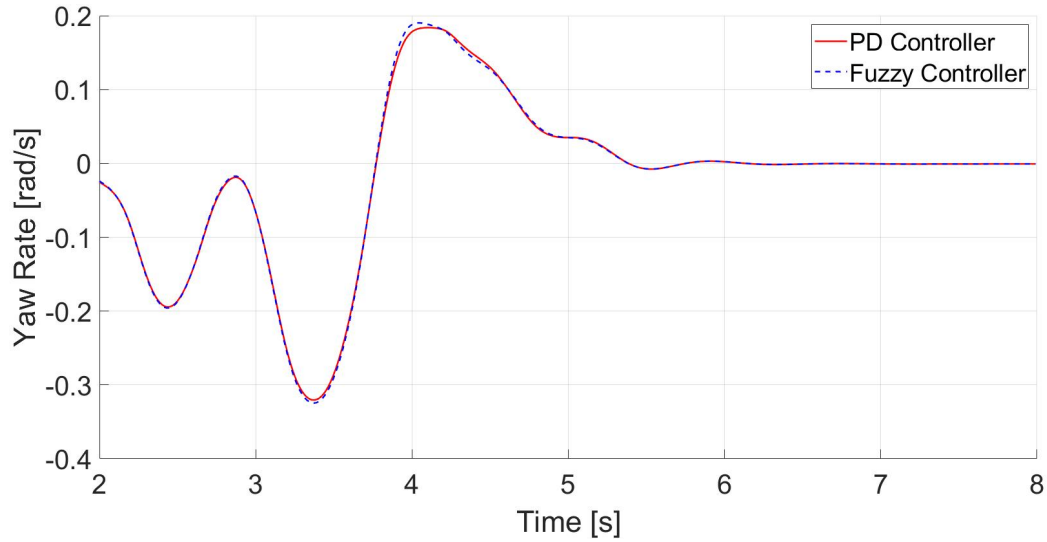

Figure 4.30: Yaw rate against time for the PD controller and the fuzzy controller during the double lane change manoeuvre at a velocity of 100 km/h.

A comparison of the steering angles is given in Figure 4.31. This too shows very similar lines, but the PD controller line is distinguishable in the middle of the graph.

A zoomed in view of the highest peak is shown in Figure 4.32, from which it is clearly visible that the fuzzy controller and the baseline follow a more similar trajectory than the PD controller.

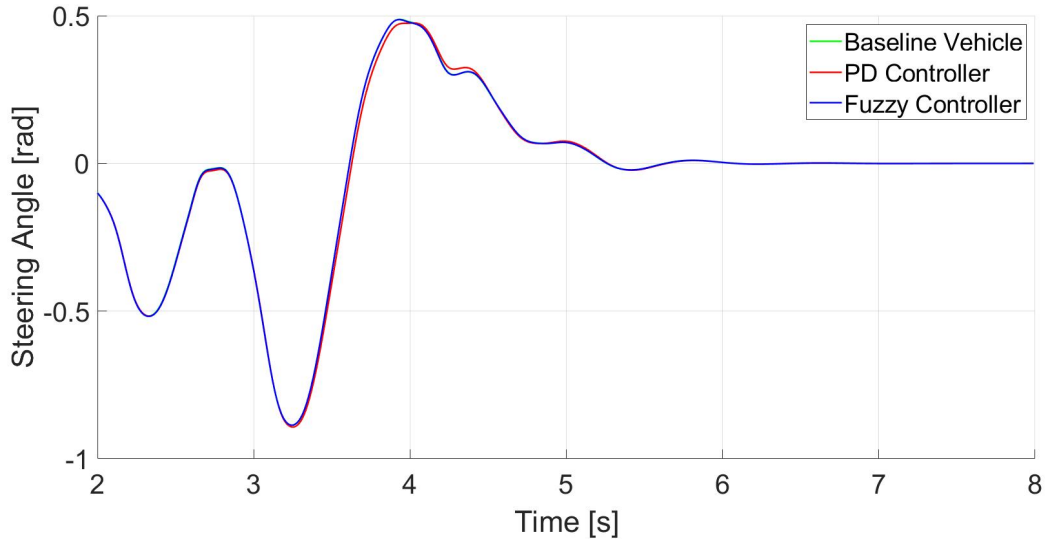

Figure 4.31: Steering angle against time for the PD controller and the fuzzy controller during the double lane change manoeuvre at a velocity of 100 km/h.

This again is due to a smaller range in commanded wheel movement, the plot of which can be found in the Appendix as Figure A.27. Plots of the yaw rate error and the control demand are also included there as Figures A.28 and A.29 respectively.

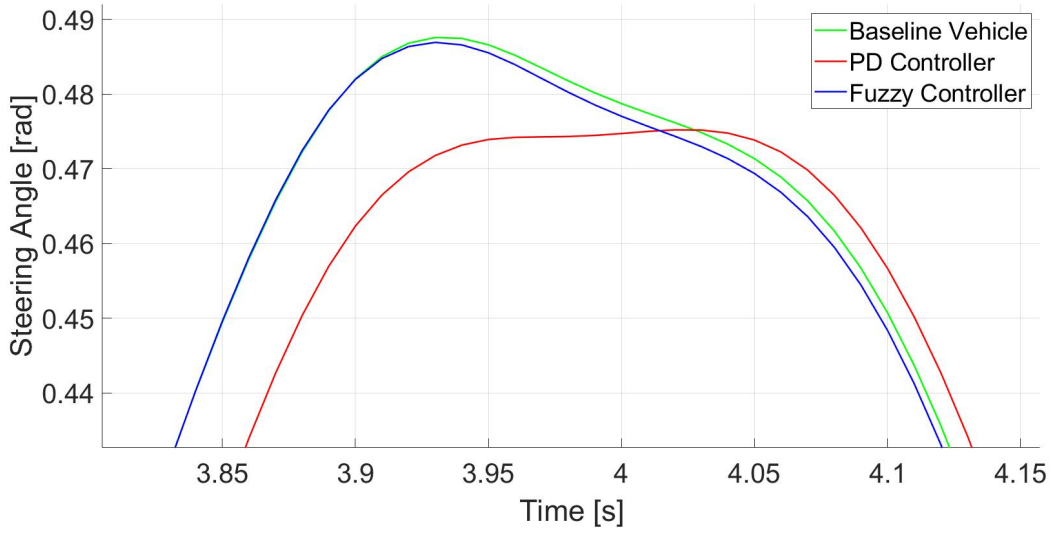

Figure 4.32: Zoomed in version of the steering angle against time for the PD controller and the fuzzy controller during the double lane change manoeuvre at a velocity of 100 km/h.

Velocity of 105 km/h

Lastly, this manoeuvre was performed at a velocity of 105 km/h. The yaw rate against time for this situation is plotted in Figure 4.33. Just as for the other two velocities, the lines are very similar except for some small outliers.

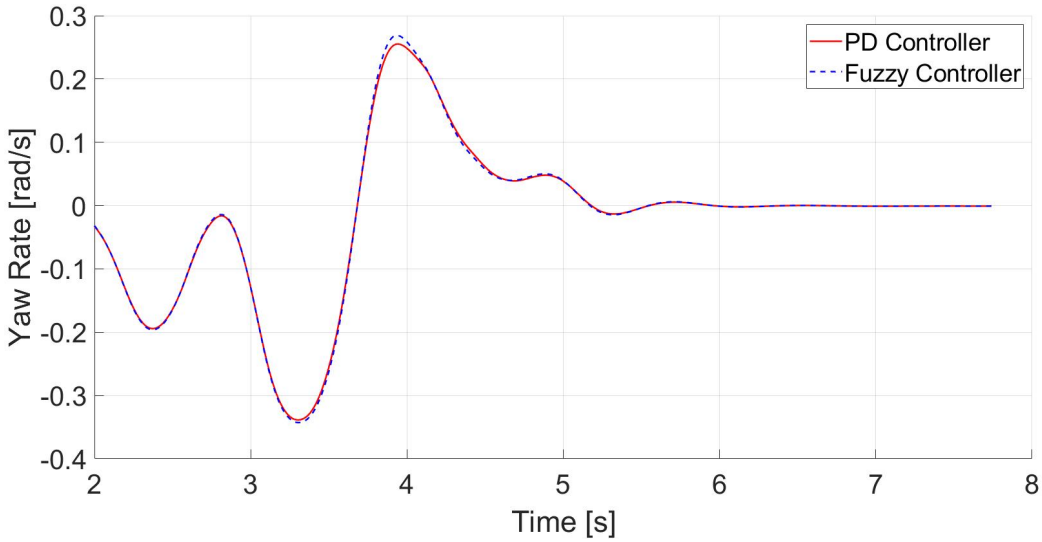

Figure 4.33: Yaw rate against time for the PD controller and the fuzzy controller during the double lane change manoeuvre at a velocity of 105 km/h.

In Figure 4.34, the steering angle against time is plotted for this situation. Again, this shows a very similar trajectory, but the red line can be distinguished at certain parts.

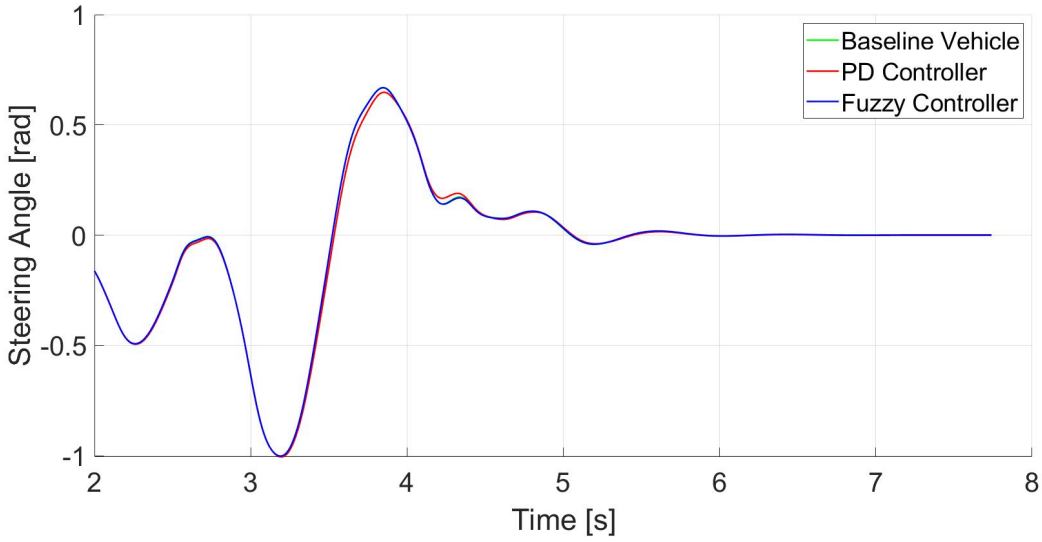

Figure 4.34: Steering angle against time for the PD controller and the fuzzy controller during the double lane change manoeuvre at a velocity of 105 km/h.

For more clarity, the zoomed in version of the highest peak is given in Figure 4.35. This shows that the fuzzy controller and the baseline are nearly identical again, whereas the PD controller deviates from them. This can be explained by the difference in range of the commanded wheel positions as well, a plot of which can be found in the Appendix as Figure A.30. Plots of the yaw rate error and the control demand are also given as Figures A.31 and A.32 respectively.

For the double lane change manoeuvre, there were no numerical results made, as it is too complex

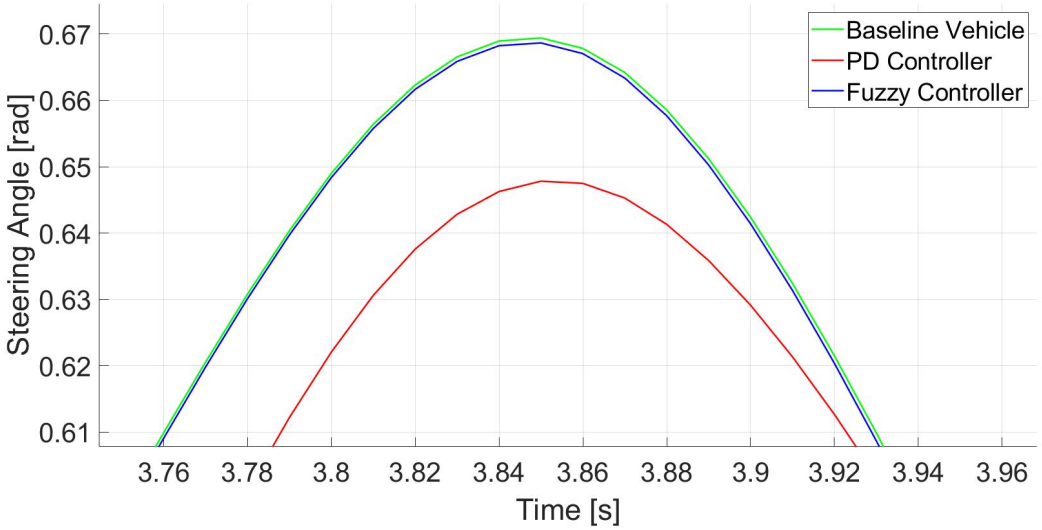

Figure 4.35: Zoomed in version of the steering angle against time for the PD controller and the fuzzy controller during the double lane change manoeuvre at a velocity of 105 km/h.

of a manoeuvre to quantify its results by a few measuring points. Additionally, it was already noted that the controller does not successfully allocate the demand for this manoeuvre.

4.3 Summary

This Chapter shows all the simulations that were done and their results. It starts off with explaining the three different manoeuvres as the step steer, the increasing circle and the double lane change. The different velocities and steering amplitudes for which these manoeuvres are tested, are given as well. Hereafter, the resulting relevant graphs of the yaw rate, commanded wheel movements, yaw rate error, control demands and steering angle are presented per manoeuvre with an explanation. For the step steer manoeuvre, the PD controller performs best compared to the fuzzy controller and the baseline vehicle. With the increasing circle, the fuzzy controller shows the best yaw rate following, but the PD controller still outperforms the baseline vehicle as well. The double lane change manoeuvre is quite inconclusive, as both controllers move too slow to keep up with the complexity of this manoeuvre.

5. Conclusion and Recommendations

5.1 Conclusion

The goal of this thesis was to research if actively changing the wheelbase could have a positive effect on the lateral vehicle dynamics. It can be concluded that such a system does affect these dynamics, however that effect is limited and dependent on manoeuvre type and actuator dynamics.

From the step steer manoeuvres, it became clear that the PD controller combined with control allocation had a closer yaw rate following than both the fuzzy controller and the baseline vehicle for every tested combination of velocity and steering amplitude. The benchmark fuzzy controller was mostly equal to or better than the baseline as well, which proves that changing the longitudinal wheel positions can indeed be used to enhance these dynamics.

However, from the increasing circle manoeuvre can be concluded that upon activation, the fuzzy controller outperforms the PD controller. Nevertheless, the PD controller did successfully allocate the control demand for this manoeuvre. Furthermore, both controllers do still equal or outperform the baseline vehicle at all times, which confirms the conclusion that it is possible for such a system to embellish the lateral vehicle dynamics.

The double lane change manoeuvre was quite inconclusive as it comes to yaw rate following. The PD controller was unable to successfully allocate the demand, which was due to the complexity of the manoeuvre. The fuzzy controller was only able to command its wheel positions in a very small range, also due to the rapidly changing yaw reference for a manoeuvre like this. Therefore, both controllers, as presented, are not applicable to fast moving manoeuvres such as this one.

From the theoretical research and results of the simulations, it can be proven that by actively changing the wheelbase, the tyre forces are modified which results in a change in yaw moment. This means that such a system could indeed be used to provide more agility at higher velocities. The predominantly positive results from both of these relatively simple controllers, mean that a system like this does have potential to perform much better in the future. With this in mind, some recommendations for future work will be given in the next section.

5.2 Recommendations

With these promising results, further research into this subject is definitely recommended. Firstly, it is recommended to test the controller with more different manoeuvres. The test scenarios of this research were very simplified manoeuvres to just study the way the controller commands the vehicle in such situations. These tests could, for example, be made to feature a difference in friction values. It would also be interesting to adjust the controller for urban applications and observe how it performs there, to see if it is possible to achieve both agility at high velocities, and manoeuvrability at lower velocities. Moreover, the vehicle model was simplified as well, by taking out the gear shifting for example, so it would also be interesting to look at different, more complex vehicle models.

Furthermore, it is recommended to look into different, more advanced controllers, such as a well tuned proportional integral derivative controller or sliding mode control to stabilize the non-linearities in the system. Additionally, the control allocation block could be extended by using model predictive control allocation. This way, the system can react better to actuator dynamics, meaning it would have less trouble following a more complex manoeuvre. The reference model could also be adjusted to account for the dynamic vehicle response, by changing the values in the transfer function from fixed ones to velocity dependent ones.

Lastly, it is highly recommended to look into the influence of a reconfigurable wheel track as well. The mathematical arguments provided to support the use of a reconfigurable wheelbase for enhanced lateral dynamics, can be made similarly for the wheel track. Designing a controller that could actively move all wheels in both longitudinal and lateral direction, can only be expected to yield much more evident and interesting results.

Bibliography

[1] A. Soltani, A. Goodarzi, M. H. Shojaiefard, and A. Khajepour, "Developing an active variable-wheelbase system for enhancing the vehicle dynamics," *Proceedings of the Institution of Mechanical Engineers, Part D: Journal of Automobile Engineering*, vol. 231, no. 12, pp. 1640–1659, 2017.

[2] *Road vehicles—Test procedure for a severe lane-change manoeuvre (Standard No. ISO/TR 3888:1975)*. Geneva, Switzerland: International Organization for Standardization (ISO), 1975.

[3] R. Bosch, "Safety, comfort and convenience systems: function, regulation and components," *Bentley Robert Inc*, 2006.

[4] C. Hong, G. Xun, H. Yun-Feng, L. Qi-Fang, G. Bing-Zhao, and G. Hong-Yan, "Automotive control: the state of the art and perspective," *Acta Automatica Sinica*, vol. 39, no. 4, pp. 322–346, 2013.

[5] A. Khajepour, M. S. Fallah, and A. Goodarzi, *Electric and hybrid vehicles: technologies, modeling and control-a mechatronic approach*. John Wiley & Sons, 2014.

[6] Y. Shibahata, "Progress and future direction of chassis control technology," *Annual Reviews in Control*, vol. 29, no. 1, pp. 151–158, 2005.

[7] D. Cao, X. Song, and M. Ahmadian, "Editors' perspectives: road vehicle suspension design, dynamics, and control," *Vehicle system dynamics*, vol. 49, no. 1-2, pp. 3–28, 2011.

[8] H. T. Smakman, "Functional integration of slip control with active suspension for improved lateral vehicle dynamics," 2000.

[9] Renault, "Renault morphoz concept." `https://www.renault.nl/design/morphoz-concept.html`. Accessed 17-12-2021.

[10] Audi, "Audi skysphere: een nieuwe visie op flexibele ruimte." `https://www.audi.nl/nl/web/nl/voorsprong/conceptcars/skysphere-concept.html`. Accessed 17-12-2021.

[11] Triggo, "Meet triggo, recover time wasted on daily commutes!." `https://www.triggo.city/`. Accessed 17-12-2021.

[12] R. N. Jazar, *Vehicle dynamics: theory and application*. Berlin: Springer, 2008.

[13] D. Karnopp, *Vehicle stability*. Boca Raton, Florida: CRC Press, 2004.

[14] J. Wong, "Theory of ground vehicles, new york, john willey & sons," 2001.

[15] H. Pacejka, *Tire and vehicle dynamics*. Elsevier, 2005.

Appendices

A. Additional Figures

A.1 Step Steer Manoeuvre

A.1.1 Velocity of $80\,km/h$ and Steering Amplitude of $50°$

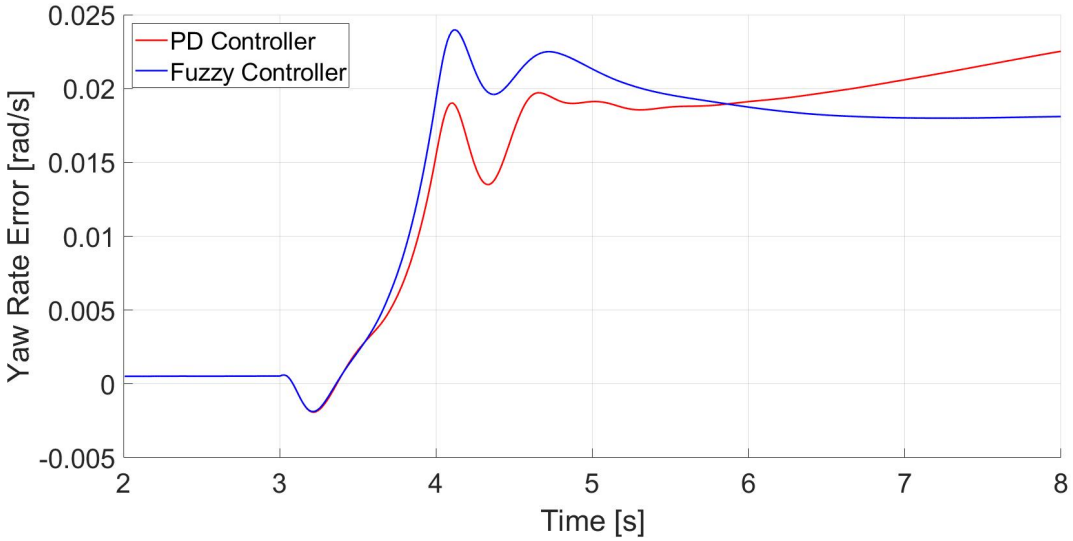

Figure A.1: Yaw rate error against time for the PD controller and the Fuzzy controller during the step steer manoeuvre at a velocity of $80\,km/h$ and a steering amplitude of $50°$.

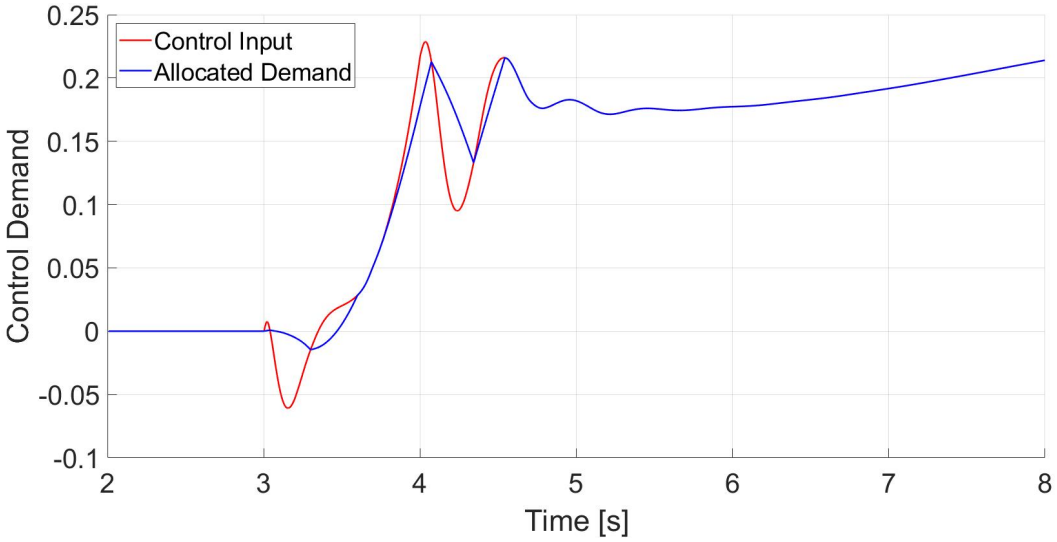

Figure A.2: Control demand against time for the PD controller during the step steer manoeuvre at a velocity of $80\,km/h$ and a steering amplitude of $50°$.

A.1.2 Velocity of $80\,km/h$ and Steering Amplitude of $30°$

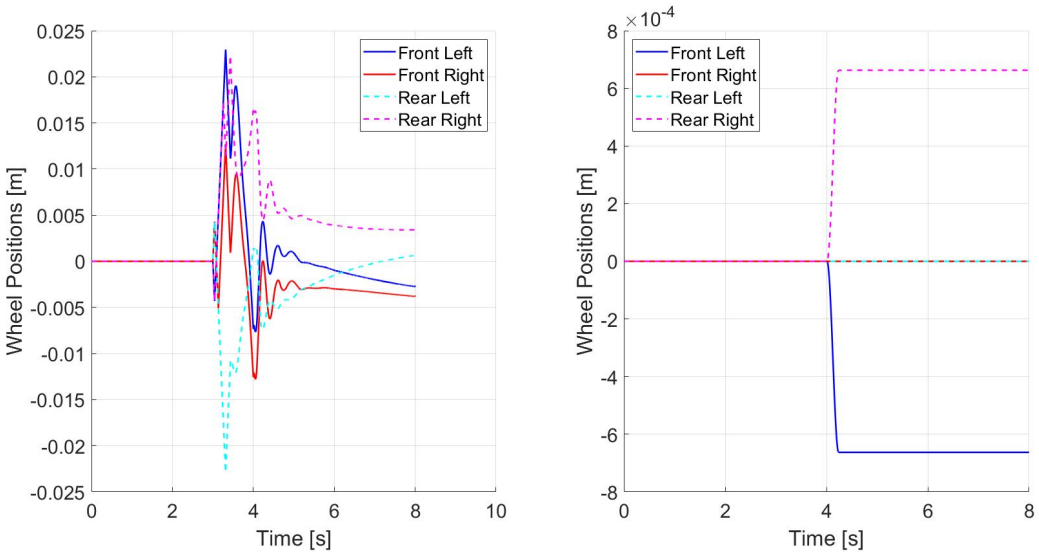

Figure A.3: Commanded wheel displacement in longitudinal direction against time for the PD controller (left) and the fuzzy controller (right), during the step steer manoeuvre at a velocity of $80\,km/h$ and a steering amplitude of $30°$.

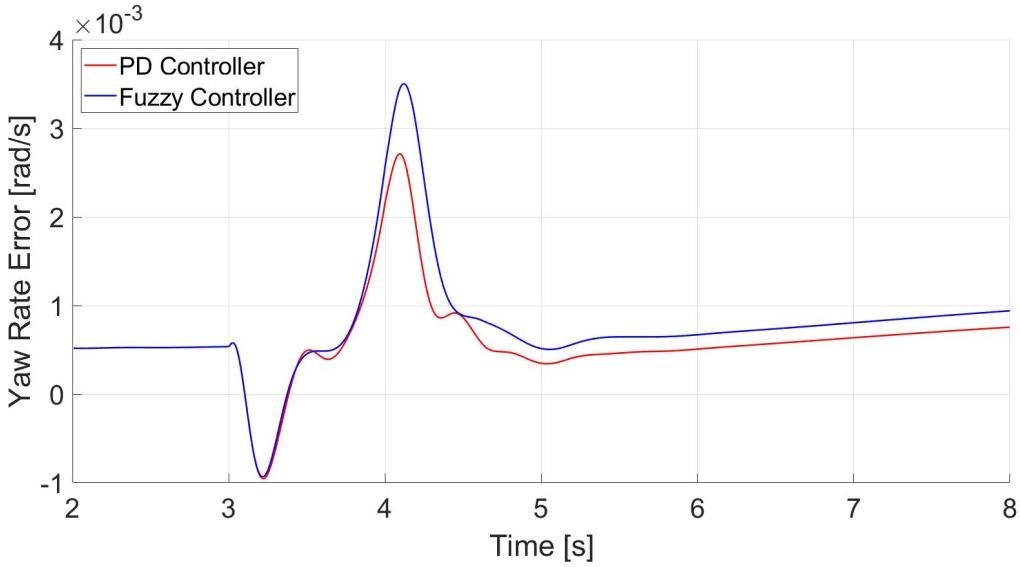

Figure A.4: Yaw rate error against time for the PD controller and the Fuzzy controller during the step steer manoeuvre at a velocity of $80\,km/h$ and a steering amplitude of $30°$.

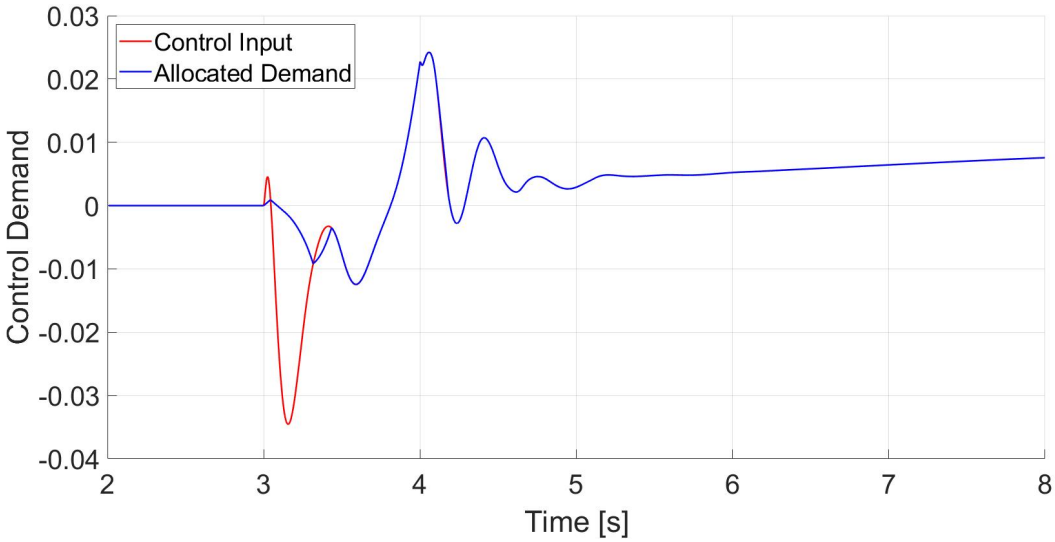

Figure A.5: Control demand against time for the PD controller during the step steer manoeuvre at a velocity of $80\,km/h$ and a steering amplitude of $30°$.

A.1.3 Velocity of $100\,km/h$ and Steering Amplitude of $50°$

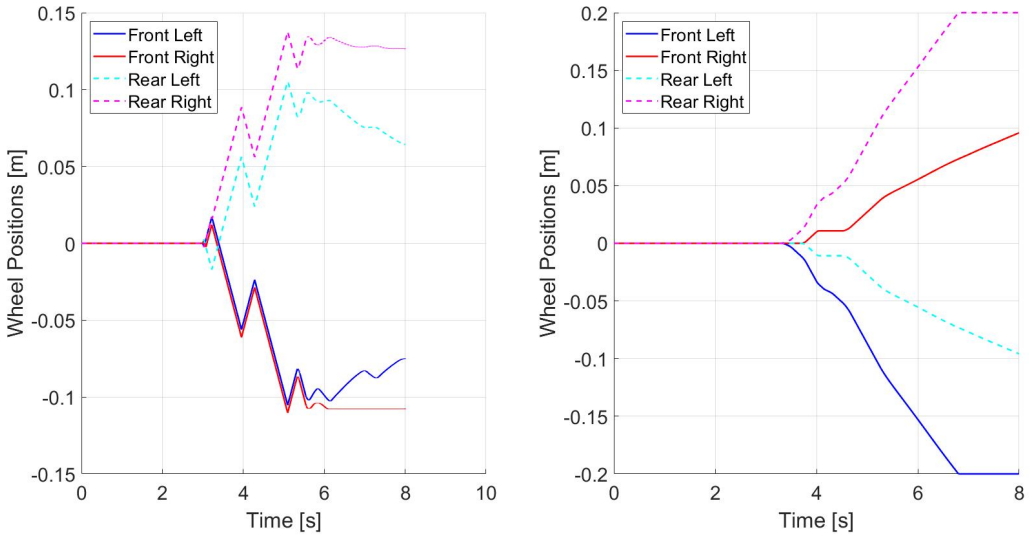

Figure A.6: Commanded wheel displacement in longitudinal direction against time for the PD controller (left) and the fuzzy controller (right), during the step steer manoeuvre at a velocity of $100\,km/h$ and a steering amplitude of $50°$.

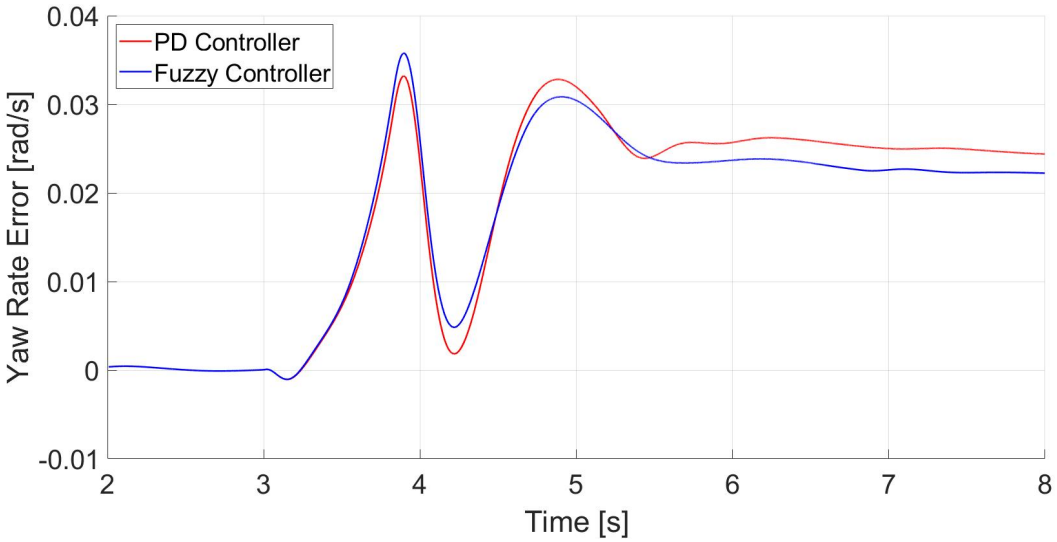

Figure A.7: Yaw rate error against time for the PD controller and the Fuzzy controller during the step steer manoeuvre at a velocity of 100 km/h and a steering amplitude of 50°.

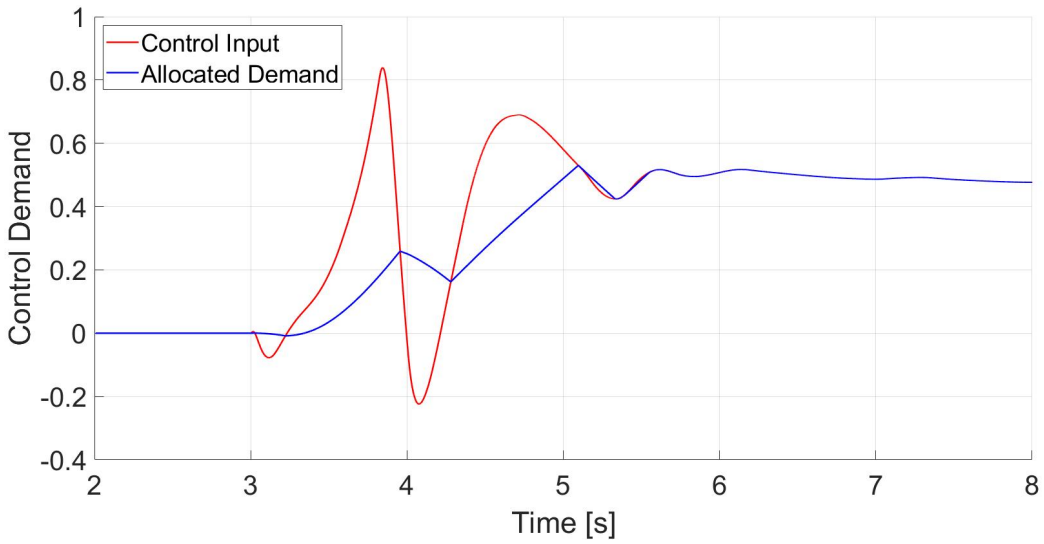

Figure A.8: Control demand against time for the PD controller during the step steer manoeuvre at a velocity of 100 km/h and a steering amplitude of 50°.

A.1.4 Velocity of $100\,km/h$ and Steering Amplitude of $30°$

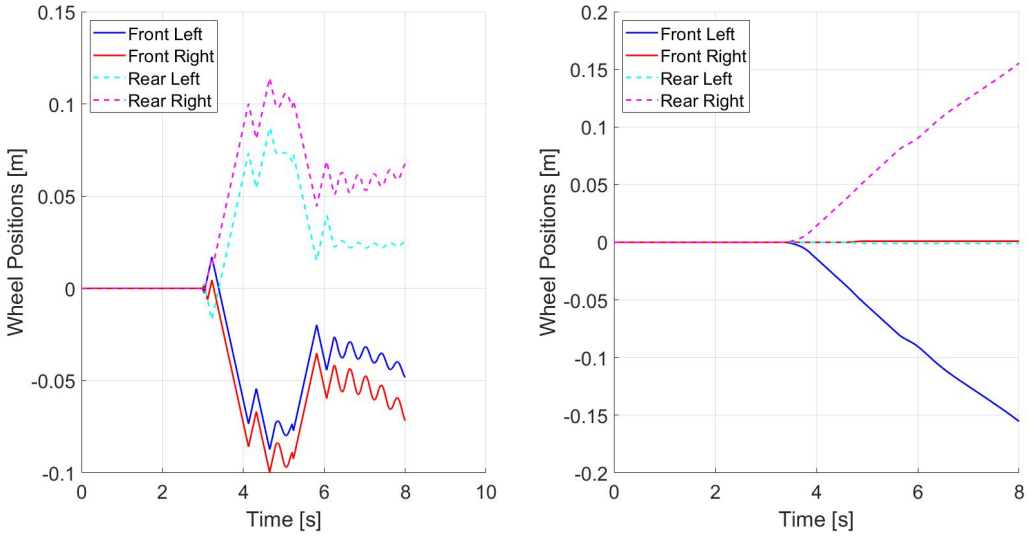

Figure A.9: Commanded wheel displacement in longitudinal direction against time for the PD controller (left) and the fuzzy controller (right), during the step steer manoeuvre at a velocity of $100\,km/h$ and a steering amplitude of $30°$.

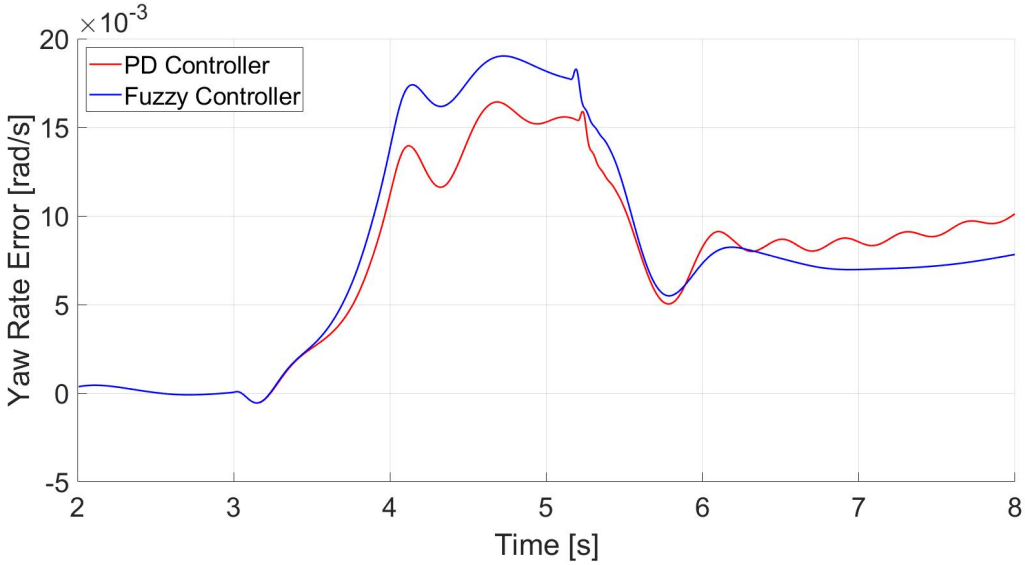

Figure A.10: Yaw rate error against time for the PD controller and the Fuzzy controller during the step steer manoeuvre at a velocity of $100\,km/h$ and a steering amplitude of $30°$.

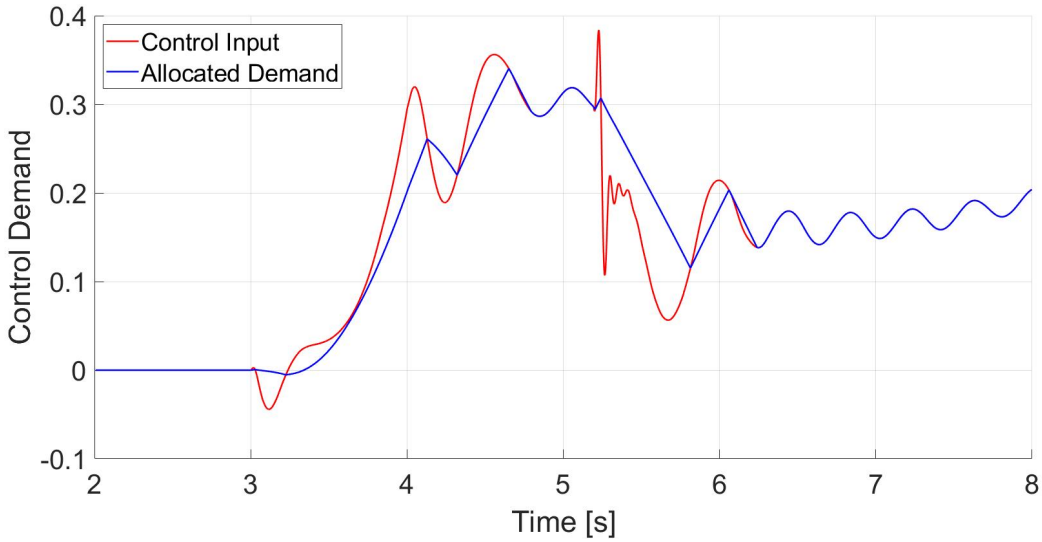

Figure A.11: Control demand against time for the PD controller during the step steer manoeuvre at a velocity of 100 km/h and a steering amplitude of 30°.

A.1.5 Velocity of 105 km/h and Steering Amplitude of 50°

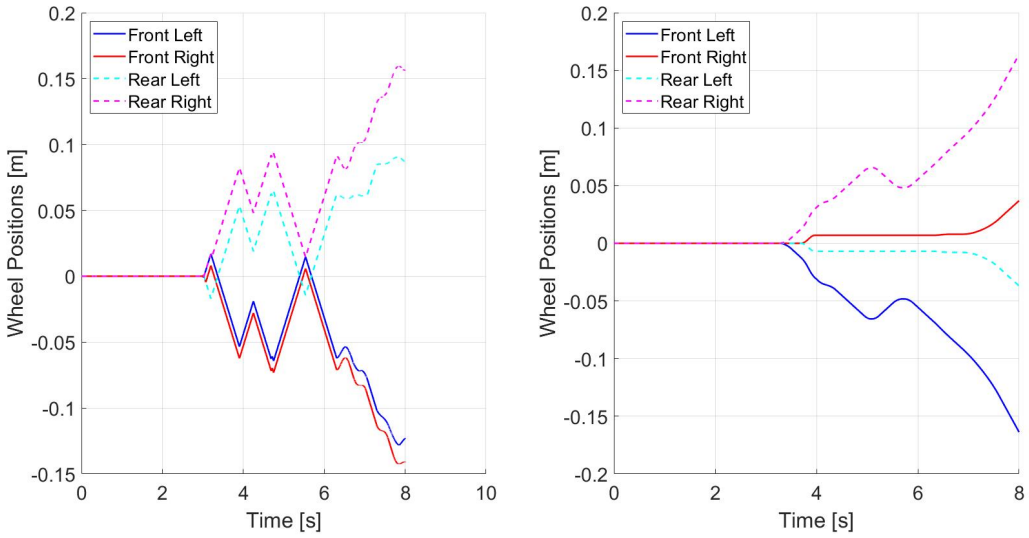

Figure A.12: Commanded wheel displacement in longitudinal direction against time for the PD controller (left) and the fuzzy controller (right), during the step steer manoeuvre at a velocity of 105 km/h and a steering amplitude of 50°.

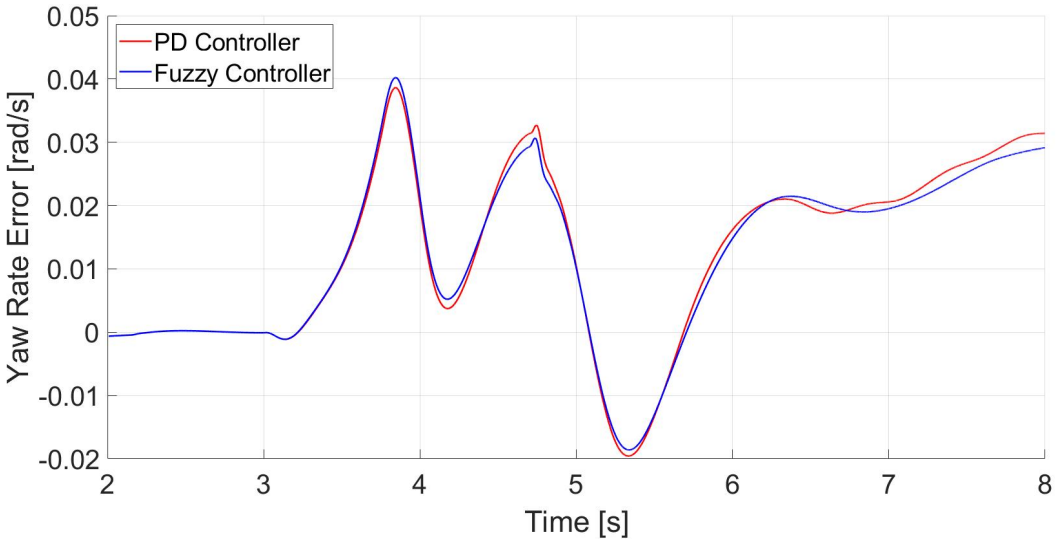

Figure A.13: Yaw rate error against time for the PD controller and the Fuzzy controller during the step steer manoeuvre at a velocity of 105 km/h and a steering amplitude of 50°.

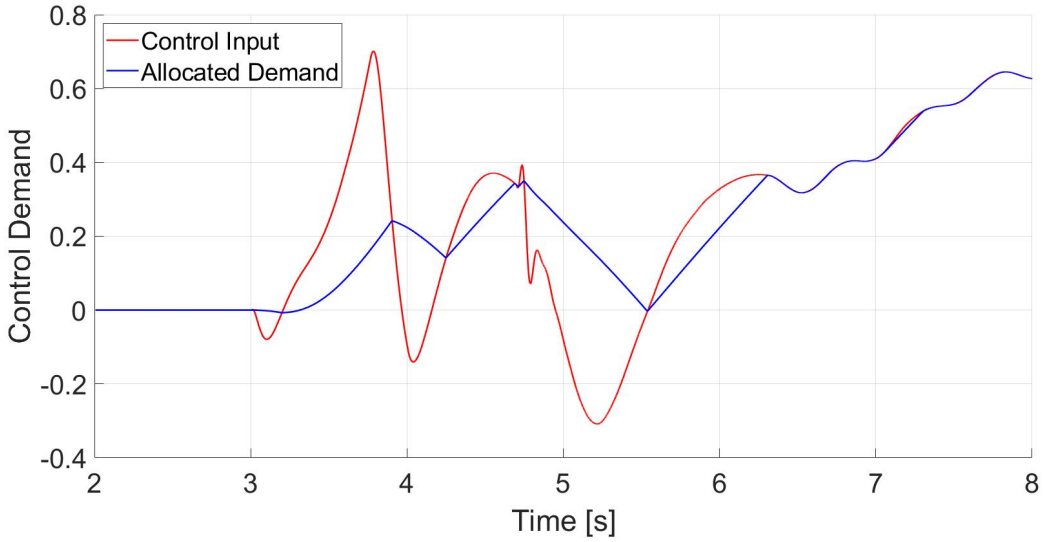

Figure A.14: Control demand against time for the PD controller during the step steer manoeuvre at a velocity of 105 km/h and a steering amplitude of 50°.

A.1.6 Velocity of $105\,km/h$ and Steering Amplitude of $30°$

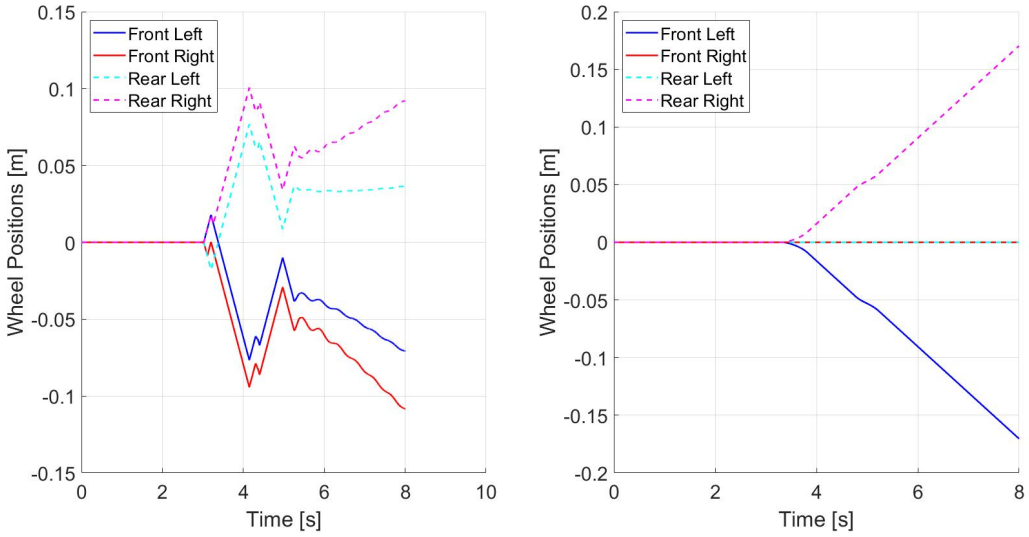

Figure A.15: Commanded wheel displacement in longitudinal direction against time for the PD controller (left) and the fuzzy controller (right), during the step steer manoeuvre at a velocity of $105\,km/h$ and a steering amplitude of $30°$.

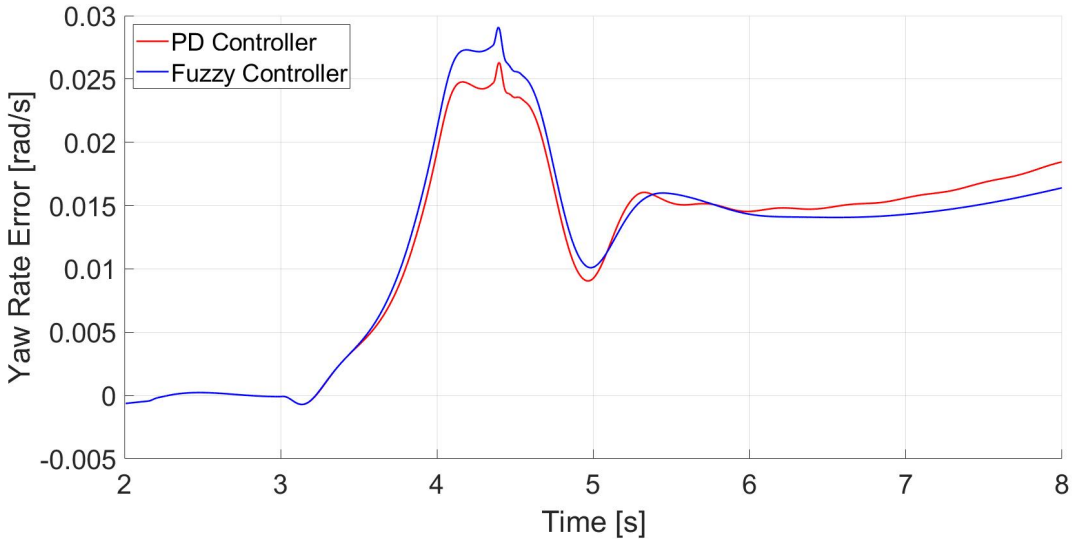

Figure A.16: Yaw rate error against time for the PD controller and the Fuzzy controller during the step steer manoeuvre at a velocity of $105\,km/h$ and a steering amplitude of $30°$.

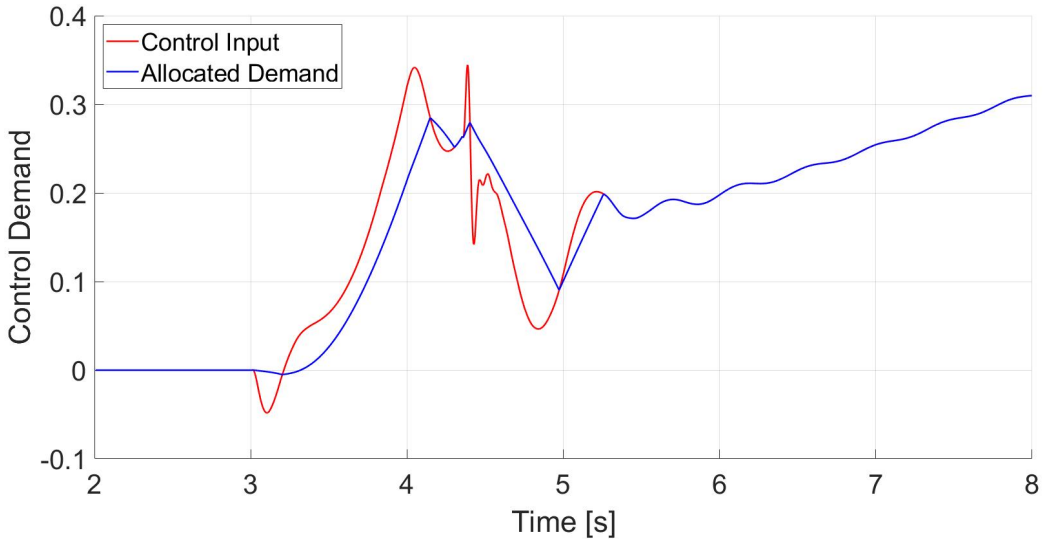

Figure A.17: Control demand against time for the PD controller during the step steer manoeuvre at a velocity of 105 km/h and a steering amplitude of 30°.

A.1.7 Velocity of 60 km/h and Steering Amplitude of 50°

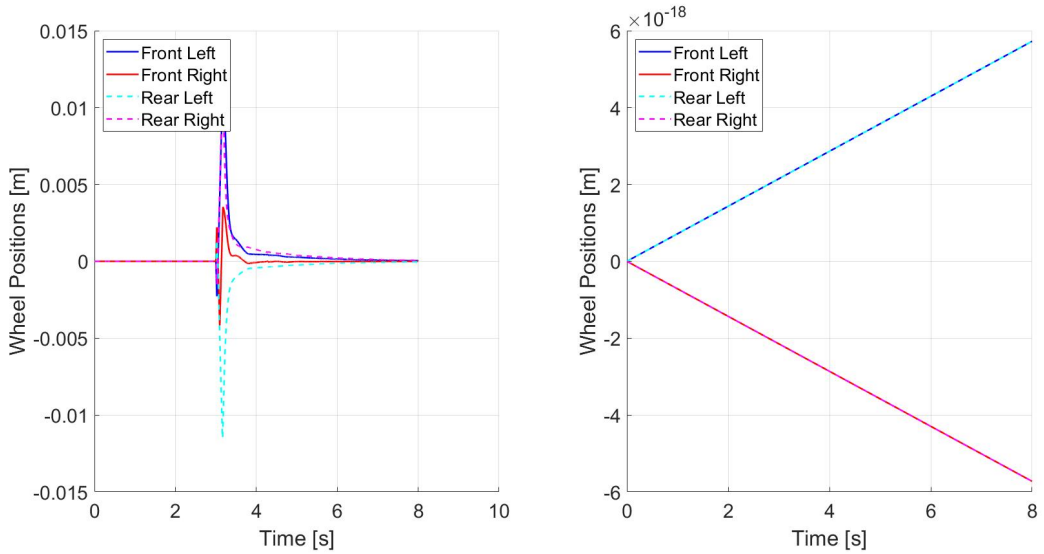

Figure A.18: Commanded wheel displacement in longitudinal direction against time for the PD controller (left) and the fuzzy controller (right), during the step steer manoeuvre at a velocity of 60 km/h and a steering amplitude of 50°.

A.1.8 Velocity of $110\,km/h$ and Steering Amplitude of $50°$

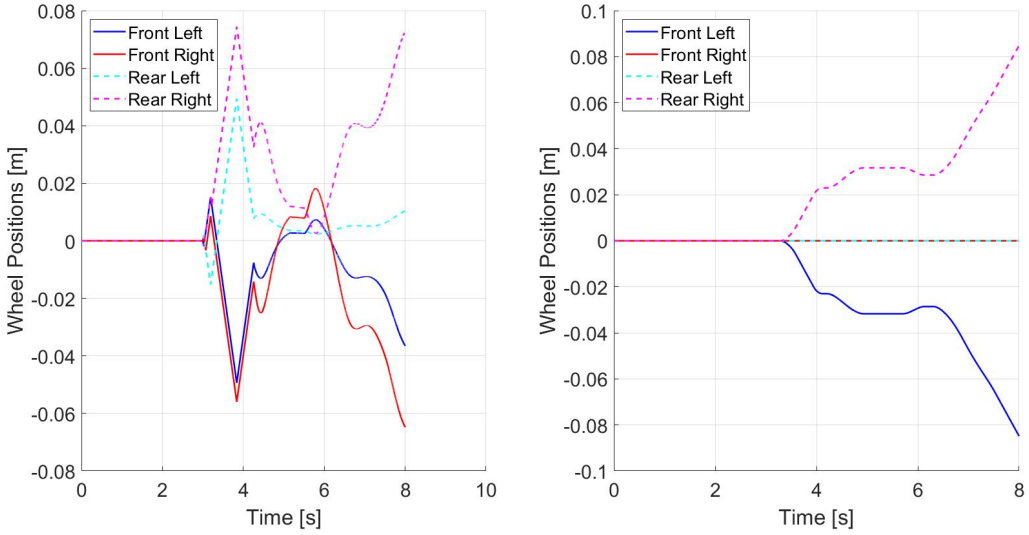

Figure A.19: Commanded wheel displacement in longitudinal direction against time for the PD controller (left) and the fuzzy controller (right), during the step steer manoeuvre at a velocity of $110\,km/h$ and a steering amplitude of $50°$.

A.2 Increasing Circle

A.2.1 Steering Amplitude of $30°$

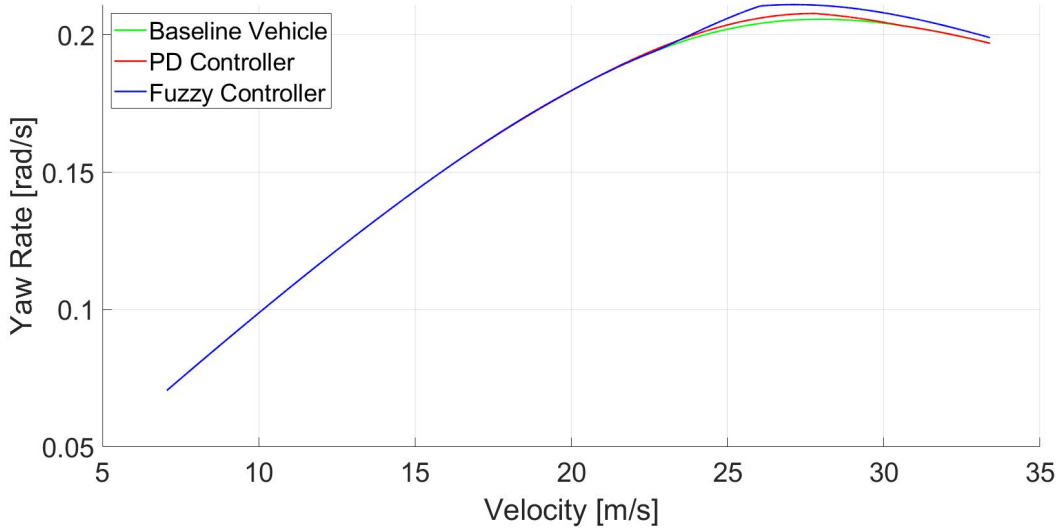

Figure A.20: Yaw rate against velocity for different controllers during the increasing circle manoeuvre at a steering amplitude of $30°$.

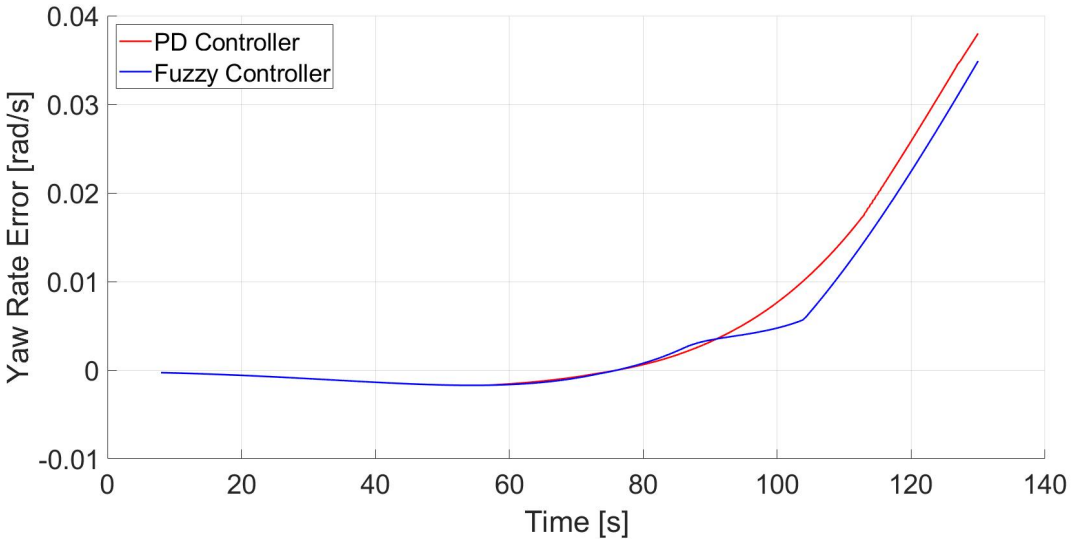

Figure A.21: Yaw rate error against time for the PD controller and the Fuzzy controller during the increasing circle manoeuvre at a steering amplitude of 30°.

A.2.2 Steering Amplitude of 50°

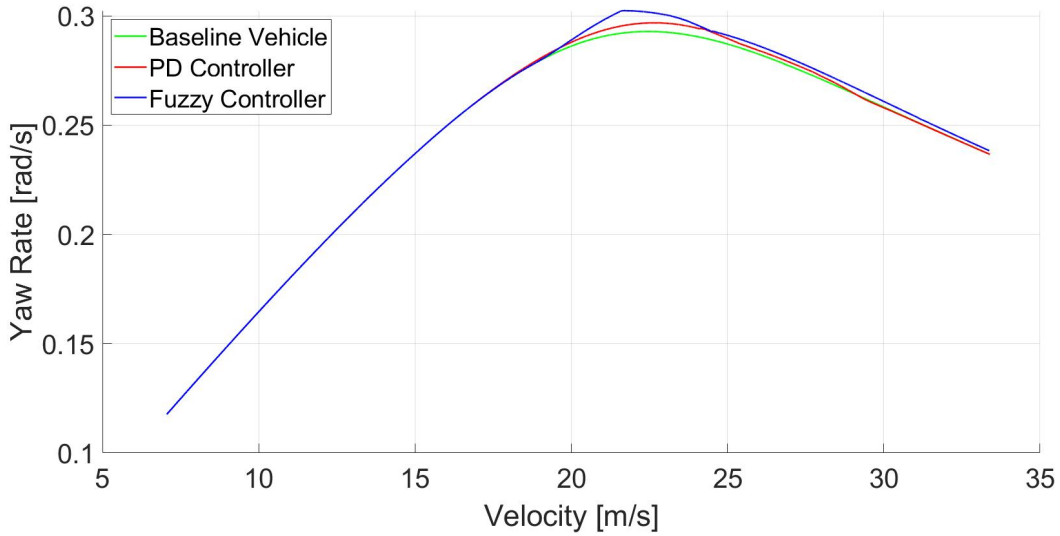

Figure A.22: Yaw rate against velocity for different controllers during the increasing circle manoeuvre at a steering amplitude of 50°.

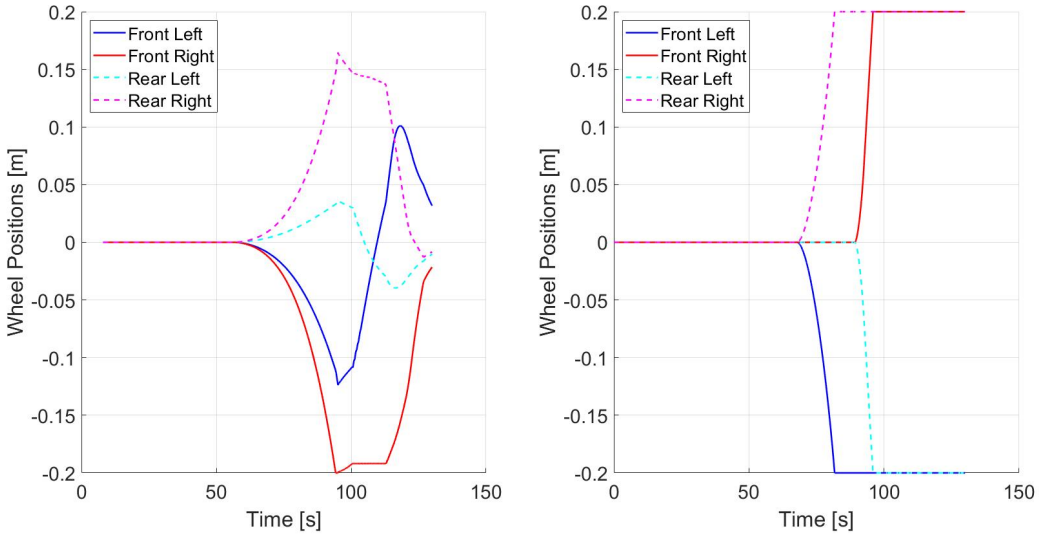

Figure A.23: Commanded wheel displacement in longitudinal direction against time for the PD controller (left) and the fuzzy controller (right), during the increasing circle manoeuvre at a steering amplitude of 50°.

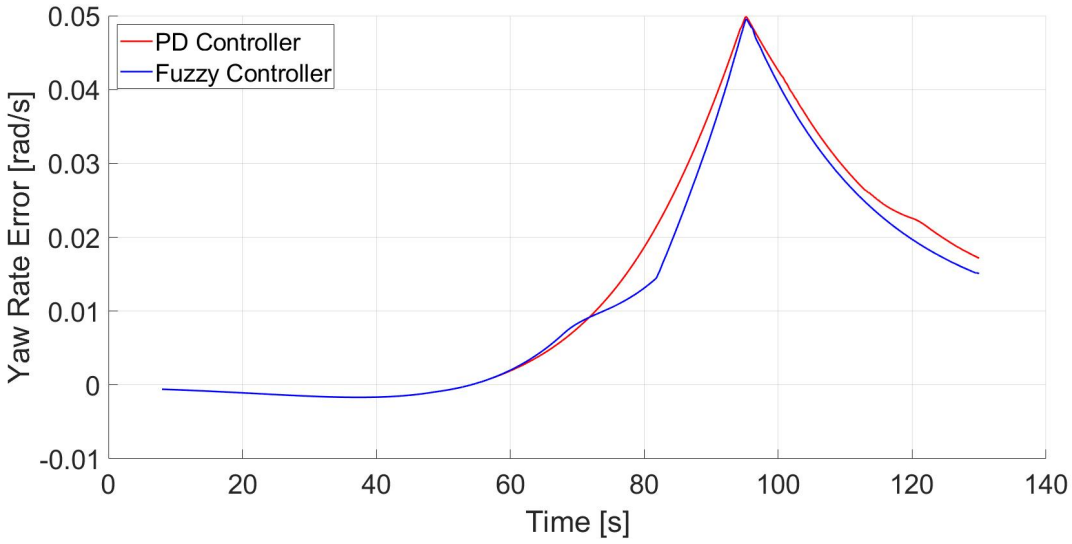

Figure A.24: Yaw rate error against time for the PD controller and the Fuzzy controller during the increasing circle manoeuvre at a steering amplitude of 50°.

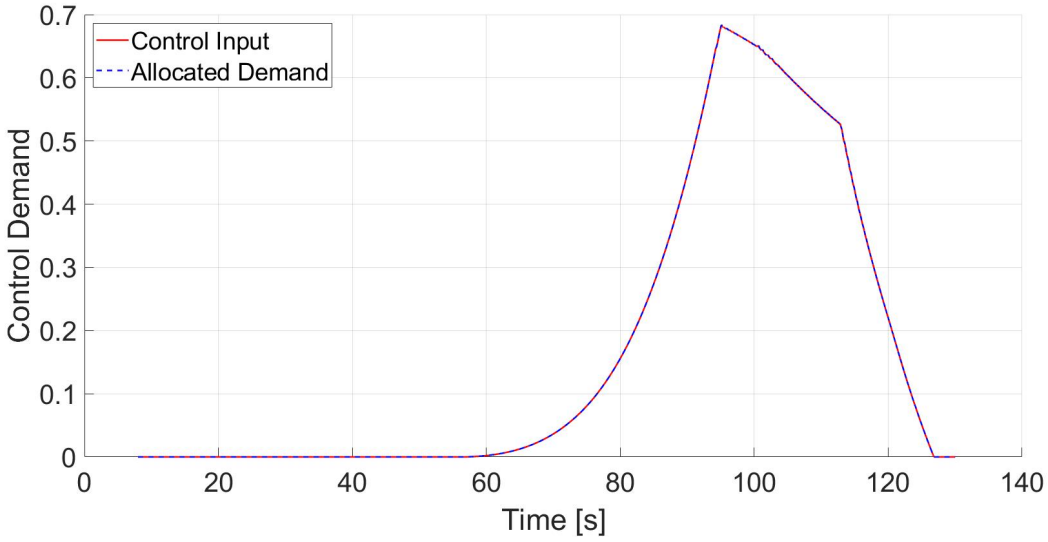

Figure A.25: Control demand of the PD controller against time during the increasing circle manoeuvre at a steering amplitude of 50°.

A.3 Double Lane Change

A.3.1 Velocity of $80\,km/h$

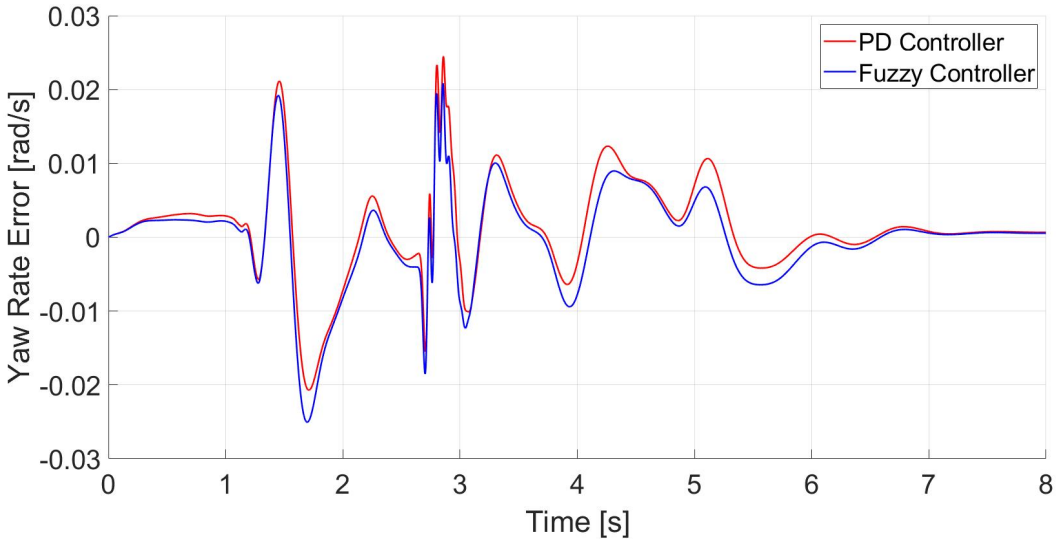

Figure A.26: Yaw rate error against time for the PD controller and the Fuzzy controller during the double lane change manoeuvre at a velocity of $80\,km/h$.

A.3.2 Velocity of $100\,km/h$

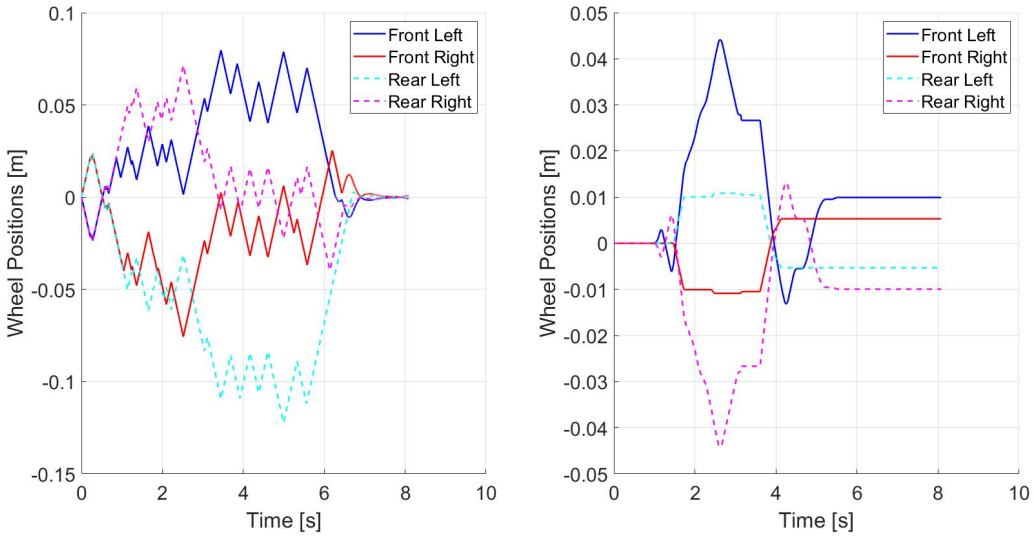

Figure A.27: Commanded wheel displacement in longitudinal direction against time for the PD controller (left) and the fuzzy controller (right), during the double lane change manoeuvre at a velocity of $100\,km/h$.

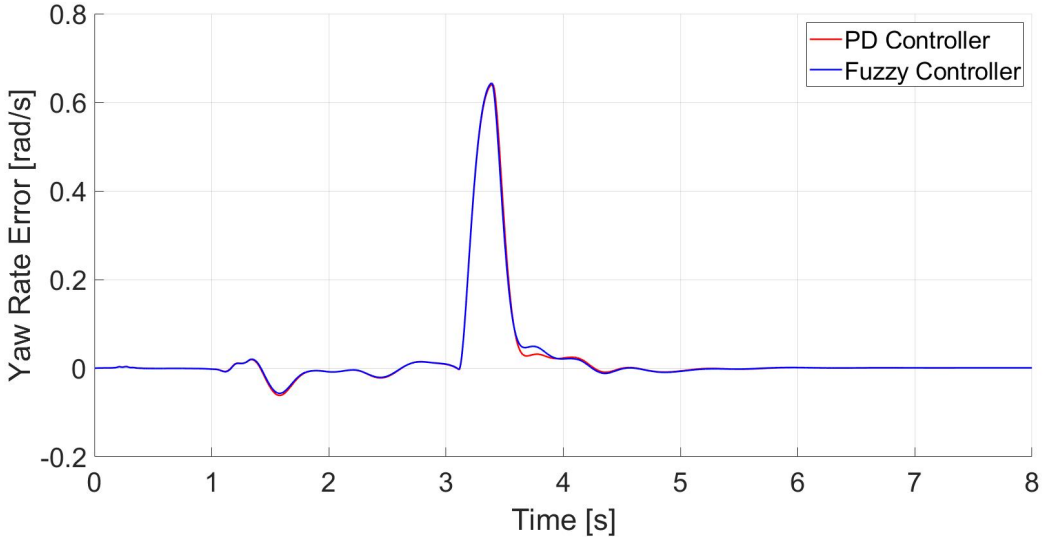

Figure A.28: Yaw rate error against time for the PD controller and the Fuzzy controller during the double lane change manoeuvre at a velocity of 100 km/h.

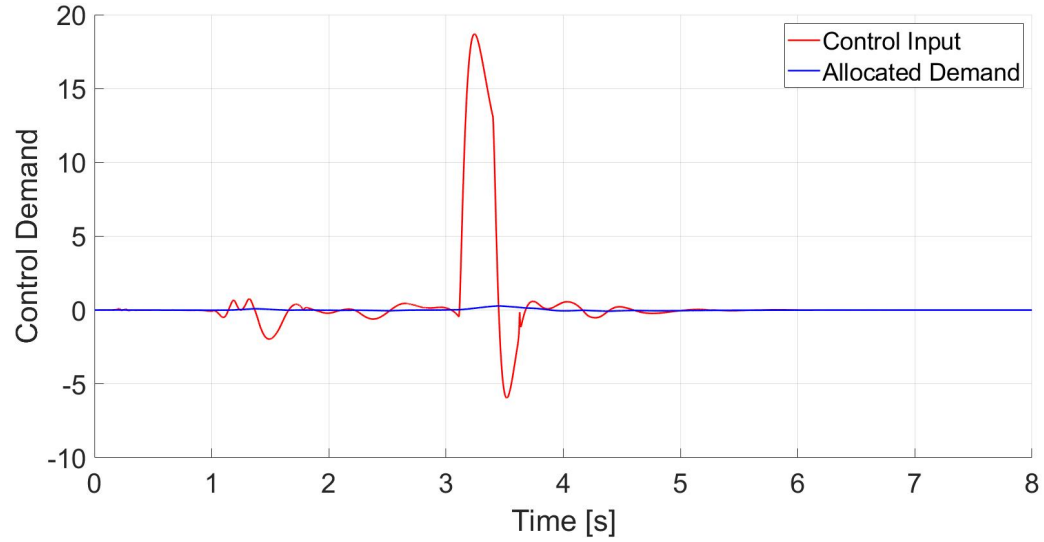

Figure A.29: Control demand of the PD controller against time during the double lane change manoeuvre at a velocity of 100 km/h.

A.3.3 Velocity of $105\,km/h$

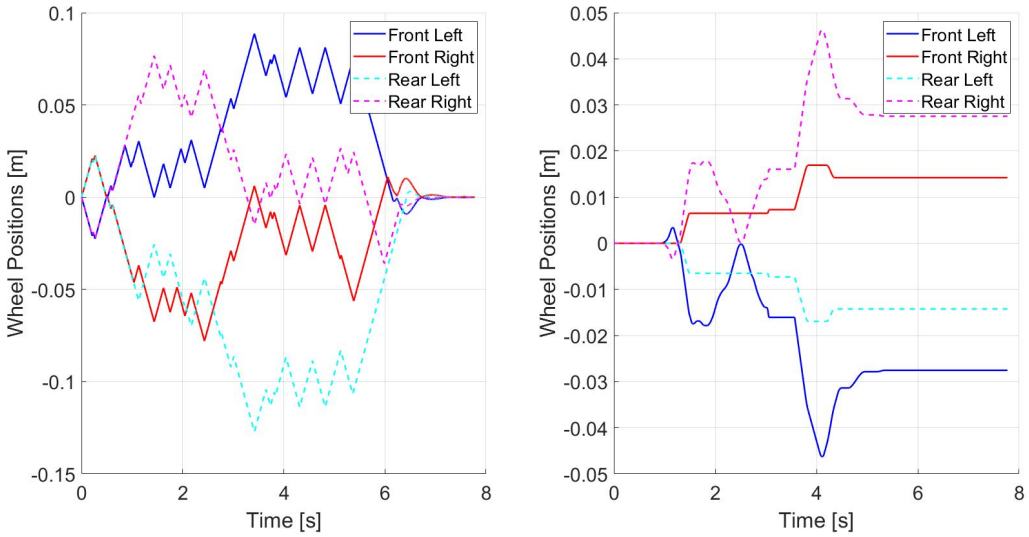

Figure A.30: Commanded wheel displacement in longitudinal direction against time for the PD controller (left) and the fuzzy controller (right), during the double lane change manoeuvre at a velocity of $105\,km/h$.

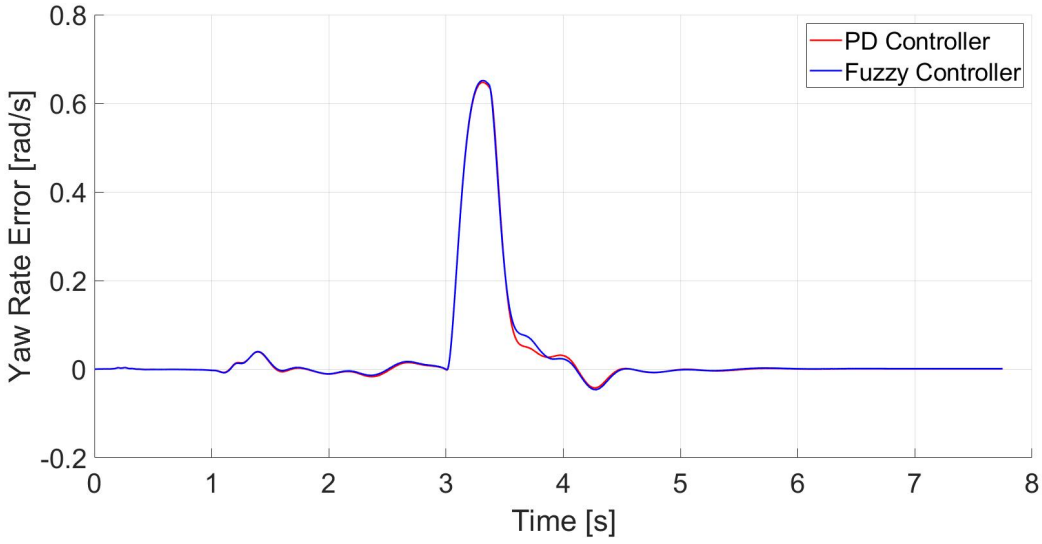

Figure A.31: Yaw rate error against time for the PD controller and the Fuzzy controller during the double lane change manoeuvre at a velocity of $105\,km/h$.

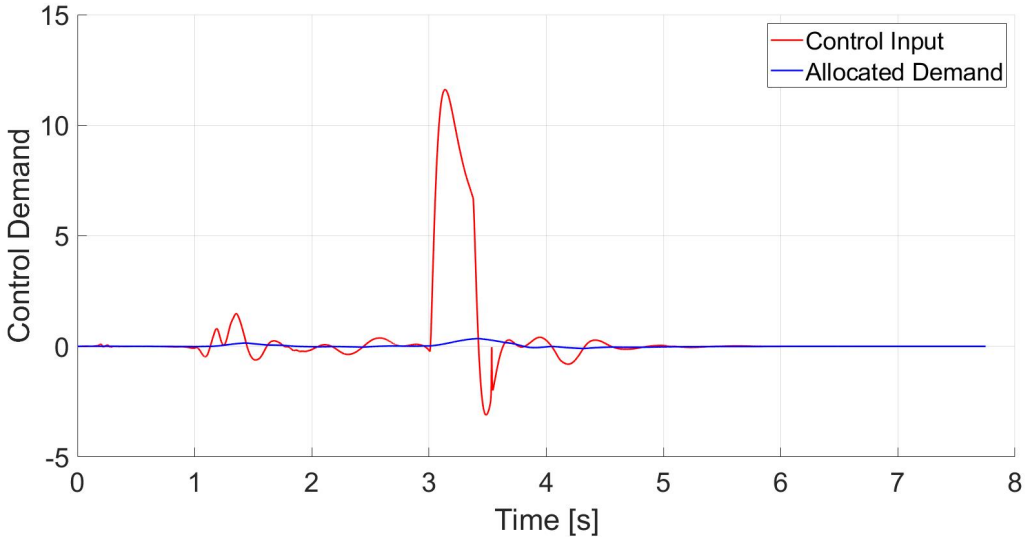

Figure A.32: Control demand of the PD controller against time during the double lane change manoeuvre at a velocity of 105 km/h.